
The role of Cysteine-rich with EGF-like domains 2 in the maintenance of metabolic homeostasis and regulation of the unfolded protein response

Dissertation

zur

Erlangung des Doktorgrades (Dr. rer. nat.)

der

Mathematisch-Naturwissenschaftlichen Fakultät

der

Rheinischen Friedrich-Wilhelms-Universität Bonn

vorgelegt von

Paul Kern

aus

Kochschetau

Bonn

August, 2018

Angefertigt mit Genehmigung der Mathematisch-Naturwissenschaftlichen Fakultät der
Rheinischen Friedrich-Wilhelms-Universität Bonn

1. Gutachter: Prof. Dr. Dr. Michael Hoch

2. Gutachter: PD Dr. Reinhard Bauer

Tag der Promotion: 30.01.2019

Erscheinungsjahr: 2019

Zusammenfassung

Das Ziel dieser Arbeit war es, die Rolle von Creld2 bei der Aufrechterhaltung der metabolischen Homöostase unter Normalbedingungen und bei der Regulation der UPR unter ER Stressbedingungen zu untersuchen. Metabolische Analysen von *Creld2*^{-/-} Mäusen zeigten eine Anfälligkeit von 1-jährigen Männchen für die Entwicklung von Hepatosteatose und Insulinresistenz, welche von einer fehlregulierten *Pgc1α* Genexpression und einer reduzierten Genexpression der Glukosetransporter Glut2 und Glut4 begleitet wird. Weibliche *Creld2*^{-/-} Mäuse sind wahrscheinlich aufgrund geschlechtsspezifischer Hormonregulationsunterschiede vor Lebersteatose geschützt. *In vitro*-ER-Stressanalysen von Wildtyp und Creld2-defizienten MEFs zeigten, dass *Creld2*^{-/-} -Zellen den entstehenden Stress nicht so gut wie *Creld2*^{+/+}-Zellen tolerieren können und folglich apoptotisch werden, wenn sie mit ER-Stress konfrontiert werden. Eingehende Analysen der drei UPR-Signalwege zeigten eine verzögerte und mangelhafte Antwort von *Creld2*^{-/-}-Zellen auf ER-Stress, welches zu einem unvollständigen ER-Stressabbau und zur Akkumulation von ER-Stress führt, was die Funktionalität der Zellen beeinträchtigt. Diese *in vitro*-Ergebnisse stützen die Hypothese, dass das Fehlen von Creld2 zu nicht aufgelöstem ER-Stress und der nachfolgenden Entwicklung von Lebersteatose führt. Darüber hinaus zeigen die Co-Präzipitationsstudien von Creld2 eine Bereicherung zahlreicher Faltungsproteine und Proteinen, welche am Kohlenhydratstoffwechsel beteiligt sind auf. Dies deutet darauf hin, dass Creld2 mit solchen Proteinen interagiert und dadurch deren Funktion beeinflussen könnte. Schlussfolgernd deuten die Ergebnisse dieser Arbeit darauf hin, dass Creld2 an der Regulation von Stoffwechselprozessen beteiligt ist, indem es eine angemessene ER-Stressantwort, durch die zeitliche Koordination und Verstärkung des UPRs, ermöglicht.

"The most beautiful experience we can have is the mysterious. It is the fundamental emotion that stands at the cradle of true art and true science"

–Albert Einstein–

Contents

1	Introduction	1
1.1	Cysteine-rich with EGF-like domains family	1
1.2	CrelD1	1
1.3	CrelD2	1
1.4	ER stress and the unfolded protein response	3
1.4.1	The Perk pathway	4
1.4.2	The Atf6 α pathway	4
1.4.3	The Ire1 α pathway	6
1.5	UPR signalling & disease	6
1.6	Glucose & Lipid metabolism and non-alcoholic fatty liver disease	8
1.7	Bone structure, growth and remodelling	10
1.8	Aim of the thesis	14
2	Materials	15
2.1	Equipment	15
2.2	Consumables	16
2.3	Chemicals & solutions	17
2.4	Standards and Kits	17
2.5	Bacterial strains	18
2.6	Buffers & solutions	18
2.7	Media	20
2.8	Antibodies	21
2.9	Plasmids	23
2.10	Primer & gene blocks	24
2.10.1	Genotyping primer	24
2.10.2	Cloning primer	24
2.10.3	qRT-PCR primer	24
2.10.4	Gene blocks	26

3	Methods	28
3.1	Histological stainings	28
3.1.1	Preparation of organ samples for histological analysis	28
3.1.2	Preparation of bone samples for histological analysis	28
3.1.3	Paraffin embedding	28
3.1.4	Cryo embedding	28
3.1.5	Hematoxilin & Eosin staining	28
3.1.6	Masson-Goldner Trichrome staining	29
3.1.7	Oil-red O staining	29
3.2	Isolation of RNA	29
3.3	Reverse transcription of RNA into cDNA	30
3.4	PCR techniques	30
3.4.1	Genotyping PCR	30
3.4.2	Cloning PCR	31
3.4.2.1	Cloning of N-terminally tagged Creld2	31
3.4.2.2	Cloning of C-terminally tagged Creld2	31
3.4.2.3	Cloning of the SF-mock vector	32
3.4.3	qRT-PCR	32
3.4.4	Total lipid extraction in solution by Bligh & Dyer	33
3.5	Western blotting	33
3.6	Antibody binding and ECL detection	33
3.7	Cell culture	34
3.7.1	Isolation and culture of mouse embryonic fibroblasts	34
3.7.2	Induction of ER stress	34
3.7.2.1	Induction of acute ER stress	34
3.7.2.2	Induction of chronic ER stress	35
3.7.2.3	Induction of transient ER stress	35
3.7.2.4	Cell viability assay	35
3.7.2.5	Electroporation of cells	35
3.7.3	Tandem affinity purification	36
3.7.4	Analysis of mass-spectrometric data	36

3.8	Work with <i>Mus musculus</i>	37
3.8.1	Animal housing	37
3.8.2	Glucose tolerance test	37
3.8.3	Insulin tolerance test	37
4	Results	38
4.1	General phenotypic analysis	38
4.2	Analysis of metabolism	39
4.2.1	Analysis of liver lipid homeostasis	41
4.2.2	Transcriptional regulation of lipid metabolism genes	41
4.2.3	Glucose metabolism	44
4.3	Analysis of liver injury status	47
4.4	Steady state UPR in 1-year-old mice	50
4.5	Analysis of bones	50
4.5.1	Analysis of bone structure	50
4.5.2	Analysis of the hematopoietic stem cell niche	54
4.6	<i>In vitro</i> analysis of the UPR	55
4.6.1	Chronic ER stress	56
4.6.1.1	Cell viability during chronic ER stress	56
4.6.1.2	Regulation of ER stress markers during chronic ER stress	58
4.6.1.3	Perk pathway regulation during chronic ER stress	58
4.6.1.4	Atf6 α pathway regulation during chronic ER stress	61
4.6.1.5	Ire1 α pathway regulation during chronic ER stress	61
4.6.2	ER stress recovery	63
4.6.2.1	Establishment of the ER stress recovery model	63
4.6.2.2	Marker regulation during ER stress recovery	66
4.6.2.3	Perk pathway regulation during ER stress recovery	68
4.6.2.4	Atf6 α pathway regulation during ER stress recovery	68
4.6.2.5	Ire1 α pathway regulation during ER stress recovery	68
4.7	Identification of Creld2 interaction partners	71

5 Discussion	75
5.1 General phenotype of the <i>Creld2</i> -knockout-mouse	75
5.2 Metabolic aberrations in the <i>Creld2</i> -knockout-mouse	75
5.2.1 Gender-specific differences	75
5.2.2 NAFLD in <i>Creld2</i> ^{-/-} mice	76
5.3 Liver injury and inflammation	78
5.4 Impaired UPR as the trigger of hepatosteatosis	79
5.4.1 Chronic ER stress	81
5.4.2 ER stress recovery	81
5.4.3 Chronic ER stress versus ER stress recovery	83
5.5 <i>Creld2</i> in bone development and maintenance	84
5.6 <i>Creld2</i> interaction partners	86
5.7 Conclusion	89
6 Summary	90
Acknowledgements	91
References	91
List of Figures	107
List of Tables	109
List of abbreviations	110
Appendix	113

1 Introduction

1.1 Cysteine-rich with EGF-like domains family

The cysteine-rich with EGF-like domains (Creld) 2 gene was identified early this century as a homologue of Creld1, the other member of the Creld protein family. In human, these proteins exhibit 38 % identity and 51 % similarity [1]. Proteins of the Creld family are highly conserved across species and possess an N-terminal signal peptide for endoplasmic reticulum (ER) localisation followed by a unique tryptophane (W) and glutamic acid (E)-rich domain (WE domain) including a highly conserved nonapeptide. Following the WE domain, Creld family proteins exhibit an array of one or two epidermal growth factor (EGF)-like and Ca²⁺ binding EGF-like domains, depending on the species. The significant difference between Creld1 and Creld2 is the presence of transmembrane domains in Creld1, which are absent in Creld2. Although Creld1 and Creld2 display high domain homology, the presence or absence of a membrane anchoring renders these proteins very diverse in their functions [1,2].

1.2 Creld1

Creld1 is repeatedly found to be mutated in atrioventricular septal defect (AVSD) patients and thus was characterised as an AVSD risk factor [3–6]. Analysis of Creld1 function showed that Creld1 effects heart development by enhancing nuclear factor of activated T cells 1 (NFATc1) nuclear localisation, thereby contributing to atrioventricular septum formation [7].

1.3 Creld2

The Creld2 protein is highly conserved between species, such as human, mouse, rat, zebrafish and *Drosophila melanogaster*, with human and murine Creld2 displaying highest conservation. The length or integrity of the WE domain and the presence of one or two Ca²⁺-binding EGF-like domains are the major differences in the primary Creld2 protein structures. Creld2 was shown to be a glycoprotein [8], and differences in the predicted sites for N-glycosylation are visible between species. Minor alterations in the

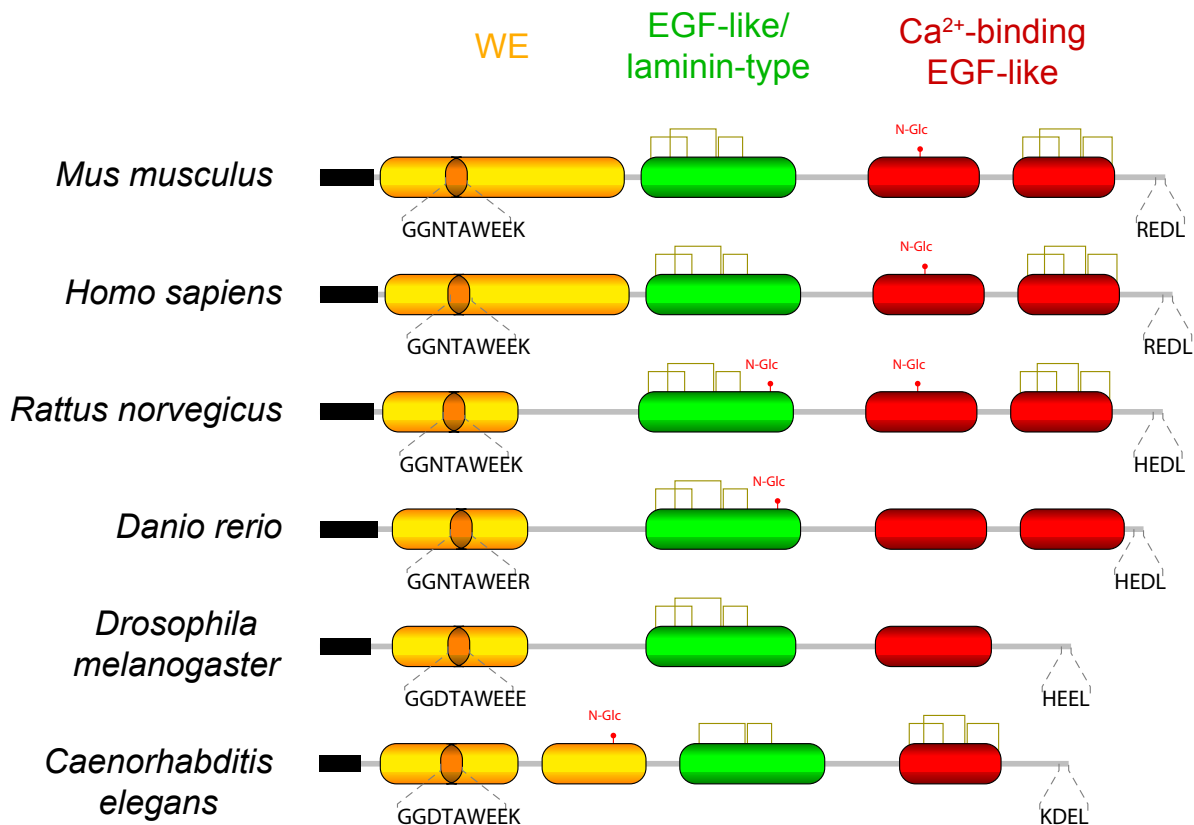


Figure 1.1: Predicted Creld2 protein structure is conserved between different species. Comparison of Creld2 primary protein structure in different species. From N- to C-terminus: Signal peptide (black), WE-domain differing in length between species (yellow) containing a conserved nonapeptide (GGNTAWEE E/K/R; orange). Followed by an epidermal growth factor (EGF)-like/laminin-type (green) and one or two Ca²⁺-binding EGF-like (red) and an ER retention signal peptide at the very C-terminus (REDL, HEDL, HEEL or KDEL). EGF-like domains contain the six characteristic disulfide bonds (olive green rectangles). Predicted sites for N-glycosylation are indicated (N-Glc). For human Creld2 only the main isoform is illustrated.

amino acid sequence of the nonapeptide (GGNTAWEE E/K/R), which is enclosed in the WE domain, and in the ER-retention motif sequence are present (Figure 1.1). Here, the human Creld2 isoform 1 and murine Creld2 display the highest conservation. While there is only one Creld2 isoform present in mouse, the human genome encompasses six *Creld2* transcripts due to alternative splicing. This results in six human Creld2 isoforms, which mainly differ in the spacing and presence or absence of EGF-like and Ca²⁺-binding domains. One isoform, however, is missing the ER retention motif. Nevertheless, the distinctive WE domain is present in all isoforms [9].

Creld2 shows ubiquitous expression and displays highest expression levels in secretory organs, for instance, the liver, pancreas, kidney and thyroid gland. [9]. Primarily, Creld2 localises in the ER due to its ER retention signal sequence, but Creld2 secretion to

the extracellular space is increased during ER stress or by the absence or masking of the ER retention sequence [8]. *Creld2* promoter analyses identified a conserved ER stress response element (ERSE) sequence. This ERSE sequence was shown to be bound by the activating transcription factor 6 (ATF6) resulting in the induction of *Creld2* expression [10]. Recently, *Creld2* was identified as a new urinary biomarker for various aberrant kidney states, for instance, acute kidney injury and tubulointerstitial kidney disease [11].

First molecular analyses indicated that *Creld2* binds the neuronal nicotinic acetylcholine receptor $\alpha 4$ and $\beta 2$ subunits, which suggests the involvement of *Creld2* in protein folding and transport to the plasma membrane [12]. Additionally, several implications of *Creld2* involvement in bone growth and homeostasis were reported, which are elucidated in section 1.7.

1.4 ER stress and the unfolded protein response

Cells have a constant need to produce proteins for the maintenance of metabolic homeostasis, proliferation or secretion of hormones and other signalling molecules. Proteins anchored to the membrane or those destined for secretion need to be correctly folded and glycosylated in the ER. However, dysregulations of Ca^{2+} levels, glucose deficiency or merely a demand for a vast amount of proteins can lead to the accumulation of unfolded proteins because these cannot be properly folded in time. This accumulation and the resulting aggregation of proteins is termed ER stress and is markedly elevated in organs with high protein turnover, such as the liver, kidney and pancreas [13]. To resolve emerging ER stress, the cell elicits a stringently controlled program called the unfolded protein response (UPR) [14].

ER stress in the cell is detected by three ER-transmembrane stress sensors, namely PERK-like endoplasmic reticulum kinase (Perk), Atf6 and inositol-requiring protein 1 α (*Ire1 α*), which evoke and orchestrate UPR pathways to ameliorate the ER stress once they are activated. Here, the three UPR branches induce transcriptional programs either independently or in a cooperative manner (Figure 1.2) [15, 16]. In principle, the UPR resolves ER stress by reducing the protein load to the ER, increasing the folding capacity and boosting degradation of ultimately misfolded proteins. Under homeostatic

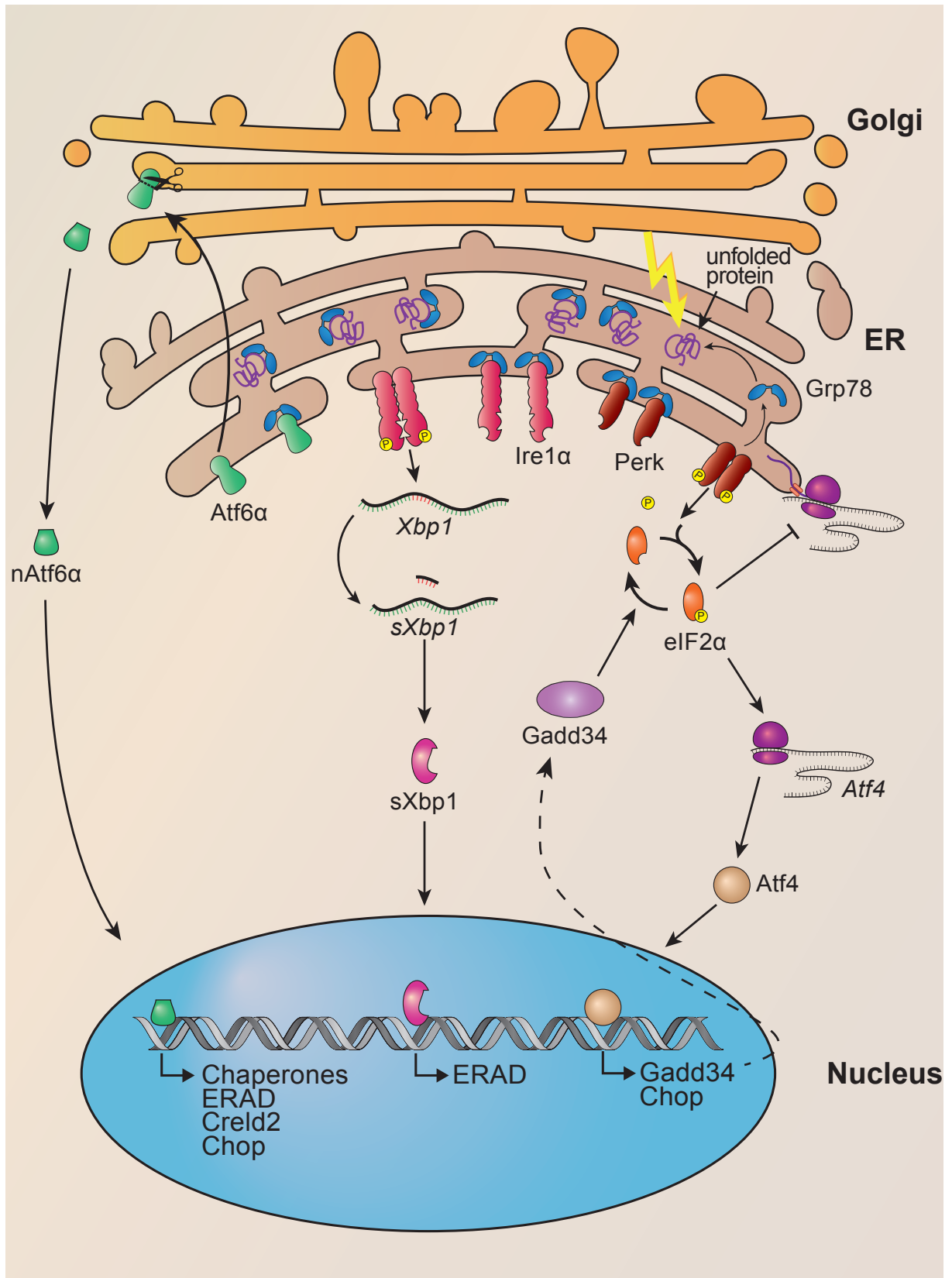
conditions, the three stress sensors are bound and deactivated by the ER stress master regulator chaperone 78 kDa glucose-regulated protein (Grp78). In case of emerging ER stress, Grp78 releases the sensors in order to bind and fold non-native proteins. This, in turn, leads to an activation of the sensors, which initiate the UPR [17]. If the cell does not succeed to eliminate the ER stress, the cell activates pathways responsible for ER stress-mediated apoptosis [18].

1.4.1 The Perk pathway

Dissociation of Grp78 from Perk leads to Perk dimerisation and autophosphorylation and renders it active. Then, Perk phosphorylates and thereby inactivates the eukaryotic initiation factor 2 α (eIF2 α). Inactivation of eIF2 α , in turn, results in a global attenuation of protein synthesis and reduces protein flux to the ER. Inhibition of eIF2 α leads to selective translation of certain proteins. One of these proteins is the activating transcription factor 4 (Atf4), which contains an internal ribosomal entry site (IRES) and induces the expression of genes important to relieve ER stress, thereby reducing reactive oxygen species (ROS) production. The growth arrest and DNA damage-inducible protein (Gadd34) is one of these important factors. Gadd34 dephosphorylates P-eIF2 α and leads to a normalisation of protein synthesis [19, 20]. However, if the ER is perturbed for extended periods, the prolonged induction of CCAAT-enhancer-binding protein homologous protein (Chop) by Atf4 results in ER stress-induced apoptosis of the cell [21, 22].

1.4.2 The Atf6 α pathway

Inactive Atf6 α is bound by Grp78. Activation of the Atf6 α branch starts with the detachment of Grp78 from Atf6 α . Subsequently, Atf6 α is translocated to the Golgi-apparatus where it is proteolytically cleaved by site-1 protease (S1P) and site-2 protease (S2P), which leads to the release of the cytoplasmic and active transcription factor Atf6 α form, termed nuclear Atf6 α (nAtf6 α) [23]. nAtf6 α was shown to induce gene expression of sets of chaperones, ER-associated protein degradation (ERAD) components and other genes involved in protein folding and glycosylation. Known downstream targets are *Grp78*, *Grp94*, *Chop*, *ER degradation enhancing alpha-mannosidase like protein 1 (Edem1)*, *Derlin 3 (Derl3)* and *Creld2* [10, 24]. Further,



it was shown that for full activation of this UPR branch, nAtf6 α dimerises and induces gene expression with the transcription factor spliced X-box binding protein 1 (sXbp1) [25]. Overexpression of Creld2 in NIH3T3 fibroblasts triggers a selective up-regulation of the ER stress-inducible gene *Chop* and an increase of *Xbp1* splicing, while other ER stress-related genes, such as *Grp78*, *Atf6 α* or *Gadd34* remained unaltered in expression levels [2].

1.4.3 The Ire1 α pathway

For the activation of Ire1 α and induction of its downstream target genes, Ire1 α undergoes dimerisation and trans-autophosphorylation after detachment from Grp78 [26]. When active, Ire1 α exerts its endoribonuclease activity and splices *Xbp1* mRNA, which then results in the active transcription factor sXbp1 [27]. sXbp1 was shown to induce genes involved in protein folding [28] and ERAD [29]. However, as mentioned above, sXbp1 executes its functionality to a large extent in combination with nAtf6 α .

1.5 UPR signalling & disease

The UPR is an essential control machinery for virtually all cells in an organism since every living cell requires a homeostatic metabolism involving the synthesis, proper folding, potential secretion of proteins as well as an accurate sensing of non-native proteins. If the quality control is impaired either in recognising ER stress or in eliciting the appropriate responses, the cells' metabolism will eventually become imbalanced

Figure 1.2 (preceding page): Overview of the unfolded protein response. ER stress sensors Atf6 α , Ire1 α and Perk are bound and inactivated by Grp78 under non-stressed conditions. When unfolded proteins accumulate in the ER causing ER stress, Grp78 dissociates from the ER stress sensors to assist in folding, thereby leading to activation of these sensors. (From left to right) Activation of Atf6 α leads to its translocation to the Golgi-apparatus where it is proteolytically cleaved, releasing the active transcription factor nAtf6 α . Subsequently, nAtf6 α induces gene expression of chaperones (e.g. *Grp78* and *Grp94*), components of the ERAD machinery (e.g. *Edem1* and *Der13*), *Creld2* and *Chop*. Grp78 dissociation from Ire1 α triggers Ire1 α dimerization and trans-autophosphorylation initiating its endoribonuclease activity. Ire1 α splices *Xbp1* resulting in the active transcription factor sXbp1, which induces gene expression of various ERAD machinery components. Perk dimerises and trans-autophosphorylates after Grp78 detachment. Active Perk inactivates eIF2 α by phosphorylation leading to attenuation of global protein synthesis resulting in selective translation of Atf4, which induces *Gadd34* and *Chop* gene expression. Gadd34 reverts inhibition of eIF2 α by dephosphorylating it.

leading to aberrant or senescent regulation of metabolic processes and result in apoptosis, eventually. Numerous implications connect impaired UPR signalling to aberrant metabolic states and diseases [13, 30, 31].

Major metabolic abnormalities of altered UPR signalling are diabetes type I and II, hepatosteatosis and impaired fatty acid metabolism [17, 32]. Primarily, this is accounted to the fact that the three UPR branches not only induce transcriptional programs explicitly directed to the elimination of ER stress but simultaneously drive expression of important metabolic regulators. Atf4 and sXbp1 are reported to control the expression of genes involved in cholesterol and triacylglycerol metabolism [33, 34]. Although Ire1 α full-knockout mice are embryonically lethal [35], hepatocyte-specific Ire1 α ablation leads to severe steatosis [36], which is consistent with the sXbp1 phenotype. Similar phenotypes are also observable for impairments in the Atf6 α branch. Atf6 α -knockout mice display fatty liver development and dysregulated expression of several lipid metabolism master regulators after challenge with the ER stressor tunicamycin (Tm) [15]. Furthermore, Atf6 α -knockout mice were found to be glucose intolerant and to develop liver steatosis after challenge with a high-fat diet (HFD) [37], and it was suggested that Atf6 α impedes hepatosteatosis by enhancing fatty acid β -oxidation via regulation of *peroxisome proliferator-activated receptor α* (Ppar α) gene expression [38].

Other diseases associated with impaired UPR involve the innate immune system and bone growth. sXbp1 was reported to be an important transcription factor for plasma B cell differentiation [39] and the development and viability of dendritic cells [40]. Furthermore, it was shown that chondrocyte differentiation is inhibited in conditions of unresolved ER stress, which leads to Schmid metaphyseal chondrodysplasia (MCDS), a pathological condition characterised by dwarfism due to arrested or aberrant bone growth [41, 42].

1.6 Glucose & Lipid metabolism and non-alcoholic fatty liver disease

The food that we eat contains, besides other molecules, carbohydrates and lipids. Once the food is digested, carbohydrates and lipids enter into the bloodstream inducing the secretion of insulin by the pancreas. The signalling molecule insulin promotes the uptake of glucose into cells and therefore is crucial for controlling the blood glucose level. The other key player is glucagon, which stimulates the release of glucose into the blood in conditions of starvation. The liver is the most sensitive organ to glucagon. It is the primary site of glycogen storage due to its capability of trapping large amounts of glucose and converting it to glycogen. These reserves can be mobilised rapidly through conversion to glucose in states of low blood sugar levels.

Glucose is used for adenosine triphosphate (ATP) synthesis via the glycolysis pathway, where glucose is converted to pyruvate, which then is converted to acetyl-coenzyme A (CoA) to be completely oxidised in the citric acid cycle (CAC) (Figure 1.3).

Dietary lipids are transported in the bloodstream by lipoprotein vesicles. The contained lipids are either absorbed by the liver, transported to adipose tissue for storage or to the muscles, where lipids are oxidised for energy production. In adipocytes, lipids are stored as triacylglycerides (TAGs). One TAG molecule is composed of one glycerol and three fatty acids (acyls). When liver glycogen stores are deprived, TAG stores from adipose tissue are mobilised via lipolysis and secreted to the bloodstream as glycerol and free fatty acid (FFA) to serve as energy source for other organs. Glycerols are taken up by the liver and converted to pyruvate via glycolysis or to glucose via gluconeogenesis. FFAs can be taken up by organs and activated by linking the fatty acid to CoA to produce acyl-CoA, which then can be degraded by β -oxidation. Each round of β -oxidation generates one acetyl-CoA, which can enter the CAC to generate ATP. However, acetyl-CoA can only enter the CAC after condensation with oxaloacetate, which is a glucose metabolite produced during glycolysis. When glucose levels are low, e.g. during starvation or in untreated diabetes, lipolysis increases, FFAs are released and β -oxidation predominates for ATP synthesis. Severe hypoglycemia results in the production of excess acetyl-CoA in the liver, which exceeds

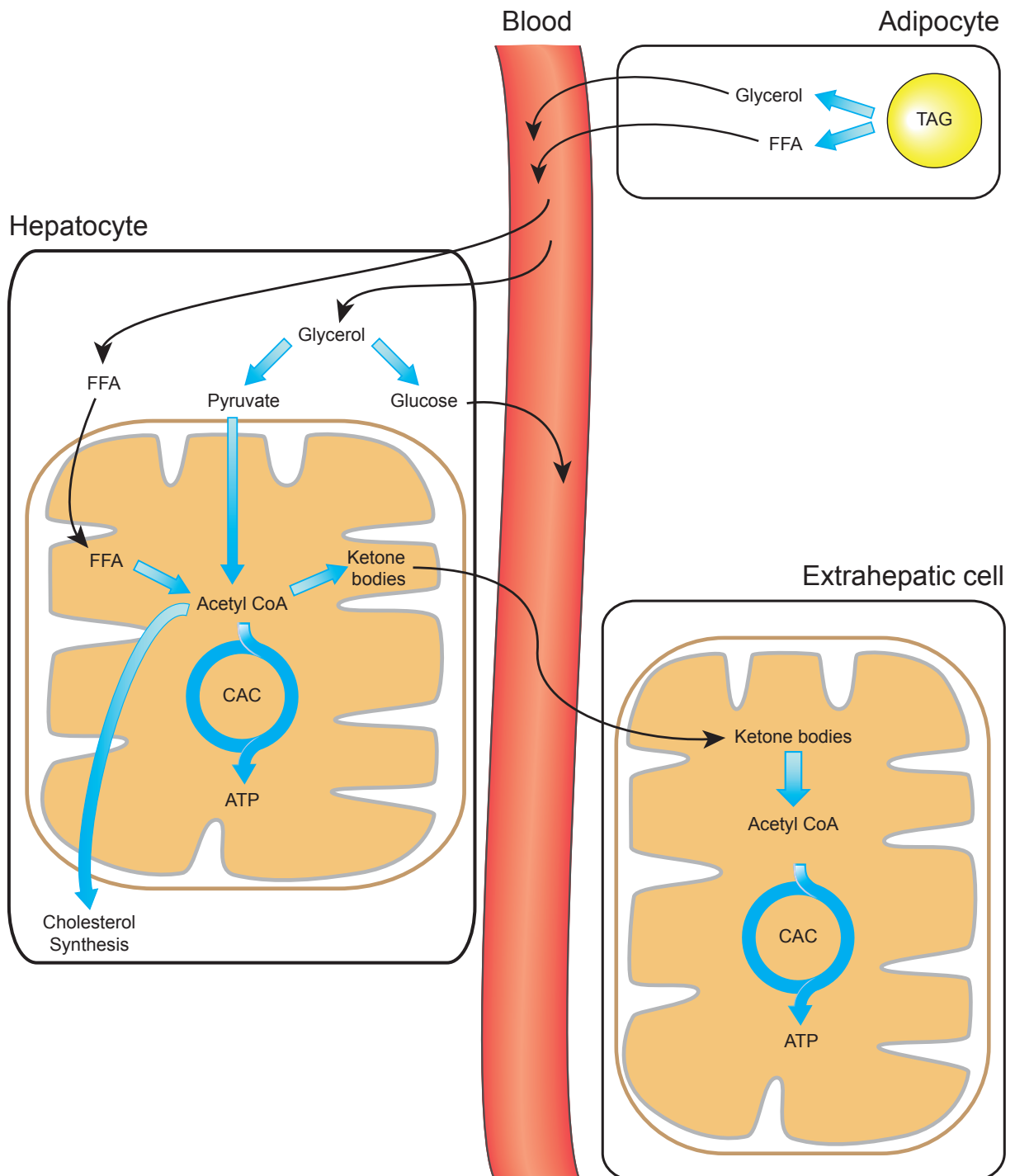


Figure 1.3: Overview of fatty acid metabolism. Lipolysis of TAGs in adipocytes results in the release of glycerol and FFAs into the bloodstream. These are taken up by the liver. Glycerols are either converted to pyruvate, which enters the CAC in the form of acetyl CoA, or to glucose and secreted into the bloodstream for usage by extrahepatic cells. FFAs are oxidized producing acetyl CoAs, which are used for ATP synthesis in the CAC. Excess acetyl CoA are either converted to ketone bodies for usage as fuel source by extrahepatic tissues or can serve as fundamental building blocks in cholesterol synthesis. Figure modified from "Biochemistry" by Stryer et al. [43].

the capacity to be oxidised in the CAC. This is due to the liver consumption of oxaloacetate for gluconeogenesis to maintain constant blood glucose levels, thereby

depriving the required molecule for further acetyl-CoA degradation. In this condition, the liver converts acetyl-CoA to acetoacetate or β -hydroxybutyrate, which are collectively termed ketone bodies. These ketone bodies are water soluble and released by the liver into the blood. Ketone bodies diffuse through membranes and can be utilised by extrahepatic organs as a fuel source, whereas the liver cannot use them for ATP synthesis because it lacks an enzyme to activate ketone bodies.

Acetyl-CoA plays a further important role in the synthesis of cholesterol because it is the building blocks of cholesterols. Cholesterols are esterified for storage or incorporated into the plasma membrane in its unesterified form.

Non-alcoholic induced fatty liver disease (NAFLD) is characterised by the accumulation of a significant amount of fatty acids, mostly TAGs, in hepatocytes and can be caused by multiple factors. Nowadays, the leading causes of NAFLD are obesity and diabetes type II. The pathogenesis of NAFLD involves a broad range of dysregulation in glucose and lipid metabolism and, if untreated, NAFLD can progress to steatohepatitis, fibrosis and cirrhosis [44, 45]. *Creld2* was observed to be upregulated in NAFLD induced mice by feeding of an HFD [46]. Additionally, epigenome-wide association studies (EWAS) in obese people found that CpG islands in the *CRELD2* locus are methylated. Thus *CRELD2* transcription is inhibited [47, 48], suggesting a potential role of *CRELD2* in lipid metabolism.

Initial phenotypic analyses of the *Creld2* full-knockout-mouse revealed that 1-year-old *Creld2*^{-/-} mice develop NAFLD, visible as excessive staining intensities in histological oil-red-O stainings, which stain lipids in red (Figure 1.4). Furthermore, mice livers revealed aberrant expression of genes important for glucose and fatty acid metabolism.

1.7 Bone structure, growth and remodelling

The body's skeleton is composed of bones, a solid yet very dynamic type of connective tissue that enables locomotion, which serves as a protection for internal organs and is the major site of hematopoiesis. Bones come with distinct shapes and sizes depending on their specific function in the body. However, besides this variety of different bones, there are only two ways of bone formation resulting in the same bone tissue.

Flat bones are formed through intramembranous ossification, while long bones

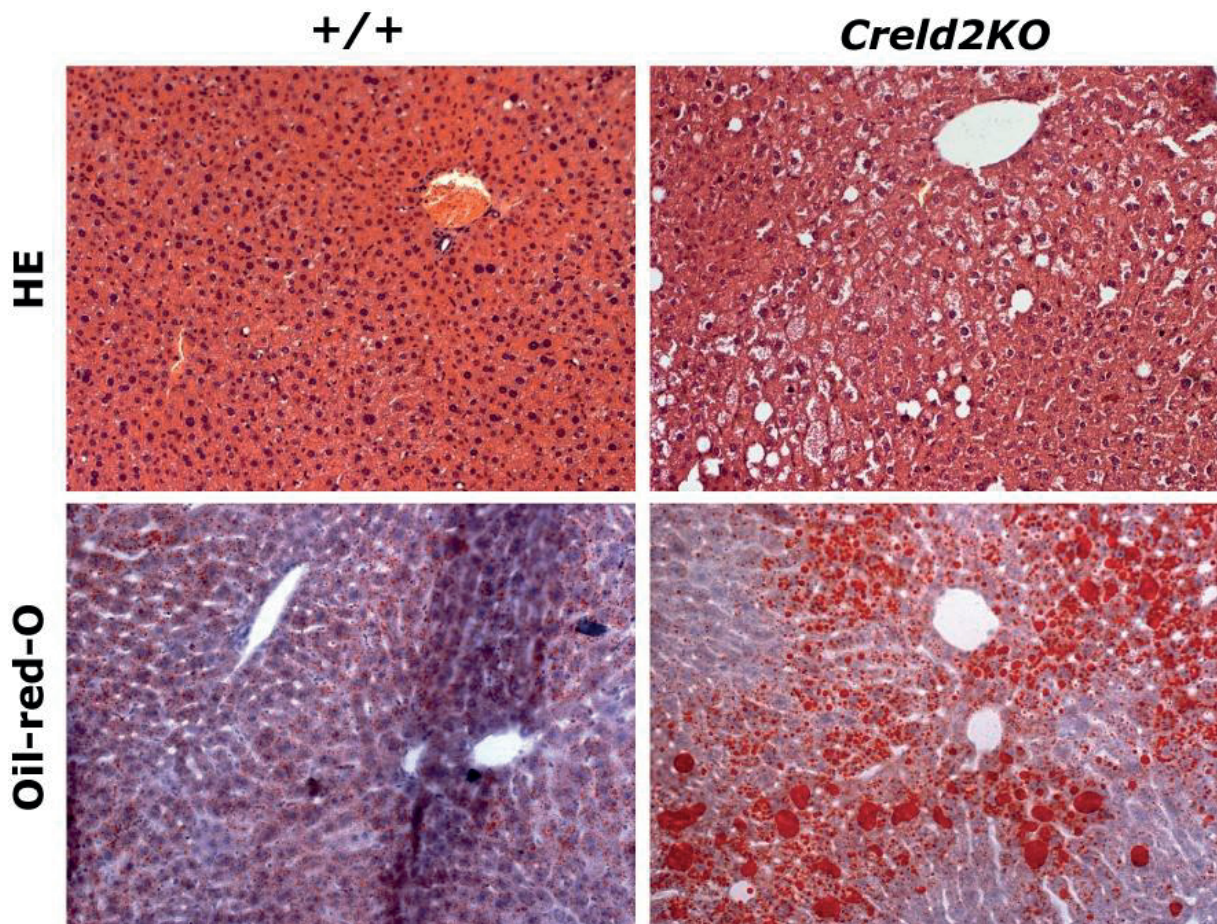


Figure 1.4: Histological analysis of *Creld2KO* liver sections. One year old *Creld2KO* animals suffer from liver steatosis, which is visualised by a hematoxylin/eosin (HE) staining. Cells in the area around the vessel harbor vesicles that were identified as lipid droplets using an Oil-red-O staining. Figure and figure caption reprinted from Mass, 2013 [2].

are formed via endochondral ossification. The main difference between these two ways of bone formation is that in intramembranous ossification bone is formed directly from mesenchymal connective tissue, whereas during endochondral ossification, mesenchymal stem cells (MSCs) first differentiate into chondrocytes, which then provide the necessary ossification precursor cells for long bone formation. Thus, endochondral bone formation involves the continuous supply of cartilage by chondrocytes, which is replaced by bone tissue, afterwards. The continuous cartilage supplies enable the bone to grow in length.

Long bones can be separated into three zones. The epiphysis, metaphysis and diaphysis. The epiphysis is located at each end of the long bone and consists of trabecular or spongy bone, a bone structure characterised by its porous appearance. The metaphysis is a narrow bone region located between the epiphysis and the

diaphysis and harbours the epiphyseal growth plate, which is responsible for longitudinal bone growth. The diaphysis is the midsection of a long bone and makes up the largest portion. It is a hollow shaft, called medullary cavity, which is surrounded by cortical or compact bone. The medullary cavity is innervated by blood vessels, which carry osteogenic cells. The medullary cavity is the storage and synthesis site for bone-marrow (Figure 1.5a).

The crucial part for bone growth in the metaphysis is the epiphyseal growth plate comprising a set of proliferating chondrocytes, which are responsible for longitudinal bone growth (Figure 1.5b). The growth plate is divided into four zones. Adjacent to the epiphysis is the reserve zone, where quiescent chondrocytes are situated within a cartilage matrix. In the direction of the diaphysis, this layer is followed by the proliferative zone, which consists of strongly proliferative chondrocytes. Chondrocytes produced by mitotic proliferation are displaced toward the diaphysis and are constituents of the third layer, the maturation and hypertrophy zone. Here, chondrocytes become larger as they mature and travel closer and closer to the diaphysis. The zone of calcification is following the maturation layer and is the layer where chondrocytes go into apoptosis because the cartilage matrix starts to calcify. As the ossification layer is pushed closer to the diaphysis due to the dividing chondrocytes in the proliferative zone, the calcified chondrocyte tissue is innervated by blood vessels and osteoblasts. Osteoblasts are bone-producing cells, which replace the calcified matrix by bone tissue. Eventually, proliferation of chondrocytes in the epiphyseal growth plate stops and the growth plate is replaced by trabecular bone tissue.

Trabecular bone in the epiphysis is constantly remodelled due to an interplay between bone forming osteoblasts and bone reabsorbing osteoclasts. The process of bone formation and resorption is tightly regulated. In principle, osteoclasts are activated by osteoblasts, which secrete signalling molecules that induce osteoclastic bone resorption. Vice versa, osteoclasts activate osteoblasts during the process of bone resorption to ensure subsequent bone renewal (Figure 1.5c). Aberrant osteoblast or osteoclast function leads to pathologies, such as osteoporosis, which is the reduction of bone mass, or osteopetrosis, the increase of bone mass (Figure 1.5d) [49].

Creld2 analyses in models of multiple epiphyseal dysplasia (MED) suggest that

Cred2 interacts with non-native cartilage extracellular matrix (ECM) proteins in a substrate-specific manner. It was further proposed that Cred2 exhibits protein disulfide isomerase (PDI)-activity and thereby assists in the folding of these ECM proteins [50]. Furthermore, Cred2 was suggested to augment bone formation by enhancing expression of bone morphogenic protein 9 (BMP9) downstream targets, which are important for osteogenic differentiation of MSCs [51].

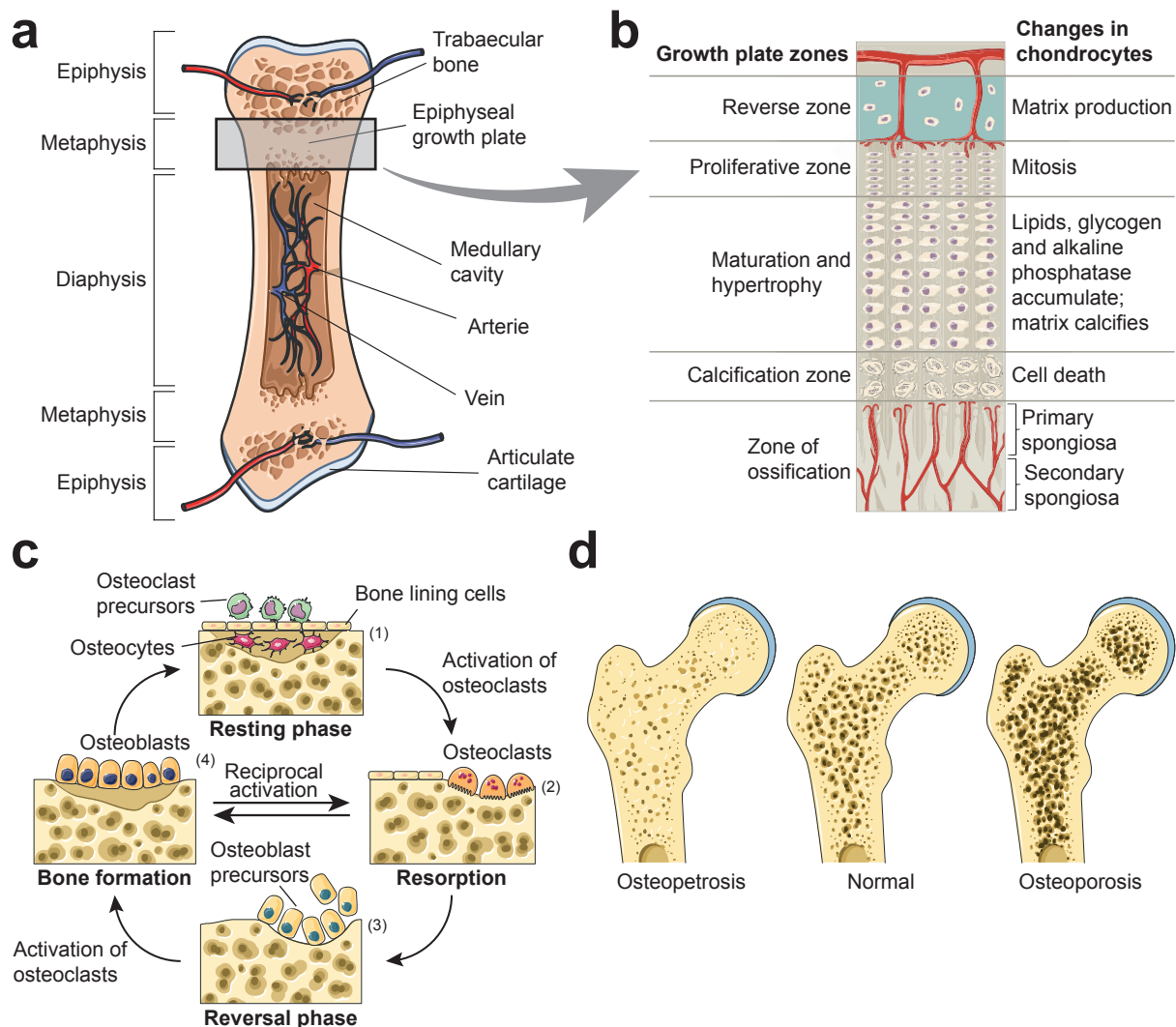


Figure 1.5: Long bone growth and structure. (a) Separation of long bones into the epiphysis, metaphysis and diaphysis. (b) Detailed depiction of the epiphyseal growth plate. **Left:** Growth plate zone classification. **Right:** Changes induced in differentiating chondrocytes in the respective growth plate zones. (c) Regulation of bone remodelling by osteoblasts and osteoclasts. Reciprocal activation of osteoblasts and osteoclasts by released factors during bone formation and resorption, respectively. (d) Defects in bone remodelling cells can result in increased bone density (Osteopetrosis, left) or reduced bone mass and bone (Osteoporosis, right) compared to normal bone structure (center). Figures in (a), (c) and (d) were adapted and modified from Smart Servier [52]. Figure in (b) was adapted and modified from Schatz, 2016 [53].

1.8 Aim of the thesis

Although *Creld2* was identified nearly 20 years ago, only little is known about its physiological or molecular function. In this work, the role of *Creld2* under steady state as well as stress conditions was investigated *in vivo* and *in vitro* utilising a *Creld2*^{-/-} mouse model and *Creld2*^{-/-} mouse embryonic fibroblasts (MEFs), respectively.

2 Materials

2.1 Equipment

Table 2.1: Equipment

Equipment	Company/ Model
Agarose gel electrophoresis chamber	Thermo scientific Owl Electrophoresis Systems B2
Autoclave	H+P Varioklav Dampfsterilisator EP-2
Bacteria incubator	Innova 44 NEW Brunswick scientific
Balances	Sartorius BL 150; Sartorius B211 D
Binocular	Zeiss Stemi 2000
Centrifuges	5415R/5424 Eppendorf; Avanti J-26 XP Beckman Coulter; Biofuge primo R Heraeus; Rotina 420 R
Cryostat	Leica
Electro pipette	Accu Jet
Electroporator	Biorad Gene Pulser Xcell
Embedding carousel	Leica TP 1020
Gel documentation	Benda Biostep Dark Hood DH-40/50
Incubators/shaker	Heiz Thermo Mixer MHR13 HLC (Memmert); Innova 44 NEW Brunswick scientific
Microplate reader	Tecan Infinite 200 Pro
Microwave	Panasonic
Photometer	Nano Drop 2000 PeqLab;
Power supply	Pover Pac HC BioRad
Radiographic cassettes	Radiographic Products
RealTime PCR thermo cycler	CFX96 BioRad
Thermo cycler	C1000 Thermal Cycler BioRad

Table 2.1: continued from previous page

Equipment	Company/ Model
Turbo-blotter	BioRad Tans-Blot Turbo Transfer System
Vortexer	Vortex Genie2
Water bath	Jubalo SW22
Western blotting equipment	Biorad
X-ray film developer machine	Curix 60 AGFA

2.2 Consumables

Table 2.2: Consumables

Consumables	Company
1.5/ 2 ml reaction tubes	Eppendorf
Cover slips	VWR
Electroporation cuvettes 0.4 cm	Biorad
Embedding cassettes	Simport
Immobilon PVDF membrane	Merck
Microscope slides	VWR
PCR reaction tubes	Sarstedt
Plastic wares	Greiner
Protein purification columns	BioRad Micro Bio-Spin Columns 0.8 ml
PVDF membrane	Millipore Immobilon-P Transfer membranes 0.45 μ m
Superfrost Plus adhesive microscope slides	Thermo scientific
Syringes	BBraun Injekt-F
Tissue-Tek	Sakura
TLC plates	Millipore HPTLC Silica gel 60
X-ray films	Fuji Medical X-Ray Film Super RX

2.3 Chemicals & solutions

Table 2.3: Chemicals

Chemical	Company
Crystal violet	Roth
Eosin	VWR
Fetal calf serum	PAN-Biotech
Hematoxylin	VWR
Oil-red O	Sigma
Paraffin	Medim-Plast
Penicillin/Streptomycin	Invitrogen
Thapsigargin	Sigma
Tissue-Tek	Sakura
Trypsin	Sigma
Tunicamycin	Sigma

2.4 Standards and Kits

Table 2.4: Standards and Kits

Name	Company
2-Log DNA ladder, 1 kb DNA ladder	NEB
Complete Protease Inhibitor Cocktail tablet	Roche
DAPI-Fluoromount G	Biozol
ECL Western Blotting Substrate	Pierce
FLAG M2 Affinity Gel	Sigma-Aldrich
Flag peptide	Sigma-Aldrich
Fluorescence microscope	Zeiss AxioCam MRm; Olympus SZX 12
iQ TM SYBR Green Supermix	BioRad
Masson-Goldner trichrome staining kit	Merck
Microtome	Leica RM2255
NBT/BCIP stock solution	Roche

Table 2.4: continued from previous page

Name	Company
Nova Red	Vector Laboratories
Nucleic Acid & Protein Purification, NucleoBond, PC 100	Macherey & Nagel
Nucleic Acid & Protein Purification, NucleoSpin, RNAII	Macherey & Nagel
NucleoSpin Gel and PCR Clean-Up	Macherey & Nagel
NucleoSpin RNA XS	Macherey & Nagel
NucleoSpin RNA/Protein	Macherey & Nagel
PCR Nucleotide Mix	Roche
Pierce BCA protein Assay kit	Thermo scientific
Precision plus Protein All Blue Standards	BioRad
QuantiTect, Reverse Transcription Kit	Qiagen
Ready-to-use System for fast Purification of Nucleic Acids, NucleoSpin, Extract II	Macherey & Nagel
Strep-Tactin Sepharose	IBA
Tissue homogenizer	Precellys Peqlab

2.5 Bacterial strains

Table 2.5: Bacterial strains

Strain	Genotype	Origin
DH5 α	F- φ 80/ <i>lacZ</i> Δ M15 Δ (<i>lacZYA-argF</i>)U169 <i>deoR recA1</i> <i>endA1 hsdR17</i> (r _K ⁻ , m _K ⁺) <i>supE44</i> <i>gyrA96</i> (Nal ^r) <i>thi-1 relA1</i>	Stratagene

2.6 Buffers & solutions

Table 2.6: Buffers

Buffer/Solution	Recipe
Agarose	1–2.5 % agarose (w/v) in TAE
Ammonium persulfate (APS)	10 % APS

Table 2.6: continued from previous page

Buffer/Solution	Recipe
Ampicillin (−20 °C) 1000x stock	50 mg/ml Ampicillin
Blocking solution	5 % skim milk powder in TBST
Decalcifying solution	14 % EDTA, 3 % Ammonium Hydroxyde, pH 7.1 in ddH ₂ O
Fixation solution	freshly prepared 4 % MeOH-free Formaldehyde (PFA) in DPBS
Flag elution buffer	200 µg/ml Flag peptide in TBS (1x)
Flag peptide stock (−80 °C)	5 mg/ml Flag peptide in TBS (1x)
Glycerine jelly mounting medium	10 g Gelatin, 60 ml ddH ₂ O, 70 ml Glycerol, 0.25 g Phenol
Laemmli loading buffer (1x)	2 % SDS, 2 µM Dithiothreitol (DTT), 5 % (v/v) Glycerol, 50 µM Tris-HCL (pH 6.8), 0.01 % (w/v) Bromophenol blue
Laird buffer	0.1 M Tris (pH 8.0), 0.2 % SDS, 0.2 M NaCl, 5 µM EDTA
Lysozyme (−20 °C)	10 mg/ml in TE-buffer
Oil-red O stock solution	0.5 % Oil-red O in isopropanol
Oil-red O working solution	30 ml Oil-red O stock solution in 20 ml ddH ₂ O
PBS (20x)	4 g KCl, 160 g NaCl, 28.6 g Na ₂ HPO ₄ , 4 g KH ₂ PO ₄
PBST	0.1 % Tween20 in PBS (1x)
Proteinase K stock (−20 °C)	20 mg/ml in DEPC
SDS	10 % SDS
SDS-PAGE running buffer (10x)	250 µM Tris-HCL, 1.92 M Glycine, 1 % SDS
TAE buffer	40 µM Tris-Acetate (ph 8.0), 1 µM EDTA

Table 2.6: continued from previous page

Buffer/Solution	Recipe
TAP-elution buffer	50 μ M Desthiobiotin in TBS (1x)
TAP-lysis buffer	For 10 ml: 1 ml TBS (10x), 200 μ l Complete Protease Inhibitor Cocktail (50x), 100 μ l Phosphatase Inhibitor Cocktail (PIC) I and II, 50 μ l NP40, 8.55 ml H ₂ O
TAP-wash buffer	For 10 ml: 1 ml TBS (10x), 100 μ l PIC I and II, 10 μ l NP40, 8.79 ml H ₂ O
TBS (10x)	5.6 g Tris-base, 24 g Tris-HCl, 87.8 g NaCl in 1000 ml of H ₂ O, pH 7.5
TBST	0.1 % Tween20 in TBS (1x)
TE buffer	10 μ M Tris-HCL (pH 7.5), 0.15 M NaCl, 0.05 % Tween20
Transfer buffer	30.3 g Tris, 144.2 g Glycine in 1 l H ₂ O

2.7 Media

Table 2.7: Media for bacterial culture

Medium	Recipe
LB-medium	10 g NaCl, 10 g tryptophan, 5 g yeast extract, add 1 l of H ₂ O (pH 7.0)
LB-ampicillin medium	LB-medium with 50 μ g/ml ampicillin
LB-kanamycin medium	LB-medium with 25 μ g/ml kanamycin
LB-ampicillin agar	LB-medium with 20 g agar and 50 μ g/ml ampicillin
LB-kanamycin agar	LB-medium with 20 g agar and 25 μ g/ml kanamycin

Table 2.8: Media for cell culture

Cell line	Recipe
Hek293, MEFs	10 % Fetal calf serum, 1 % Penicillin/Streptomycin in DMEM

2.8 Antibodies

Table 2.9: Antibodies

Antibody	Conjugate	Species	Method (dilution)	Company
Akt	–	rab	WB (1:1000)	Cell Signaling
β -Actin (AC-15)	–	mouse	WB (1:5000)	Novus Biologicals
CD117 (c-KIT) (2B8)	PE or APC Cy7		FACS (1:100)	Biolegend
CD11b (M1/70)	PE or PE Cy7		FACS (1:100)	BD Pharmingen
CD150 (TC15-12F12.2)	PE Cy7		FACS (1:100)	Biolegend
CD16/32 (2.4G2)	Uncoupled		FACS (1:100)	BD Pharmingen
CD19 (1D3)	BV711		FACS (1:100)	BD Pharmingen
CD3 (145-2C11)	PE		FACS (1:100)	Biolegend
CD335 (NKp46) (29A1.4)	PE		FACS (1:100)	ebioscience
CD45 (30-F100)	AF780		FACS (1:100)	ebioscience

Table 2.9: continued from previous page

Antibody	Conjugate	Species	Method (dilution)	Company
CD48 (HM48-1)	APC		FACS (1:100)	Biolegend
Chop (L63F7)	–	mou	WB (1:500)	Cell Signaling
Creld2 (G-17)	–	rab	WB (1:750)	Santa Cruz
eIF2 (9722)	–	rab	WB (1:1000)	Cell Signaling
F4/80 (2M8)	eF450 or APC or BV605		FACS (1:100)	eBioscience
Flag M2	–	mouse	WB (1:500)	Sigma
Gadd34 (H-193)	–	rab	WB (1:400)	Santa Cruz
GFP	–	rab	WB (1:300)	Santa Cruz
Gr1 (RB6-8C5)	e450 or FITC or PE		FACS (1:100)	BD Pharmingen
Grp78	–	rab	WB (1:2000)	StressMarq Biosciences
Hoechst 33258	–		FACS (1 µg/ml)	Invitrogen
Ly-76 (Ter119)	BV650 or PercP		FACS (1:100)	BD Pharmingen
Mouse	HRP	Donkey	WB (1:15000)	Santa Cruz

Table 2.9: continued from previous page

Antibody	Conjugate	Species	Method (dilution)	Company
Perk (C33E10)	–	rab	WB (1:750)	Cell Signaling
Phospho-Akt (S473) (D9E)	–	rab	WB (1:750)	Cell Signaling
Phospho-eIF2 (Ser51) (D9G8)	–	rab	WB (1:500)	Cell Signaling
Phospho-Perk (T980) (16F8)	–	rab	WB (1:500)	Cell Signaling
Rabbit	HRP	Donkey	WB (1:15000)	Santa Cruz
Sca1 (D7)	BV421		FACS (1:100)	BD Pharmingen
Tim4 (RMT4-54)	AF647		FACS (1:100)	Biologend

2.9 Plasmids

Table 2.10: Plasmids used

Plasmid	Source
pcDNA3.1Zeo+	AG Hoch (T. Krsmanovic)
FS-C2 in pcDNA3.1Zeo+	P. Kern
C2-SF in pcDNA3.1Zeo+	P. Kern
SF-mock in pcDNA3.1Zeo+	P. Kern

2.10 Primer & gene blocks

2.10.1 Genotyping primer

Table 2.11: Primer for genotyping

Primer name	Primer sequence (5'–3')
Creld2 wt genotype fw	CCTGAGCTGTCCTTAGAAAGTTGCTAG
Creld2 ko genotype fw	GCCCGACAACCACTACCTGAGC
Creld2 genotype rev	GGGGTTCATGTCCATGGGCCAC

2.10.2 Cloning primer

Table 2.12: Primer for cloning

Primer name	Primer sequence (5'–3')
NheI-Kozak-mC2-SF-tag fw	CTAGCTAGCGCCACCATGCACCTGCTGCTTGCA
Creld2-KpnI	TATGGTACCTCACAAATCCTCACGGGAGGG
KpnI-Flag rev	TAGGGTACCTCACTTGTCGTCGTC
NheI-SF-tag fw	CTAGCTAGCATGGGTGGAGGTTCTGGA
KpnI-SF-tag rev	GGAGCTCTGGATGGTACCTCACTTGTC

2.10.3 qRT-PCR primer

Table 2.13: Primer for quantitative real time PCR

Gene	Forward primer (5'–3')	Reverse primer (5'–3')
Acox1	GCCTTTGGACCTTCACTTGG	GATGAGTTCCATGACCCATCT CT
Apcs	TGTGGGACTATGTGCTGACC	ATCTCAATCCCAGACACGGG
ApoB100	GGAATCCCCCAGATGGTTGT	ACTCCAGACGAGGACACTTG
Apoc2	GCTTTGTTGGCCAGGACTTT	TGTCTGGGACCTGAATGTAGT G
Atf6	AATGGGGCCCTCCTCAGGGG	GGGCCTGTGCTAGCGCACAA
Chop	TCACCTCCTGTCTGTCTCTCC	TACCCTCAGTCCCCTCCTC
Creld2	GGCTACACCAAGGAGAGTGG	GGACACACGCACACGAAG
Derl1	GAAACCTTGTCGGCCATCTT	GGTAGCCAGCGGTACAAAAA
Derl2	TTCTAAACTTCCAGGCCCCC	CTGCAATACCCAAAAGGTCCA
Derl3	CTTCGTGTTCCGCTACTGC	CCAGGAATCCCAGCAGAGT

Table 2.13: continued from previous page

Gene	Forward primer (5'–3')	Reverse primer (5'–3')
Dgat1	TCAAGGCCAAAGCTGTCTCTA	AGGTCAGGTTGTCTGGATAG C
Dgat2	TATCCTTCCTGGTGCTAGGAG T	CTTTCTTGGGCGTGTTCCAG
Dr5	AAAAGAGGCTGTGAACGGGA	GCTAGATGTCTGTCCGGTCCA
Edem1	GGTCTTCGAAGCTACGATAAG G	GGGCTGTTTGGAAATCAGTTAT TA
Edem2	ACTACAGGGAGCGAGTCAAG	GTCCAGGGCATCAATTAGCG
Edem3	GATGGGAAGGACACAGACGA	TCCATTTCCGGATCTCGGTC
Erk1	GATCCGACAGATGAGCCAGT	ATCCAAAAGGACAGGGGTGT
Erk2	CCCAAGTGATGAGCCCATTG	ACACCGACATCTGAACTCGT
Fit2	GCAACGTCCTCAACGTGTATT	AGGTGGTAGTTGGTAAGGGC
Fsp27	TCATGAGGTGTGCGAGAGAG	GCATTCCCTAAGGTCCCTCC
Gadd34	ACGATCGCTTTTGGCAAC	GACATGCTGGGGTCTTGG
GFP	TGAGCAAAGACCCCAACGA	CGTCCATGCCGAGAGTGAT
Glut2	GGGACTTGTGCTGCTGGATA	AATTGCAGACCCAGTTGCTG
Glut4	CCGAAAGAGTCTAAAGCGCC	GCTCTCTCTCCAACCTCCGT
Grp78	CGACAAGCAACCAAAGATG	CCAGGTCAAACACAAGGATG
Grp94	GCGGCGGATTAAGGAAGATG	TACGCCTTGGTGTCTGGTAG
Hprt	TCCCAGCGTCGTGATTAGCG ATGA	AATGTGATGGCCTCCCATCTC CTTCATGACAT
Il1b	AGCTTCCTTGTGCAAGTGTC	TCTTTTGGGGTCCGTCAACT
Il6	GTGGAAATGAGAAAAGAGTTG TGC	GTTTTCTGCAAGTGCATCATC G
Ire1a	TGCTGAAACACCCCTTCTTC	CTCCCGCCTCTCTCCAAC
Lsr	TTGGCAGGACCTCAGAAGC	CCACAAAGAGCCAATCTTCCA A
Perk	CGGGACAAGTAGGGACCAAG	GGTGCTGAATGGGTAGAGGA G
Pgc1a	GTGTGCTGTGTGTCAGAGTG	ACCAGAGCAGCACACTCTATG
Pgc1b	AACTTCAGACGTGAGAGCAG A	TATACCACACGGCCTTCACC
Plin2	CGGTTGCCAATACCTATGCC	CACTGGCAACAATCTCGGAC

Table 2.13: continued from previous page

Gene	Forward primer (5'–3')	Reverse primer (5'–3')
Ppara	CATTTGGGCGTATCTCACCG	AACTTCAACTTGGCTCTCCTC T
Ppia	GCGTCTCCTTCGAGCTGTT	AAGTCACCACCCTGGCA
Saa3	AAGTCATCAGCGATGCCAGA	ACTGGTCAGCTCTTGAGTCC
sXbp1	CTGAGTCCGCAGCAGGT	CCAAGTTGTCCAGAATGCCC
Tnf	GCCCACGTCGTAGCAAAC	GGAGTAGACAAGGTACAACC CA

2.10.4 Gene blocks

Table 2.14: Gene blocks used for cloning

Gene block	Sequence (5'–3')
N-term FS-C2	CTAGCTAGCGCCACCATGCACCTGCTGCTTGCAGCCGC GTTTCGGGCTGCTGCTGCTGCTGCCGCCGCCCGGGGCC GTAGCCGACTACAAGGACGACGACGACAAGGGCGCCA GCGGCGAGTGGAGCCACCCCCAGTTCGAGAAGGGAGG TGGATCAGGCGGTGGATCTGGTGGAGGTTCTGGTTCG CATCCACAATTTGAAAAGGGTGGAGGTTCTGGAGGTGG TTCAGGAGGAGGTAGTTCCCGGAAGCCGACGATGTGCC AGAGATGCCGGACGCTGGTGGACAAGTTCAACCAGGG GATGGCCAACACGGCCAGGAAGAATTTCCGGTGGCGGC AACACGGCGTGGGAAGAGAAGACGCTGTCTAAGTACGA ATTCAGTGAGATCCGGCTTCTGGAGATCATGGAGGGTC TG

Table 2.14: continued from previous page

Gene block	Sequence (5'–3')
C-term C2-SF	GAAAAAGCCTGTAAGAGGAAAAACGAAAAGCTGCTACAA TGTTCCGGGGAGCTTCGTGTGCGTGTGTCCGGAAGGCT TTGAGGAGACAGAAGACGCTTGTGTGCAGACAGCAGAA GGCAAAGTCACAGAGGAAAACCCACACAGCCACCCTC CCGTGAGGATTTGGGTGGAGGTTCTGGAGGTGGTTCAG GAGGAGGTAGTTGGAGCCACCCCCAGTTCGAGAAGGG AGGTGGATCAGGCGGTGGATCTGGTGGAGGTTCCCTGG TCGCATCCACAATTTGAAAAGGGCGCCAGCGGCGAGGA CTACAAGGACGACGACGACAAGTGAGGTACCGAGCTCG GATCCACTAGTCCAGTGTGGTGGGTCTAGAGGGCCC

3 Methods

3.1 Histological stainings

3.1.1 Preparation of organ samples for histological analysis

For histological staining, organs were fixed in fixation solution for 24 h at 4 °C. Subsequently, fixed organ samples were embedded either in Paraffin or processed for cryo-sectioning. Embedded tissue samples were sectioned at 10 µm depth.

3.1.2 Preparation of bone samples for histological analysis

Whole bones were fixed in fixation solution for 72 h at 4 °C with constant agitation. After fixation, bones were washed twice in PBS for 10 min. Subsequently, bones were decalcified in decalcifying solution for 96 h at 4 °C with constant agitation. Decalcified bones were washed twice in PBS for 10 min prior to paraffin or cryo embedding.

3.1.3 Paraffin embedding

Fixed organ samples were dehydrated in increasing ethanol concentration series (70 %, 70 %, 80 %, 80 %, 90 %, 96 %, 100 %, 100 %) followed by incubating twice in xylol and twice in wax. Tissue samples were incubated for 1 h in each step.

3.1.4 Cryo embedding

Directly after fixation, tissue samples were incubated in 30 % sucrose solution at 4 °C for 24 h. Afterwards, tissue samples were embedded in Tissue-Tek freezing resin and stored at –20 °C for short-term or –80 °C for long-term storage.

3.1.5 Hematoxilin & Eosin staining

Prior to staining of tissue sections, samples were deparaffinized in xylol rehydrated in descending ethanol series (100 %, 100 %, 96 %, 90 %, 80 %, 70 %, 60 %). Afterwards, samples were stained in Hematoxylin solution for 3 min and rinsed in running tap water for 3 min, followed by staining in Eosin solution for 3 min with subsequent rinsing under tap water for 30 sec. Stained sections were dehydrated in increasing ethanol series (as mentioned above), cleared in xylol twice and mounted in Entellan.

3.1.6 Masson-Goldner Trichrome staining

Prior to staining of tissue sections, samples were deparaffinized in xylol rehydrated in descending ethanol series (twice in 100 %, 96 %, 90 %, 80 %, 70 %, 60 %). Subsequently, sections were stained in Hematoxylin for 5 min and rinsed for another 5 min under running tap water. Afterwards, samples were rinsed in 1 % acetic acid for 30 sec and incubated in Azophloxine solution for 10 min. Sections were rinsed again in 1 % acetic acid for 30 sec, stained in orange G solution for 1 min and rinsed another time in 1 % acetic acid for 30 sec followed by incubation in light green SF solution for 2 min. Samples were rinsed in 1 % acetic acid for 30 sec, dehydrated in ascending ethanol series, cleared twice in xylol and mounted in Entellan.

3.1.7 Oil-red O staining

Cryo-embedded tissue sections were let to dry on microscope slides, fixed with fixation solution and washed under running tap water for 5 min. Sections were rinsed in 60 % isopropanol and stained with freshly prepared Oil-red O working solution for 15 min prior to rinsing with 60 % isopropanol. Subsequently, samples were stained with hematoxylin by dipping the sections 5 times into the solution, rinsed with ddH₂O and mounted in glycerine jelly mounting medium.

3.2 Isolation of RNA

RNA was isolated either using the Nucleospin RNA II kit according to the manufacturer's protocol or, in case of limited sample amount, by cytoplasmic extraction of RNA. For the cytoplasmic extraction of RNA tissue or cell pellet was homogenized in 200 µl cytoplasmic RNA lysis buffer and incubated on ice for 10 min to lyse cells. Afterwards, the lysate was centrifuged for 10 min at 4 °C to sediment nuclei. The supernatant was recovered, SDS and proteinase K were added to a final concentration of 1% and 0.5 mg/ml, respectively followed by digestion at 37 °C for 3 h. After digestion of proteins, RNAs were extracted twice by adding 150 µl Phenol/Chloroform (1:1), centrifugation of the mixture for 10 min at RT and the upper aqueous phase was recovered. Subsequently, the harvested lysates were washed twice with 150 µl chloroform alone to remove potential phenol contaminations. The aqueous phase was

harvested and 15 μl of 3M NaOAc (pH 4.8–5.5) and RNA was precipitated O/N at $-80\text{ }^{\circ}\text{C}$ after addition of 500 μl absolute EtOH. Afterwards, the mixture was centrifuged for 15 min at $4\text{ }^{\circ}\text{C}$, the supernatant was discarded and the RNA pellet was dried shortly to eliminate EtOH contamination. Pure RNA was resuspended in 20–40 μl H_2O .

3.3 Reverse transcription of RNA into cDNA

cDNA was synthesized by reverse transcription of isolated RNA using Qiagen QuantiTect reverse transcription kit including rDNaseI treatment according to the manufacturer's protocol. Up to 500 ng of total RNA was used in a 10 μl reaction and filled up to 50 μl with aqua bidest after cDNA synthesis.

3.4 PCR techniques

Primer stock concentration for PCR was 100 pmol/ μl unless otherwise stated.

3.4.1 Genotyping PCR

Table 3.1: Genotyping PCR Protocol

Component	Volume / 20 μl reaction
H_2O	14.7 μl
5x GoTaq reaction buffer	4 μl
DNTPs	0.4 μl
Forward primer 1	0.1 μl
Forward primer 2	0.1 μl
Reverse primer	0.1 μl
DNA template	0.5 μl
GoTaq DNA polymerase (5 U/ μl)	0.1 μl

Table 3.2: Genotyping PCR program

Step	Temperature ($^{\circ}\text{C}$)	Time	Number of cycles
Initial denaturation	95	3 min	1
Denaturation	95	20 sec	30
Annealing	57	15 sec	
Extension	72	15 sec	
Final extension	72	5 min	1

Table 3.3: PCR Protocol *Creld2* cDNA amplification

Component	Volume / 20 μ l reaction
5x Phusion buffer	4 μ l
DNTPs	0.4 μ l
NheI-Kozak-mC2-SF-tag fw	0.1 μ l
Celd2-KpnI rev	0.1 μ l
Template DNA	1 μ l
Phusion polymerase	0.2 μ l
ddH ₂ O	14.2 μ l

Table 3.4: *Creld2* cDNA amplification PCR program

Step	Temperature ($^{\circ}$ C)	Time	Number of cycles
Initial denaturation	98	30 sec	1
Denaturation	98	10 sec	5
Annealing	65	15 sec	
Extension	72	30 sec	
Denaturation	98	10 sec	25
Annealing	72	15 sec	
Extension	72	30 sec	
Final extension	72	5 min	1

3.4.2 Cloning PCR

3.4.2.1 Cloning of N-terminally tagged *Creld2*

The N-term FS-C2 gene block (gBlock) was cut out of the Topo vector with NheI-HF and EcoRI-HF and purified from an agarose gel. *Creld2* cDNA was amplified and digested with EcoRI-HF and KpnI-HF and the 3' fragment was purified from an agarose gel. Purified gBlock and 3' PCR product were ligated and subcloned into the pcDNA3.1Zeo+ vector for transfection of cells.

3.4.2.2 Cloning of C-terminally tagged *Creld2*

Subcloned *Creld2* cDNA in a pcDNA3.1Zeo+ vector was digested with EcoNI and XbaI and the vector containing the 5' *Creld2* fragment was purified. The C-term C2-SF gBlock was digested with EcoNI and XbaI and ligated with the pcDNA3.1Zeo+ vector containing the 5' *Creld2* part.

Table 3.5: PCR Protocol SF-mock tag amplification

Component	Volume / 20 μ l reaction
5x Phusion buffer	4 μ l
DNTPs	0.4 μ l
NheI-SF-tag fw	0.1 μ l
KpnI-SF-tag rev	0.1 μ l
Template gBlock	1 μ l
Phusion polymerase	0.2 μ l
ddH ₂ O	14.2 μ l

Table 3.6: SF-mock tag amplification PCR program

Step	Temperature ($^{\circ}$ C)	Time	Number of cycles
Initial denaturation	98	30 sec	1
Denaturation	98	10 sec	5
Annealing	55	15 sec	
Extension	72	10 sec	
Denaturation	98	10 sec	30
Annealing	72	15 sec	
Extension	72	10 sec	
Final extension	72	5 min	1

3.4.2.3 Cloning of the SF-mock vector

For generation of the SF-mock tag, the SF-tag was amplified from one of the used gBlocks and subcloned into the pcDNA3.1Zeo+ vector.

3.4.3 qRT-PCR

qRT-PCR primer were designed either by using the Universal Probe Library (Roch Applied Science) or by using Primer-Blast (NCBI). Primers were desalted and without 5' or 3' modifications from IDT and supplied lyophilized.

Table 3.7: qRT-PCR Protocol

Component	Volume / 15 μ l reaction
Template cDNA	0.75 μ l
Forward primer	0.375 μ l (5 pmol/ μ l)
Reverse primer	0.375 μ l (5 pmol/ μ l)
2x SYBR-Green Supermix	7.5 μ l
ddH ₂ O	6 μ l

3.4.4 Total lipid extraction in solution by Bligh & Dyer

Total lipids were extracted from mice livers. On ice, tissue samples were weighed, cut into small pieces and transferred to Precellys tubes. Sample concentration was adjusted to 50 mg/ml with respect to the tissue's wet weight and homogenized in a Precellys tissue homogenizer until samples were free of intact tissue pieces. In case of homogenization iterations samples were placed on ice for 2 min. Subsequently, 0.8 ml of the homogenate were transferred into a Pyrex glass tube and 3 ml of 1:2 (v/v) CHCl_3 :MeOH were added. Mixture was vortexed for 10 sec. Afterwards, 1 ml of CHCl_3 and 1 ml of ddH₂O were added consecutively. Mixtures were vortexed as mentioned above after each addition and centrifuged at 1000 x g for 5 min at RT. Following centrifugation as much as possible of the bottom, solvent, phase was recovered with a Pasteur pipette without contaminating it with the aqueous phase. Subsequently, the same amount of recovered solvent phase of each sample was transferred to a new Pyrex tube and solvents were evaporated under a stream of N₂ gas. Finally, extracted lipids were resuspended in 100 μl of 1:1 (v/v) CHCl_3 :MeOH. The final concentration of extract in respect to the wet weight of tissue per μl was calculated and lipid extracts according to 1 mg of tissue were subjected to thin layer chromatographical analysis.

3.5 Western blotting

Proteins separated by SDS-PAGE were transferred to a PVDF membrane. The membrane was activated with methanol for 1 min and equilibrated in transfer buffer. SDS-PAGE gels and Whatman papers were equilibrated in transfer buffer and assembled to a transfer sandwich. The membrane was oriented to the anode, whereas the gel was oriented to the cathode. Proteins were blotted in the turbo-blotter using standard protocol for mixed molecular weight protein transfer predefined by BioRad.

3.6 Antibody binding and ECL detection

After the transfer of proteins the membrane was blocked with 5 % skim milk powder in TBST for 30 min. The membrane was incubated with primary antibody in TBST with 5 % skim milk powder o/n at 4 °C. After incubation, the membrane was washed 3 times for

5 min in TBST to reduce unspecific binding and incubated with the secondary antibody for 1 h. Membrane was washed 3 times for 5 min and the ECL substrate was added for the production of chemiluminescence. For the detection of luminescence signals X-Ray film was used. X-ray films were developed in a Curix60 developer.

3.7 Cell culture

3.7.1 Isolation and culture of mouse embryonic fibroblasts

Pregnant mice were sacrificed and embryos (E12.5) were obtained. Heads of the embryos were removed and used for genotyping. Heart and liver were removed from the embryo bodies and embryos were incubated in (0.05%) trypsin-(0.48 mmol) EDTA solution for 30 min at 37 °C with shaking at 900 rpm. Subsequently, pre warmed Dulbecco's Modified Eagle Medium (DMEM; Invitrogen) supplemented with 10% fetal calf serum (FCS; Pan Biotech) and 1% Penicillin-streptomycin (10 000 U/mL; Thermo Scientific) was added to stop trypsin-EDTA activity and the cell suspension was centrifuged at 100 x g for 5 min. After substitution of the supernatant with fresh DMEM, MEF cells were resuspended and the cell suspension was transferred onto a culture dish plate and incubated in DMEM at 37 °C in an incubator with a humidified atmosphere of 5% CO₂. Cells were passaged at a confluence of 70 % to 80 %.

3.7.2 Induction of ER stress

ER stressors Tg and Tm were resuspended in Dimethyl sulfoxide(DMSO). For the analysis of UPR pathways in Creld2^{+/+} and Creld2^{-/-} MEFs during ER stress, 0.5×10^6 MEF cells of passage 3 were seeded onto 6-well culture dishes one day prior to the start of treatment. Control cells (designated as 0 h) were incubated in DMEM supplied with FCS, appropriate antibiotics and the equivalent volume of DMSO as was used for cells treated with Tg or Tm.

3.7.2.1 Induction of acute ER stress

Seeded cells were cultured in the presence of 1 μ M Tg for 1,2,4 or 8 h. Untreated cells served as 0 h controls. After the respective treatment time, cells were harvested. A small fraction of harvested cells was seeded out for analysis of cell viability. The

remaining cells were subjected to gene expression and immunoblot analysis.

3.7.2.2 Induction of chronic ER stress

Chronic ER stress was induced in *Creld2*^{+/+} and *Creld2*^{-/-} MEFs by treatment with various concentrations of Tg for 48 h or Tm for up to 72 h. Medium and stressors were refreshed daily. At the indicated time points, cells were either sampled for molecular analysis or subjected to cell viability analysis.

3.7.2.3 Induction of transient ER stress

For induction of transient ER stress 0.5×10^6 MEF cells were seeded into 6-well culture plates the day before the experiment. The next day, ER stress in MEFs was induced by Tm (2 μ g/mL) or Tg (1 μ M) for 2 h. After the incubation with ER stressor the medium was replaced by DMEM alone and cells were incubated for 4, 8, 28 and 46 h. Control cells were incubated without ER stressor in DMEM.

3.7.2.4 Cell viability assay

To analyze cell viability of *Creld2*^{+/+} and *Creld2*^{-/-} during ER stress, MEFs were seeded into 96-well plates as doublets one day prior to the start of treatment. The following day, cells were incubated with either TM (25 ng/ml, 50 ng/ml or 100 ng/ml; Sigma-Aldrich) or Tg (2.5 nM, 5 nM or 10 nM; Sigma-Aldrich) in DMEM for 1 or 2 days. As control, cells were incubated without Tm or Tg. At the indicated time points cells were fixed with Histofix 4% (Roth) for 5 min and stained with Crystal violet (0.05% in ddH₂O; Roth) for 30 min. Stained cells were washed twice with tap water and air-dried. After drying MeOH was added to solubilize the dye and staining intensity was measured with a Fluostar Omega (BMG Labtech) plate reader at 590 nm.

3.7.2.5 Electroporation of cells

Prior to electroporation, adherent cells were trypsinized and washed twice with PBS and cell concentration was adjusted to 5×10^6 – 2×10^7 cells/ml with Optimem medium. For electroporation 0.5 ml of the cell suspension was transferred to a 4 mm electroporation

cuvette, mixed with 2.5 μg DNA per 10^6 cells without introducing bubbles and incubated for 15 min. Directly before electroporation, the mixture was resuspended by gently tapping the cuvette so that no bubbles were produced and cells were electroporated at 250 V, 950 μF , $\infty\Omega$ in exponential mode. Immediately after electroporation, 1 ml of DMEM containing 10% FCS, without antibiotics, was added to the cell suspension and cells were incubated in cell culture flasks for 24 h prior to changing the medium to DMEM containing the proper antibiotics.

3.7.3 Tandem affinity purification

The protocol for tandem affinity purification (TAP) was adapted from Gloeckner et al. [54]. Transiently over expressing HEK293 cells were cultured for 72 h post electroporation for the initial analysis of Creld2 interaction partners. For extensive investigation on Creld2 protein interactions TAP was performed with stably expressing HEK293 cells. Buffers for TAP were prepared freshly on the same day of purification. Cells were trypsinized and incubated in 1 ml/ 5×10^7 cells of ice cold TAP-lysis buffer for 20 min on ice. The lysates were centrifuged for 10 min at 10 000 xg at 4 °C and the supernatants were recovered. Afterwards, cell lysates were incubated with 100 μl Strep-tactin resin for 2 h at 4 °C on a rotating wheel. After incubation, lysates and resins were transferred to micro spin columns and washed 3 x with 500 μl TAP-wash buffer with 5 sec centrifugation steps at 100 x g between each wash. Subsequently, samples were eluted by incubation with 500 μl TAP-elution buffer for 10 min. Eluates were further incubated with 50 μl anti-FLAG M2 resin for 2 h at 4 °C on a rotating wheel. Following incubation with the anti-FLAG M2 resin, samples were washed once with 500 μl TAP-wash buffer and twice with 500 μl TBS as mentioned above. For the final elution of bound proteins, samples were incubated with 200 μl FLAG elution buffer for 10 min on ice in micro spin columns with several times of gentle mixing.

3.7.4 Analysis of mass-spectrometric data

Raw mass spectrometry data sets were processed with MaxQuant software for identification and quantification of proteins. For protein identification, peptides were searched against human protein sequences obtained from Uniprot. Statistical analysis of processed data sets was performed with Perseus software. Reactome functional

interaction analysis of enriched co-purified proteins and pathway enrichment analysis was done with Cytoscape [55] using the ReactomeFIViz plug-in.

3.8 Work with *Mus musculus*

3.8.1 Animal housing

Mice were kept under standard SPF conditions with a 12 h dark/light cycle, and normal chow and autoclaved water *ad libitum*. Isolated DNA from mouse tail tips was used for genotyping.

3.8.2 Glucose tolerance test

To analyse glucose tolerance mice were fasted for 6 h with supply of drinking water *ad libitum*. Afterwards, fasting blood glucose (0 min sample) was measured by scratching the tail tip of mice and sampling a drop of blood with a test strip for determination of blood glucose with a glucose meter. Mice were weighed and administered with a final glucose concentration of 2 g/kg by intraperitoneal (IP) injection. Subsequently, blood glucose was measured after 15, 30, 60, 90 and 120 min by withdrawing blood from the initially scratched tail tip.

3.8.3 Insulin tolerance test

For testing the insulin tolerance, mice were supplied with chow and drinking water *ad libitum* before and throughout the experiment. Initial blood glucose (0 min sample) was measured by scratching the tail tip of mice and sampling a drop of blood with a test strip for determination of blood glucose with a glucose meter. Mice were weighed and administered with a final insulin concentration of 0.75 U/kg by IP injection. Subsequently, blood glucose was measured after 15, 30, 60, 90 and 120 min by withdrawing blood from the initially scratched tail tip.

4 Results

4.1 General phenotypic analysis

After the generation of the *Creld2*-knockout-mouse, offspring from heterozygous matings were evaluated for a Mendelian distribution showing a normal distribution [2]. However, due to the mixed background of generated mice, the line was back-crossed to the C57BL/6JRcc background for a minimum of 10 generations, reaching 95 % C57BL/6JRcc background. Both, male and female *Creld2*^{-/-} mice were born in Mendelian ratio (Figure 4.1a). Further, in the assessment of the general *Creld2*^{-/-} phenotype, male wild-type and *Creld2*^{-/-} mice body weights were determined at the age of 1, 2 and 12-months and show similar weight gains throughout ageing, albeit *Creld2*^{-/-} mice weights are slightly reduced (Figure 4.1b). Comparing liver weights of *Creld2*^{-/-} and littermate control male mice at 2 and 12-months of age reveals significantly decreased liver weight in 12-months-old *Creld2*^{-/-} males (Figure 4.1c). However, assessment of the liver to body weight ratio in these mice only shows a slightly decreased ratio compared to the wild-type (Figure 4.1d).

In addition to the assessment of liver weights, livers of 1-month and 12-months-old male mice were examined histologically (Figure 4.2). Hematoxylin/Eosin (HE) stained livers of 1-month-old *Creld2*^{+/+} and *Creld2*^{-/-} mice show no differences in liver tissue structure (Figure 4.2a). On the other hand, *Creld2*^{-/-} livers of 12-months-old males reveal dilation of sinusoids and the presence of vacuoles in hepatocytes, while *Creld2*^{+/+} livers are comparable to those in 1-month-old mice (Figure 4.2b (top)). To test whether livers of *Creld2*^{-/-} mice store more lipids than wild-type controls, Oil-red-O stainings were performed. Indeed, 12-months-old livers show more intensive staining for lipids in *Creld2*^{-/-} mice compared to wild-type controls (Figure 4.2b (middle)), indicating that the observed vesicles in the HE staining are filled with neutral lipids. This is similar to the initial characterisation of the *Creld2*^{-/-} mouse [2] and could be validated in this study. The increased accumulation of vacuoles and lipids in hepatocytes is present in circa 75 % of *Creld2*^{-/-} animals. Furthermore, livers of 12-months-old mice were stained against glutamine synthetase (GS) (Figure 4.2b (bottom)), which is assessed

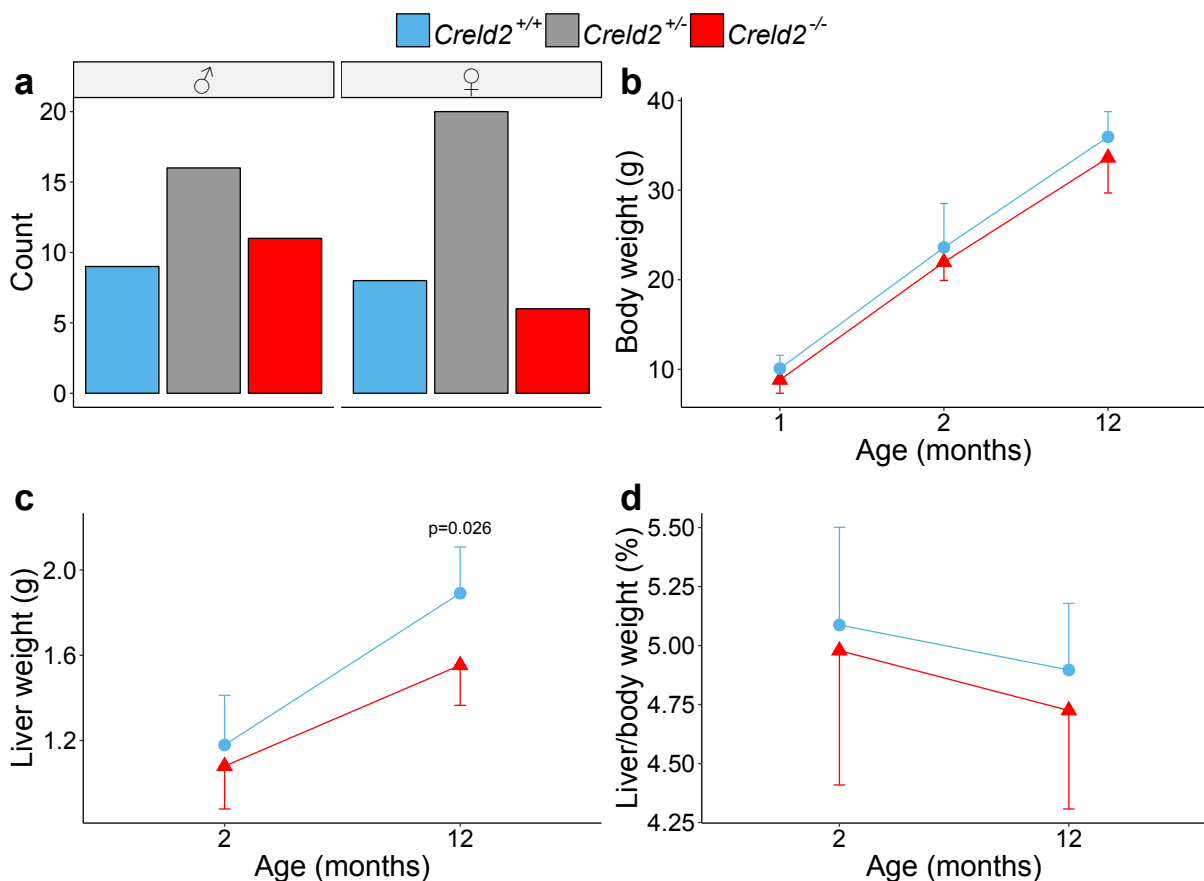


Figure 4.1: Genotype distribution and comparison of mouse weights. (a) Genotype and gender distribution of mice born from heterozygous matings (n=17 matings). (b) Body weight development of $Creld2^{+/+}$ and $Creld2^{-/-}$ male mice (for 1 and 2-months-old mice n=5–7, for 12-months-old $Creld2^{+/+}$ mice n=10 and $Creld2^{-/-}$ n=18). (c) Liver weight development of $Creld2^{+/+}$ and $Creld2^{-/-}$ male mice. Liver weight of 12-months-old $Creld2^{-/-}$ mice is significantly reduced. (d) Liver to body weight ratios in 2 and 12-months-old males (n=5 for 2-months-old mice, for 12-months-old $Creld2^{+/+}$ n=3 and $Creld2^{-/-}$ n=9 in c-d).

to examine metabolic anomalies in ammonia detoxification [56] and also serves as a marker for various metabolic liver aberrations [57,58]. In a healthy liver, the expression of GS is found exclusively in endothelial cells lining hepatic veins and may be present in another one or two layers of liver parenchymal cells [59].

However, the GS signal in $Creld2^{-/-}$ livers is frequently (approximately 75 %) exceeding the endothelial layer of hepatic veins, which indicates disturbances in liver metabolism.

4.2 Analysis of metabolism

The accumulation of neutral lipids in hepatocytes of 1-year-old $Creld2^{-/-}$ mice might underlie various aberrant conditions, such as insulin resistance, type II diabetes and anomalous genetic orchestration of metabolism [44]. To investigate and narrow down

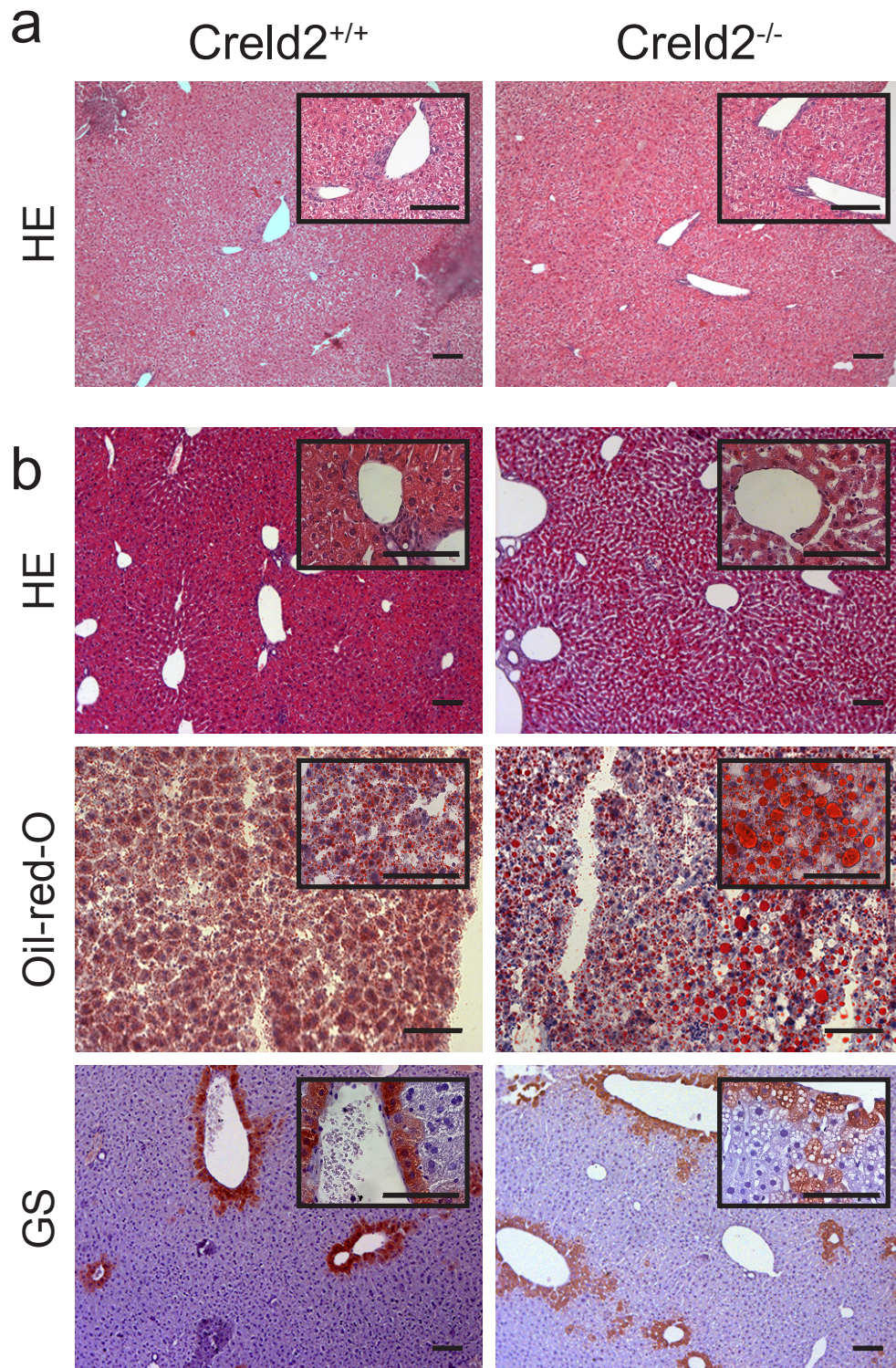


Figure 4.2: Histological analysis of livers. (a) HE staining of 1-month-old *Creld2*^{+/+} and *Creld2*^{-/-} male mice (n=2–3). (b) HE (top), Oil-red-O (middle) and GS (bottom) staining of 12-months-old *Creld2*^{+/+} and *Creld2*^{-/-} male mice livers (n=5). HE staining shows disintegrated liver structure with dilated sinusoids (overview) and vacuolar deposits in hepatocytes (inset) in *Creld2*^{-/-} mice. Oil-red-O staining of neutral lipids reveals increased accumulation of lipids in *Creld2*^{-/-} livers. Staining against GS displays vacuolar deposits in hepatocytes and diffused signal for GS. **HE:** Hematoxylin & Eosin; **GS:** Glutamine synthetase. Scale bars indicate 100 μ m.

potential causes of this steatotic phenotype, mice were subjected to systemic, lipidomic and molecular analyses of their metabolism.

In addition, the severity of this phenotype was assessed by measuring the inflammation status in the liver.

4.2.1 Analysis of liver lipid homeostasis

To assess the lipid composition of young (1 month) and old (12 months) *Creld2*^{-/-} mice and wild type controls, livers were harvested, total lipids were extracted and subjected to thin layer chromatography analysis (Figure 4.3.) To observe possible gender differences in lipid contents, male and female liver lipid extracts were analysed separately. 12-months-old male mice show significantly increased cholesterol levels, while other lipid species such as cholesteryl esters, Diacylglycerols (DAGs) and free fatty acids are elevated in both, young and old male mice. Furthermore, TAG levels in old mice show no differences in relative lipid abundance when compared to their wild type controls, whereas young *Creld2*^{-/-} mice livers show an increased TAG content (Figure 4.3a). In contrast, analyses of old female mice (Figure 4.3b) indicate no differences in relative lipid abundance of any lipid species when compared to wild type mice.

4.2.2 Transcriptional regulation of lipid metabolism genes

For a better understanding of the underlying hepatosteatosis and the differences in liver lipid composition between *Creld2*^{-/-} and *Creld2*^{+/+} mice, expression analyses of genes involved in lipid metabolism and homeostasis in the liver were performed. Genes important for fatty acid oxidation, acylglycerol metabolism, cholesterol storage and general lipid storage were examined separately for male and female mice (Figure 4.4). The results display significantly reduced *peroxisome proliferative activated receptor gamma coactivator 1 alpha* (*Pgc1 α*) expression in male *Creld2*^{-/-} mice (Figure 4.4a). *Pgc1 α* is a transcription factor playing a major role in energy metabolism by orchestrating programs responsible for mitochondrial biogenesis and function [60]. Additionally, *Pgc1 α* regulates the expression of enzymes for mitochondrial fatty acid oxidation [61]. Moreover, dysfunction in the metabolism of acylglycerols are noticeable in *Creld2*^{-/-} males as evidenced by decreased levels in *apolipoprotein C-II* (*Apoc2*) and

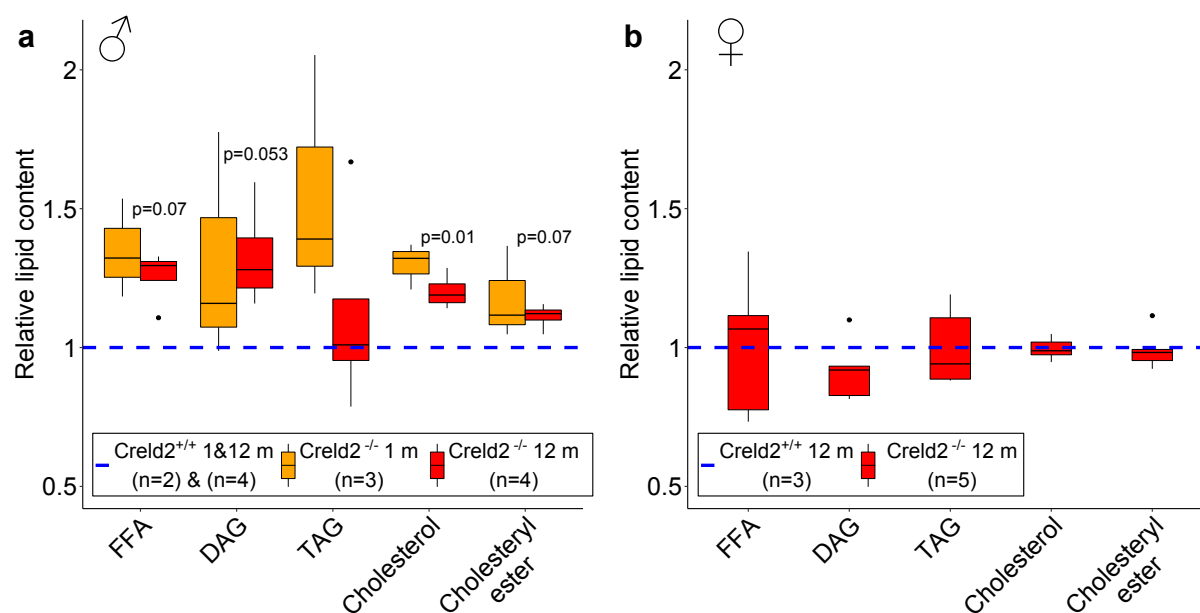
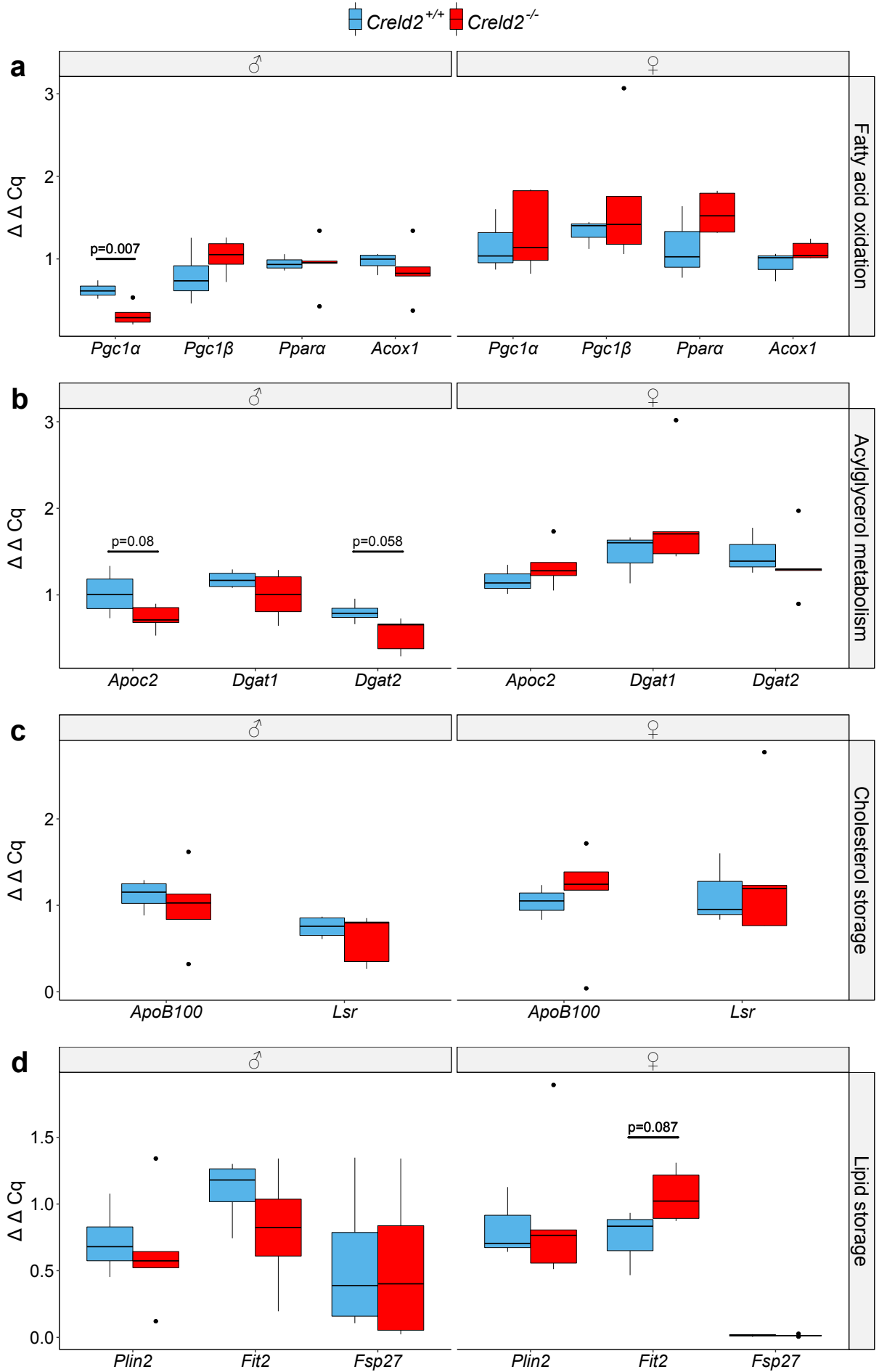


Figure 4.3: Thin layer chromatography of total lipid extracts from young and old *Creld2*^{-/-} and litter mate control mice livers. Lipid content of *Creld2*^{-/-} mice was normalized to age-matched wild type controls. Dashed line indicates mean values of *Creld2*^{+/+} mice, which were set to 1. **(a)** Lipid analysis of 1 month (1 m, orange) and 12 months (12 m, red) old male mice. Significantly elevated cholesterol contents are observable in 12-months-old males. Free fatty acids, DAGs and cholesterol esters show increased quantities in 1 and 12 month old mice. **(b)** Lipid contents in female mice. No variance in lipid species contents between *Creld2*^{+/+} and *Creld2*^{-/-} females is visible. Number of analysed mice (n) for each group is indicated in the figure key. **DAG:** Diacylglycerol; **TAG:** Triacylglycerol. Bottom and top of boxes represent the first quartile (Q₁) and third quartile (Q₃) with indicated median (bar inside box). Lower and upper whiskers represent minimum and maximum values within 1.5 x the interquartile range (IQR) of Q₁ or Q₃. Closed (black) circles represent statistical outlier. Unpaired, two-tailed student's t-test was performed for calculation of p-values. P-values below 0.1 are indicated.

diacylglycerol O-acyltransferase (Dgat2) (Figure 4.4b). *Apoc2* is a required cofactor of lipoprotein lipase for the hydrolysis of TAGs into free fatty acids and DAGs [62, 63], whereas *Dgat2* is responsible for the synthesis of TAGs [64].

In line with the analyses of liver lipid composition, there are gender-specific differences in gene expression levels. In contrast to male mice, no significant transcriptional regulation of gene expression is present in female mice. Major differences between male and female mice are visible in genes responsible for lipid storage (Figure 4.4b). Here, *fat storage-inducing transmembrane protein 2 (Fit2)* shows increased expression in *Creld2*^{-/-} females compared to the wild type controls, whereas male *Creld2*^{-/-} mice show a decrease in *Fit2*. Additionally, female mice are virtually devoid of *fat specific protein 27 (Fsp27)*, while males display a high variability in *Fsp27* levels.



4.2.3 Glucose metabolism

The development of liver steatosis may not only be the consequence of multiple abnormalities in the metabolism but might also entail various aberrations in metabolism homeostasis [44]. To obtain an insight into the metabolic status of *Creld2*^{-/-} mice, the systemic and liver-specific glucose metabolism was analysed in 1-year-old mice (Figure 4.5).

To measure systemic glucose metabolism, glucose and insulin tolerance tests were performed in *Creld2*^{-/-} and littermate control male mice (Figure 4.5a-b). Here, mice were administered either glucose or insulin, and the blood glucose levels were measured over a period of 120 min. For analysis of glucose tolerance, mice were fasted for 6 h prior to injection to establish a fasting blood glucose baseline. The fasting glucose levels in *Creld2*^{+/+} and *Creld2*^{-/-} mice is virtually equal. However, after application of glucose, *Creld2*^{-/-} mice show augmented elevation of blood glucose compared to wild-type littermates, with highest levels 15 min post-glucose administration (Figure 4.5a). To test the insulin tolerance, mice were not fasted to avoid severe hypoglycemia, so that no consistent glucose baseline levels could be obtained. Due to the dispersed initial blood glucose levels, the measured glucose of the insulin tolerance test is displayed in percent. Blood glucose levels in *Creld2*^{+/+} mice drop to approximately 60 % after insulin injection and return almost to the starting value at the end of the observation time. In contrast, *Creld2*^{-/-} mice reveal overall reduced blood glucose clearance, reaching a drop to maximally 75 %. The decrease of blood glucose is significantly diminished

Figure 4.4 (preceding page): Gene expression analysis of lipid metabolism components. Male (left, ♂) and female (right, ♀) mice were analysed separately. **(a)** Genes responsible for fatty acid oxidation. *Pgc1α* is significantly reduced in *Creld2*^{-/-} males. **(b)** Expression of genes involved in acylglycerol metabolism. *Creld2*^{-/-} male mice show reduced levels of *Apoc2* and *Dgat2* with values close to significance. **(c)** Analysis of genes involved in cholesterol storage. **(d)** Marker genes for lipid storage. Female *Creld2*^{-/-} mice show upregulated expression of *Fit2*. Expression results implicate gender-specific differences in *Fsp27*, which expression is virtually absent in females. Data set is comprised of n=3–5 for male and n=3–8 for female. Gene expression levels are represented as housekeeper normalized $\Delta\Delta Cq$ values. Bottom and top of boxes represent the first quartile (Q₁) and third quartile (Q₃) with indicated median (bar inside box). Lower and upper whiskers represent minimum and maximum values within 1.5 x the interquartile range (IQR) of Q₁ or Q₃. Closed (black) circles represent statistical outlier. Unpaired, two-tailed student's t-test was performed for calculation of p-values. P-values below 0.1 are indicated.

15 min post insulin application in *Creld2^{-/-}* mice compared to the controls. Furthermore, glucose levels after 120 min are still remaining at approximately 85 % in *Creld2^{-/-}* mice and are not normalizing as fast as in the littermate controls (Figure 4.5b).

To analyse the underlying molecular mechanisms that could explain the differences in the responses to glucose and insulin, further studies of glucose metabolism were conducted in the liver of mice because the liver is a key organ for carbohydrate metabolism.

The activation of the insulin signalling pathway is often defective in insulin resistance and type II diabetes [65]. After binding of insulin to the insulin receptor, protein kinase B (Akt) is activated by phosphorylation and stimulates glucose uptake into the cell [66]. Determination of Akt activation is one possible measure to analyse insulin sensitivity and was therefore analysed by assessing the phosphorylation of Akt 15 min post insulin administration (Figure 4.5c-d). Here, moderately increased P-Akt/Akt ratio levels are observed in *Creld2^{-/-}* mice compared to wild-type littermates.

In addition to the study of the insulin signalling pathway on protein level, livers of male and female mice were analysed for gene expression of two major glucose transporters (Glut), *Glut2* and *Glut4* (Figure 4.5e). *Glut2* is the main glucose transporter in the liver [67, 68] and shows slightly reduced expression levels in *Creld2^{-/-}* males. *Glut4* encodes a protein important for transport of glucose across the plasma membrane into adipocytes and striated muscle [69]. However, *Glut4* expression levels in wild-type livers resembles the $\Delta\Delta Cq$ values of *Glut2* in these analyses. *Creld2^{-/-}* males reveal significantly decreased *Glut4* expression compared to the wild-type. Deficiency of *Glut4* was reported to be an indirect cause for increased liver lipid production in mice [70]. Defects in insulin signalling or glucose uptake could influence the energy metabolism, leading to reduced ATP synthesis. Therefore, the content of ATP in 1-year old mice was determined (Figure 4.5f). ATP levels are reduced in *Creld2^{-/-}* males, albeit not significant due to a strong variability of ATP levels in *Creld2^{+/+}* male mice. For female mice, no definite differences are visible because of high variation in *Creld2^{-/-}* mice.

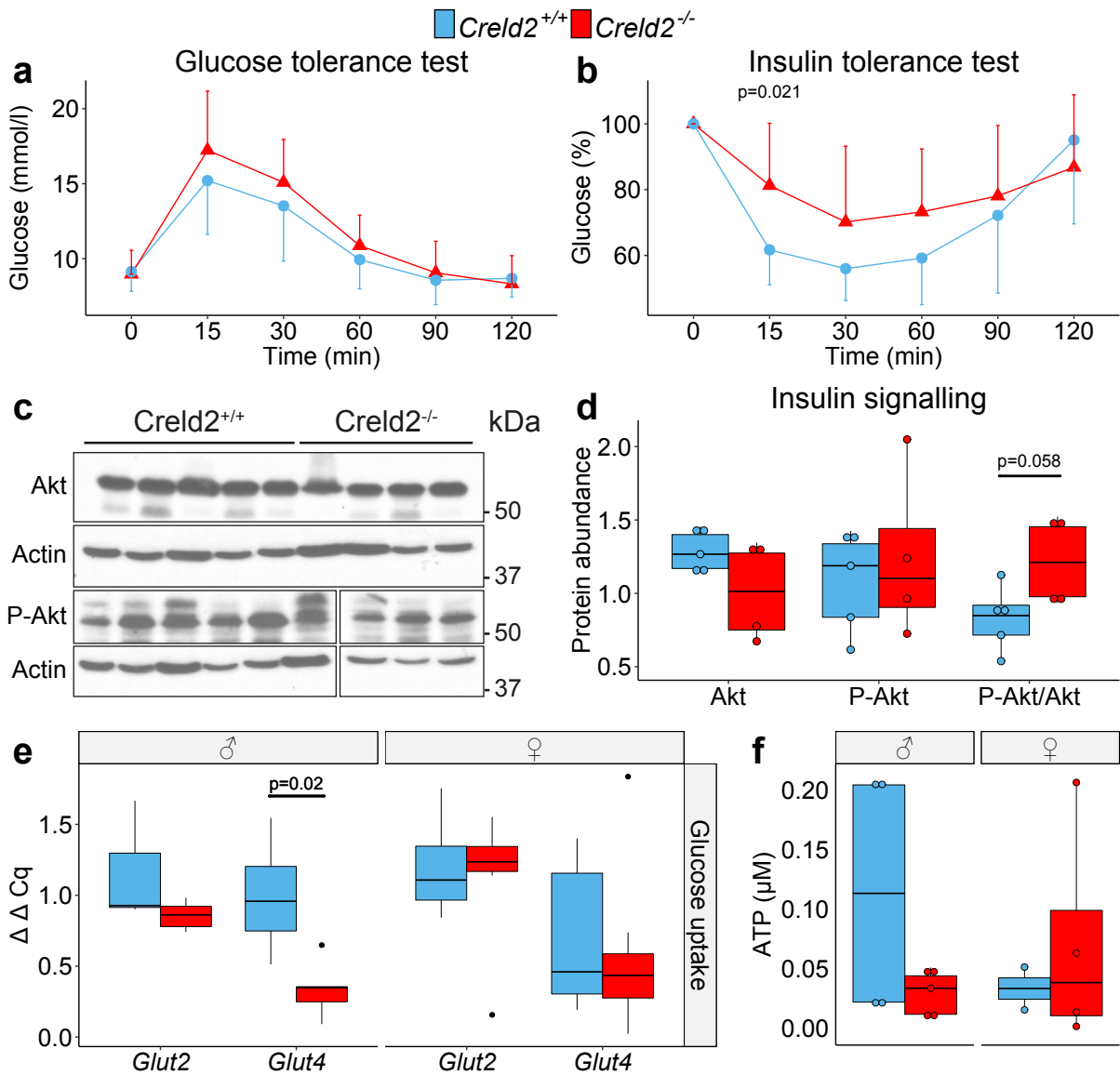


Figure 4.5: Analysis of glucose metabolism and energy state in 1-year-old mice. (a) Glucose tolerance test in *Creld2*^{+/+} (n=9) and *Creld2*^{-/-} (n=10) male mice. Glucose level is displayed in mmol/l. *Creld2*^{-/-} mice show increased blood glucose levels after 15 min to 30 min of glucose administration compared to wild type littermates. (b) The insulin tolerance test shows a significant reduction of glucose uptake into cells 15 min after insulin injection in *Creld2*^{-/-} males (n=9). Glucose uptake in *Creld2*^{+/+} mice (n=8) is increased by approximately 20%. Blood glucose is presented as percentages. (c) Insulin signalling pathway activation analysis in livers 15 min after insulin administration shows an increased P-Akt/Akt ratio in *Creld2*^{-/-} mice. (d) Immunoblots of liver samples described in (c). (e) Measurement of liver ATP levels. Liver ATP abundance is displayed in μM for male (left) and female (right) mice. ATP levels in *Creld2*^{-/-} males tend to be decreased compared to wild type controls. (f) Analysis of transporter genes for glucose uptake into the cell. Gene expression of *Glut4* in *Creld2*^{-/-} males is significantly reduced in contrast to wild-type males (for males n=4–5; for females n=7–8). Expression of *Glut2* is neither altered in females nor in males (for males n=3–5; for females n=6–8). Values in (a–b) are represented as means \pm SD. Gene expression levels are represented as housekeeper normalized $\Delta\Delta\text{Cq}$ values. Coloured circles represent individual mice. Bottom and top of boxes represent the first quartile (Q₁) and third quartile (Q₃) with indicated median (bar inside box). Lower and upper whiskers represent minimum and maximum values within 1.5 x the interquartile range (IQR) of Q₁ or Q₃. Closed (black) circles represent statistical outlier. Unpaired, two-tailed student's t-test was performed for calculation of p-values. P-values below 0.1 are indicated.

4.3 Analysis of liver injury status

Due to the developing liver steatosis and metabolic imbalances in 1-year-old *Creld2*^{-/-} mice, the livers of these mice were analysed for their state of health. For this purpose gene expression levels of markers for cell viability and inflammation were determined (Figure 4.6). As a measure of general cell cycle in the liver, gene expression of *extracellular signal-regulated kinase 1 (Erk1)* and *Erk2*, which are involved in cell growth [71] and *death receptor 5 (Dr5)*, a marker for apoptosis, were analysed (Figure 4.6a). Male *Creld2*^{-/-} mice show a slight reduction in *Erk2* expression compared to wild-type males. *Erk1* and *Dr5* expression in *Creld2*^{-/-} males and females is similar compared to *Creld2*^{+/+} mice, with *Dr5* showing slightly reduced gene expression in *Creld2*^{-/-} females in comparison to the wild-type controls.

Progressing liver steatosis is the basis for the development of NAFLD, which is a chronic inflammatory liver disease. In NAFLD, initially harmless liver steatosis can progress to steatohepatitis, fibrosis and cirrhosis [45]. Hence, the liver is experiencing increasing levels of inflammation and tissue damage in the course of NAFLD progression. Therefore, the degree of liver damage was assessed by determining the expression of acute phase response (APR) genes, which are induced upon tissue injury [72]. APR components *serum amyloid P-component (Apcs)* and *serum amyloid A-3 protein (Saa3)* were analysed for gene expression (Figure 4.6b). Both genes show similar expression in *Creld2*^{+/+} and *Creld2*^{-/-} mice of the same gender, but display increased expression in female mice compared to males.

The assessment of APR components is suited to determine the injury or inflammation status of the liver and also allows to monitor occurring inflammatory responses days later [72]. However, APR induction can be missing in the case of defective upstream signalling, which are pro-inflammatory cytokines. Therefore, the inflammation status of 1-year-old livers was assessed by measuring gene expression levels of pro-inflammatory cytokines (Figure 4.6c). Albeit the presence of a hepatosteatosis and a potential immune cell infiltrate, *tumor necrosis factor alpha (Tnf α)* and *interleukin 6 (Il6)* show decreased expression in *Creld2*^{-/-} male mice compared to wild-type males and *interleukin 1 β (Il1 β)* in *Creld2*^{-/-} females displays downregulation in comparison to *Creld2*^{+/+} female controls.

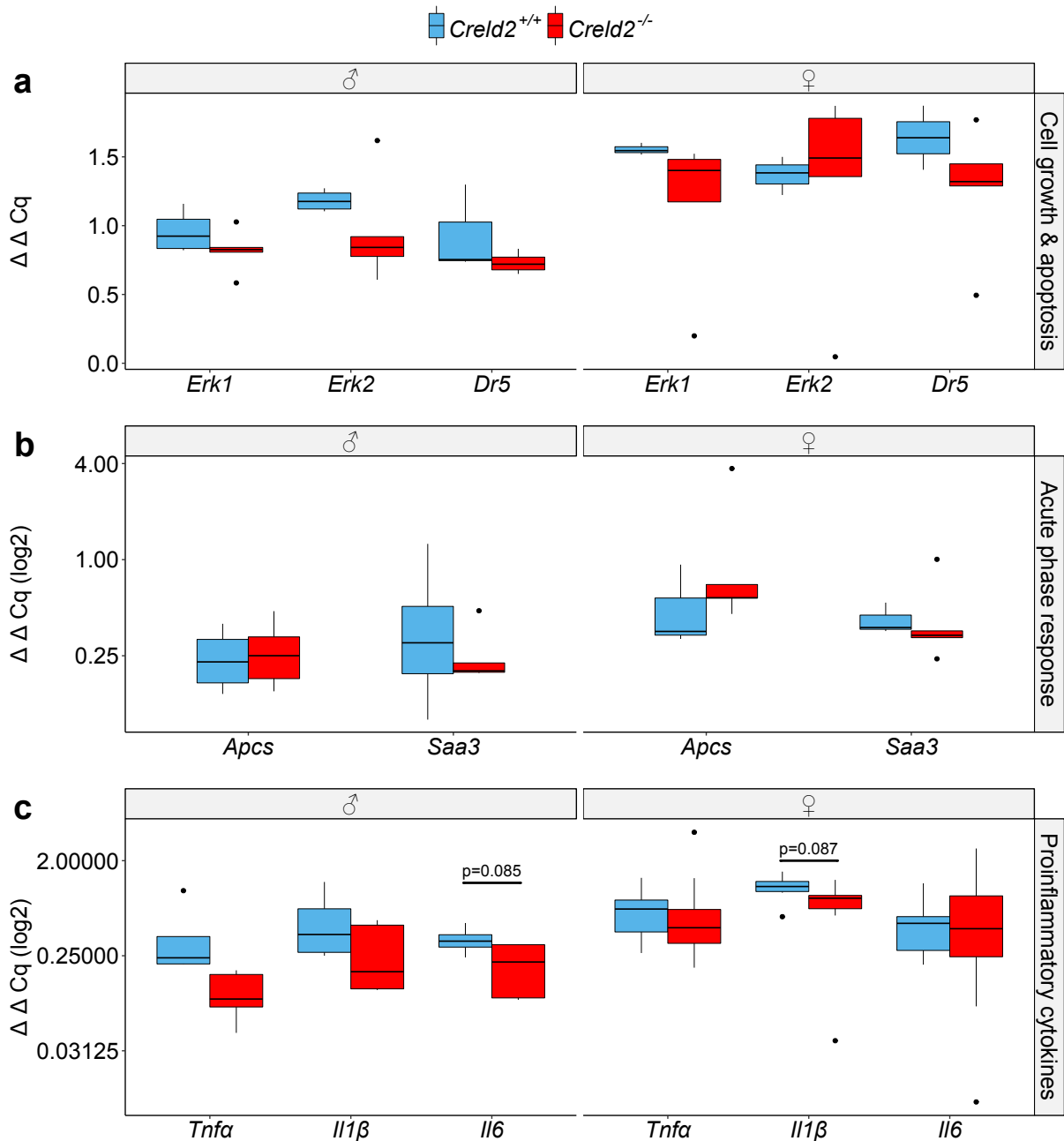


Figure 4.6: Determination of liver health state in aged mice. Male (left, ♂) and female (right, ♀) mice were analysed separately. **(a)** Expression levels of genes involved in cell proliferation and apoptosis, namely *Erk1*, *Erk2* and *Dr5*, respectively. **(b)** Analysis of acute phase response genes as tissue damage response marker. Female mice, independent of genotype, express more *Apcs* and *Saa3* than males. **(c)** Assessment of liver inflammation. *Tnfa* and *Il6* gene expression is reduced in male *Creld2*^{-/-} mice and *Il1 β* levels are decreased in female *Creld2*^{-/-} mice compared to their wild-type controls. Gene expression levels are represented as housekeeper normalized $\Delta\Delta Cq$ values. Bottom and top of boxes represent the first quartile (Q_1) and third quartile (Q_3) with indicated median (bar inside box). Lower and upper whiskers represent minimum and maximum values within 1.5 x the interquartile range (IQR) of Q_1 or Q_3 . Closed (black) circles represent statistical outlier. Unpaired, two-tailed student's t-test was performed for calculation of p-values. P-values below 0.1 are indicated.

The main cytokine producing cells in the liver are Kupffer cells. Thus, the abundance of Kupffer cells in livers of 1-year-old *Creld2*^{-/-} male mice was compared to those of age-matched wild-type controls (Figure 4.7a). However, *Creld2*^{-/-} livers rather show an increase of Kupffer cell numbers when compared to *Creld2*^{+/+} mice. This hints towards defects in activation of Kupffer cells or infiltrating macrophages from the bone-marrow. To test whether macrophage induction is dysfunctional due to *Creld2* deficiency in general, bone-marrow derived macrophages (BMDMs) of 1-year-old *Creld2*^{+/+} and *Creld2*^{-/-} males were treated with Lipopolysaccharide (LPS) to stimulate the production of pro-inflammatory cytokines and gene expression of *Tnfα*, *Il1β* and *Il6* was assessed after 4 h and 8 h of LPS treatment (Figure 4.7b). BMDMs of both genotypes display peaking cytokine gene expression after 4 h, with decreasing expression levels at 8 h of LPS stimulation, but no differences in transcript levels between both genotypes are noticeable.

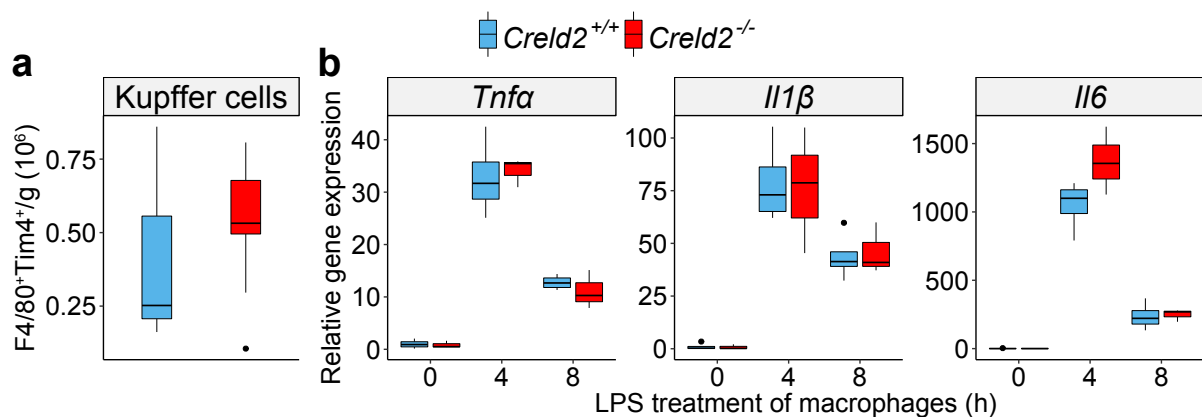


Figure 4.7: Analysis of Kupffer cells and macrophage activation. (a) Determination of Kupffer cell abundance in 1-year-old *Creld2*^{+/+} (n=3) and *Creld2*^{-/-} (n=9) male mice via flow cytometry. Kupffer cells were determined by gating on single, live, CD45⁺, CD11b low, F4/80⁺Tim4⁺ cells. (b) Analysis of bone-marrow derived macrophage (BMDM) activation after LPS treatment. Gene expression of *Tnfα*, *Il1β* and *Il6* in BMDMs from 1-year-old *Creld2*^{+/+} (n=4) and *Creld2*^{-/-} (n=3) male mice shows no differences between the genotypes. Gene expression is represented as housekeeper normalized $\Delta\Delta$ Cq values relative to the 0 h wild-type controls. Bottom and top of boxes represent the first quartile (Q₁) and third quartile (Q₃) with indicated median (bar inside box). Lower and upper whiskers represent minimum and maximum values within 1.5 x the interquartile range (IQR) of Q₁ or Q₃. Closed (black) circles represent statistical outlier. Unpaired, two-tailed student's t-test was performed for calculation of p-values. P-values below 0.1 are indicated.

4.4 Steady state UPR in 1-year-old mice

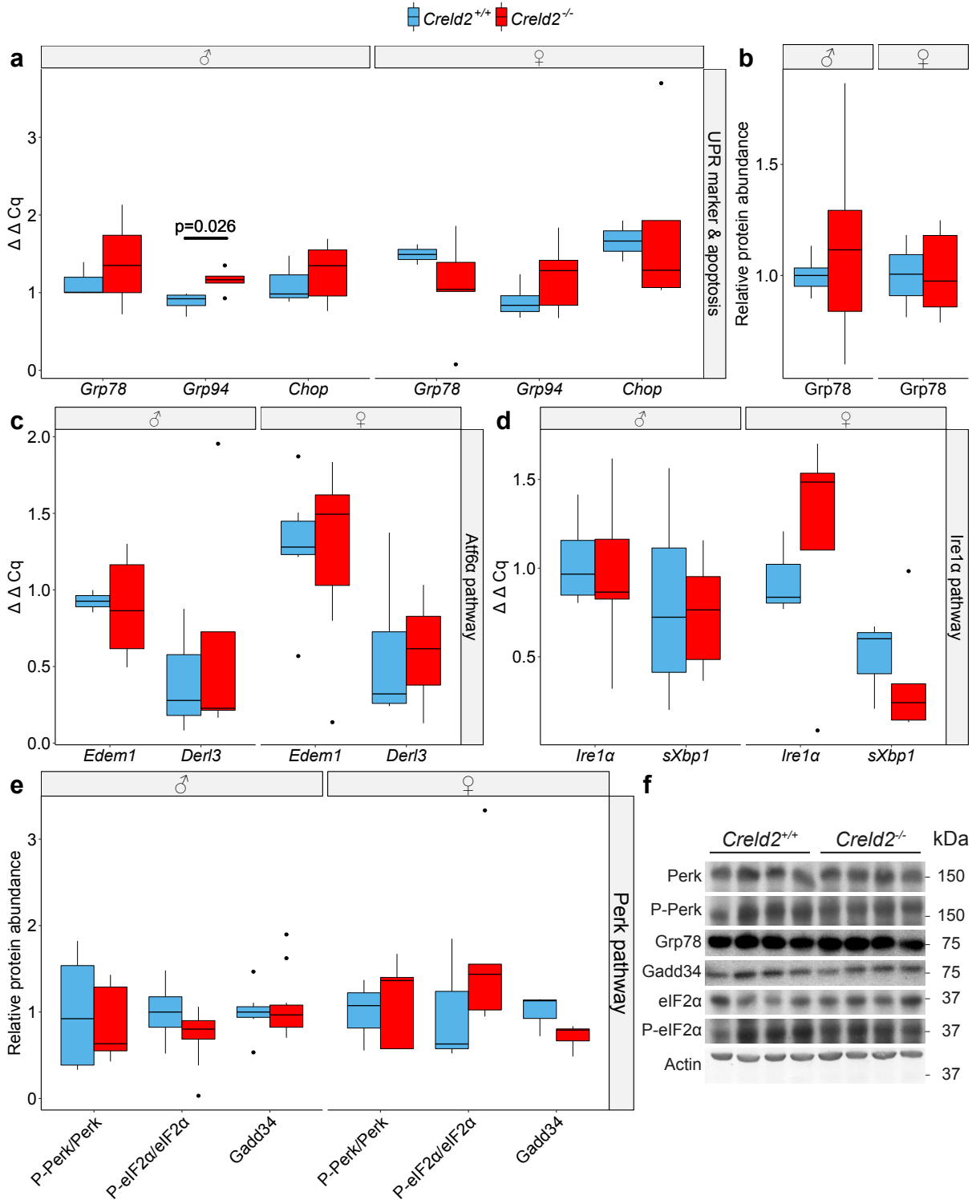
The development of liver steatosis is frequently correlated with malfunctions in the UPR pathways. Besides inducing genes for the amelioration of ER stress, each of these pathways induces sets of genes involved in fatty acid metabolism [36, 38, 31]. Since *Creld2* is induced by *Atf6 α* during ER stress and thus potentially plays a role in the regulation of the UPR, 1-year-old mice livers were analysed for their steady state UPR to determine whether *Creld2*^{-/-} mice exhibit an aberrant ER stress status. For general assessment of ER stress the expression of chaperones *Grp78*, *Grp94* and the apoptosis inducer *Chop* were analysed (Figure 4.8a). *Grp94* expression is significantly increased in male *Creld2*^{-/-} mice, whereas *Creld2*^{-/-} females show slightly elevated *Grp94* expression. *Grp78* mRNA expression is not altered between the two genotypes in males but is marginally reduced in *Creld2*^{-/-} females compared to littermate controls, which is confirmed by unaltered *Grp78* protein expression (Figure 4.8b). Furthermore, activation of the *Atf6 α* , *Ire1 α* and *Perk* pathways were analysed (Figure 4.8c,d,e). No significant differences in gene expression of *Atf6 α* (Figure 4.8c) or *Ire1 α* pathway (Figure 4.8d) downstream targets could be observed in male mice compared to littermate controls. However, female *Creld2*^{-/-} mice show an upregulation of *Ire1 α* and decreased *sXbp1* levels (Figure 4.8d). Activation of the *Perk* pathway was assessed by immunoblotting through determination of the phosphorylation status of *Perk* and *eIF2 α* , as well as expression of *Gadd34* (Figure 4.8e). These analyses show no substantial differences between wild-type and *Creld2*^{-/-} mice. Still, a minor reduction of *Gadd34* expression in female *Creld2*^{-/-} mice as compared to *Creld2*^{+/+} females is noticeable.

4.5 Analysis of bones

4.5.1 Analysis of bone structure

Recently, *Creld2* was reported to be upregulated in chondrocytes experiencing ER stress, as well as to be a component of the ECM in the epiphyseal growth plate [50]. Furthermore, Briggs et al. [73] state that cartilage-specific *Creld2*^{-/-} mice exhibit growth plate dysplasia. However, these findings are unpublished yet.

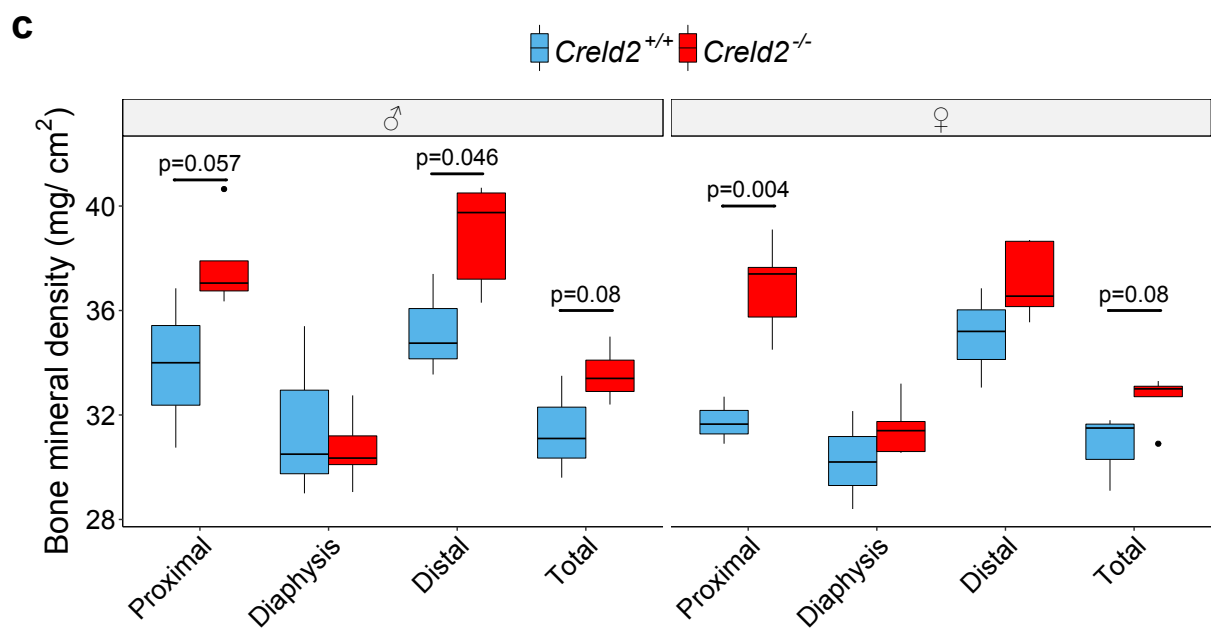
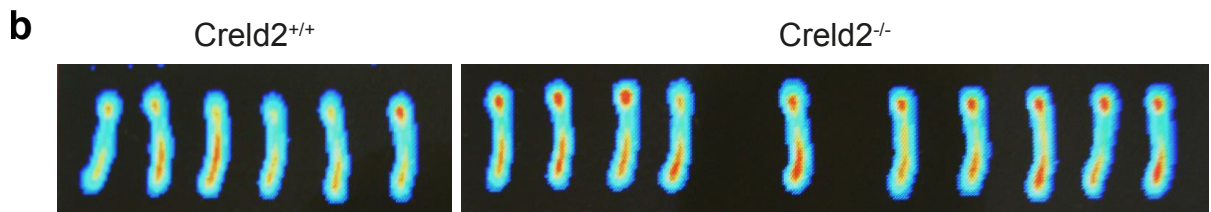
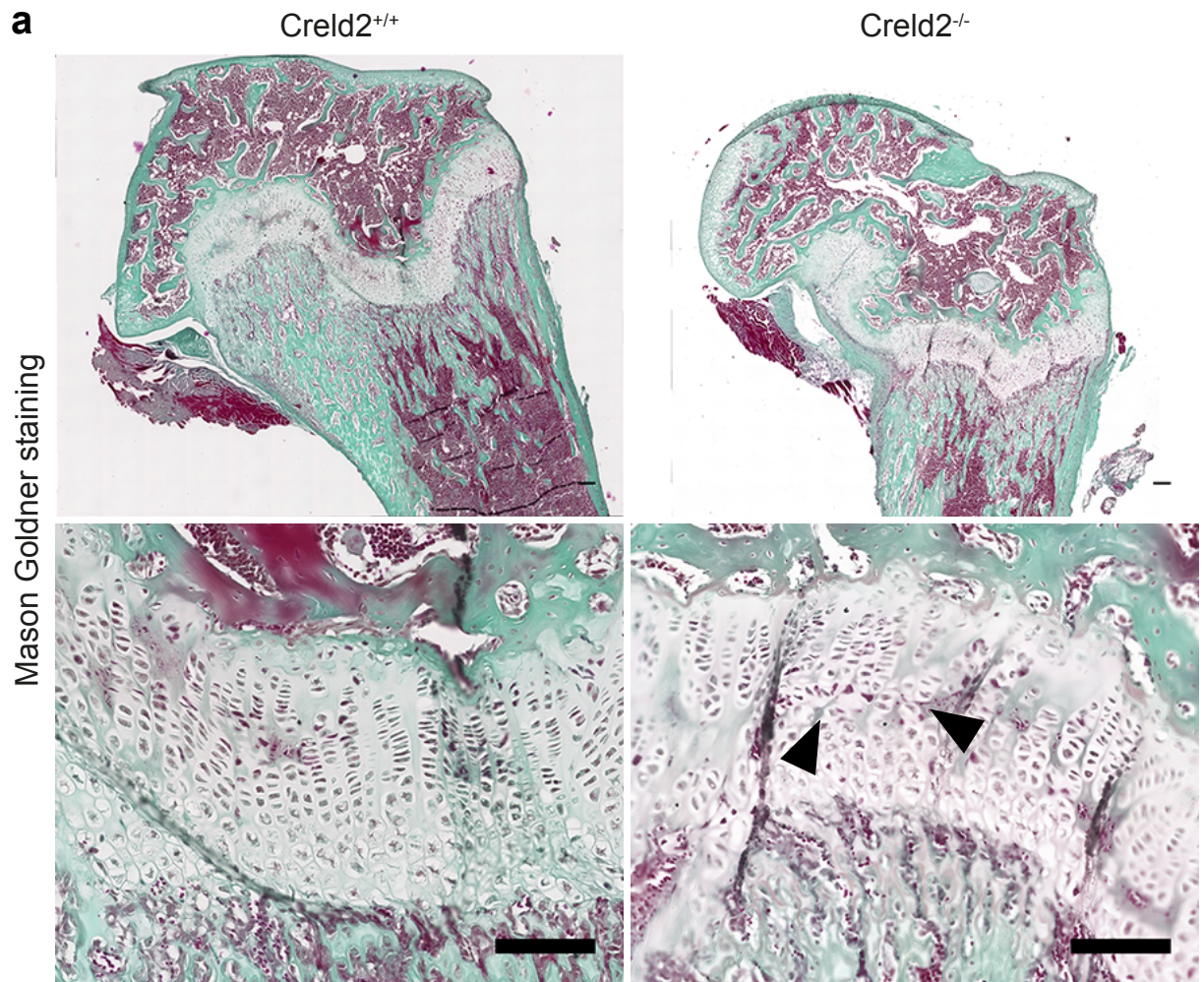
To analyse the growth plate and the overall bone structure phenotype in *Creld2*



knockout mice, femurs of 1-month-old mice were analysed histologically (Figure 4.9a). Masson-Goldner trichrome stained *Creld2*^{-/-} bones show no apparent differences in overall mineralised bone structure (green) compared to wild-type controls. However, *Creld2*^{-/-} mice occasionally display increased innervation of bone matrix by chondrocytes. Additionally, in contrast to wild-type mice, *Creld2*^{-/-} mice frequently show disrupted columnar alignment of chondrocytes in the epiphyseal growth plate and a larger hypertrophic zone, which is composed of roundly shaped chondrocytes.

In another recent report, it was found that *Creld2* enhances bone formation and matrix mineralisation *in vitro* [51]. To investigate the effect of *Creld2* on bone formation, femoral bone mineral density (BMD) was assessed in 1-year-old mice, since young mice show no apparent histological abnormalities regarding bone mass. Further, an osteopenic phenotype in *Creld2*^{-/-} mice would be visible more likely during ageing. The micro-CT analyses of bones that were performed in collaboration with the group of prof. Inada (Tokyo university of agriculture and technology, Japan) reveal a higher BMD in male and female *Creld2*^{-/-} mice compared to the wild-type, indicating a development of osteopetrosis in *Creld2*^{-/-} mice (Figure 4.9b,c).

Figure 4.8 (preceding page): Analysis of UPR pathways in livers of 1-year-old mice. Male (left, ♂) and female (right, ♀) mice were analysed separately. **(a-b)** Determination of general ER stress. **(a)** Gene expression of *Grp78*, *Grp94* and *Chop*. Increased levels of *Grp94* are present in *Creld2*^{-/-} mice of both genders with significant levels in males. For male wild-type mice n=3–4 and *Creld2*^{-/-} n=4–5. For female *Creld2*^{+/+} n=2, except for *Grp94* (n=7). *Creld2*^{-/-} female results consist of n=5, except for *Grp94* (n=8). **(b)** Protein expression of UPR regulator *Grp78* is similar in both genotypes and genders (male *Creld2*^{+/+}: n=4–7, *Creld2*^{-/-}: n=5–10; female *Creld2*^{+/+}: n=3, *Creld2*^{-/-}: n=5). **(c)** *Atf6α* pathway induced genes *Edem1* and *Derl3* do not show genotypic or gender specific differences in expression levels (n=3–5 for male and n=5–8 for female *Creld2*^{+/+} and *Creld2*^{-/-} mice). **(d)** Expression of genes regulated by the *Ire1α* pathway. A trend of increased *Ire1α* and decreased *sXbp1* is present in *Creld2*^{-/-} female mice (n=5–8) compared to wild-type controls (n=3–6). In male *Creld2*^{+/+} (n=3–4) and *Creld2*^{-/-} (n=5) mice no differences are evident. **(e)** Protein abundances of components of the Perk pathway, respectively. The steady state assessment of *Grp78* and Perk pathway components displays equal levels of relative protein abundances in males of both genotypes. For male *Creld2*^{+/+} n=4–7 and *Creld2*^{-/-} n=5–10. Female wild-type mice n=3 and *Creld2*^{-/-} mice by n=5. **(f)** Representative immunoblots of proteins displayed in **(b)** and **(e)**. Gene expression levels are presented as normalized $\Delta\Delta$ Cq values. Bottom and top of boxes represent the first quartile (Q₁) and third quartile (Q₃) with indicated median (bar inside box). Lower and upper whiskers represent minimum and maximum values within 1.5 x the interquartile range (IQR) of Q₁ or Q₃. Closed (black) circles in **(a-e)** represent statistical outlier. Unpaired, two-tailed student's t-test was performed for calculation of p-values.



4.5.2 Analysis of the hematopoietic stem cell niche

To further determine the severity and potential impact of the developing osteopetrosis in *Creld2*^{-/-} mice on the bone-marrow niche, the femoral and tibial bone-marrow in *Creld2*^{+/+}, *Creld2*^{+/-} and *Creld2*^{-/-} mice was analysed via flow cytometry (Figure 4.10). A progressing increase in bone mass eventually causes space constraints for blood vessels and bone-marrow cells and results in decreasing cell numbers in the bone-marrow niche. To analyse the progression of the osteopetrosis, total bone-marrow cell number per leg was determined, showing no differences between the three genotypes (Figure 4.10a). Despite the total cell numbers being normal in *Creld2*^{-/-} mice, the increased bone mass might have an impact on the hematopoietic stem cell (HSC) niche. Thus, different HSC populations were quantified. First, bone-marrow cells were identified by gating to Lineage negative (Lin⁻) Sca1⁺ cKit⁺ (LSK) cells, which is the surface marker expression profile by which all HSCs are defined (Figure 4.10b,c). Further gating identifies different HSC subpopulations by the expression of CD48 and CD150 [74] (Figure 4.10d). Interestingly, while LSK cells in *Creld2*^{+/-} and *Creld2*^{-/-} bone-marrow express the *green fluorescent protein (GFP)* reporter, indicating a potential need for *Creld2* by the cells (Figure 4.10c), no deviations in LSK or HSC population cell numbers is observed among the three genotypes (Figure 4.10d). Taken together, these results suggest that despite the increased bone mineral density, the osteopetrosis has not progressed to a pathogenic status.

Figure 4.9 (preceding page): Analysis of bones in 1-month and 1-year-old mice. (a) Mason Goldner staining of 1-month-old *Creld2*^{+/+} and *Creld2*^{-/-} male mice femurs. Top panel depicts an overview of the proximal (hip joint) femur. Bottom panel shows a magnification of the epiphyseal growth plate. Chondrocytes in the proliferating zone of *Creld2*^{-/-} show deviations in the columnar alignment and display a wider hypertrophic zone (roundish cell shape) when compared to the wild-type. Scale bars indicate 100 μ m. Representative for n=2–3. **(b)** Micro-CT radiographic analysis and **(c)** quantification of bone mineral density in 1-year-old male (left, σ) and female (right, ?) femurs. *Creld2*^{-/-} mice exhibit increased bone mineral density in the proximal (hip joint) and distal (knee joint) part of the femur. n=3 for *Creld2*^{+/+} and n=5 for *Creld2*^{-/-} mice in both genders. Bottom and top of boxes represent the first quartile (Q₁) and third quartile (Q₃) with indicated median (bar inside box). Lower and upper whiskers represent minimum and maximum values within 1.5 x the interquartile range (IQR) of Q₁ or Q₃. Closed (black) circles represent statistical outlier. Unpaired, two-tailed student's t-test was performed for calculation of p-values. P-values below 0.1 are indicated.

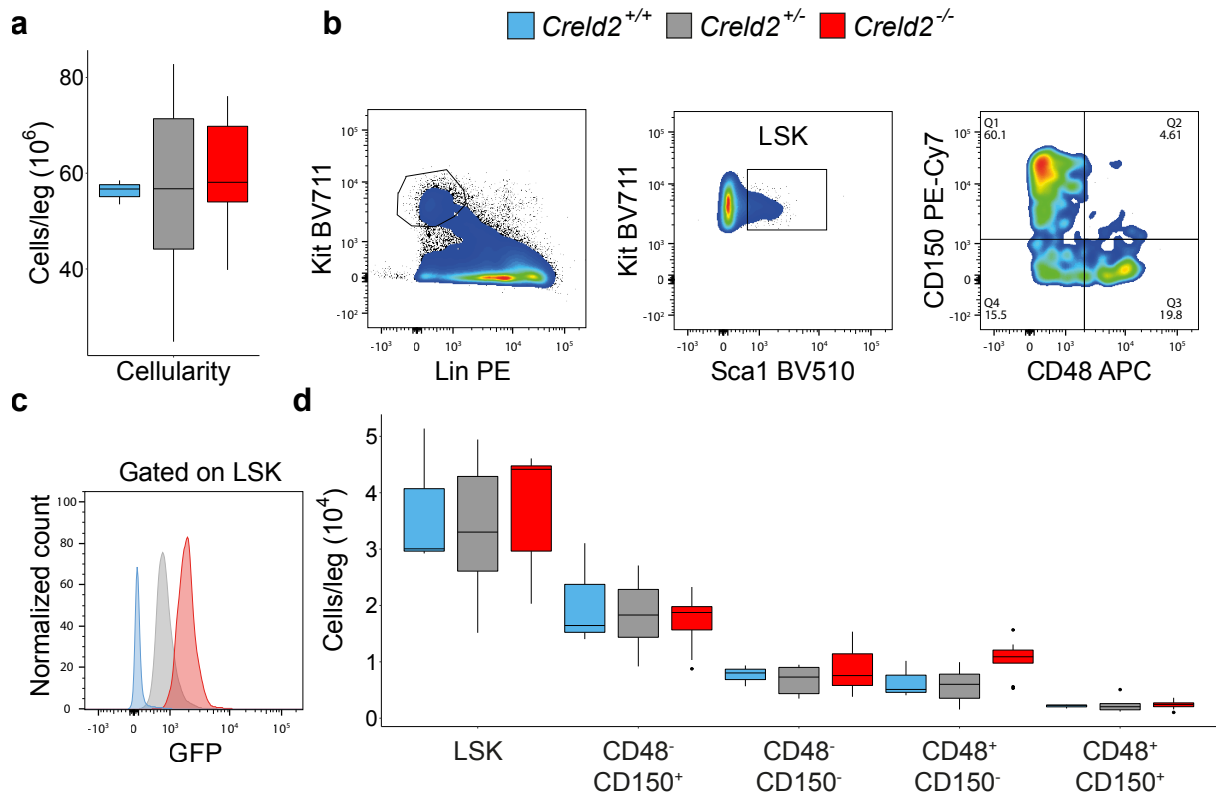


Figure 4.10: Bone-marrow analysis in 1-year-old male mice. (a) Determination of whole cell numbers per leg in bone-marrow of *Creld2*^{+/+}, *Creld2*^{+/-} and *Creld2*^{-/-} mice. (b) Gating strategy to identify LSK and HSC lineages. Gated on single live cells. (c) GFP expression in LSK cells. (d) Determination of bone-marrow HSCs (hematopoietic stem cells) in *Creld2*^{+/+} (n=3), *Creld2*^{+/-} (n=6) and *Creld2*^{-/-} (n=9) mice. n=3 for *Creld2*^{+/+}, n=6 for *Creld2*^{+/-} and n=9 for *Creld2*^{-/-}. Two-way Anova was used for statistical evaluation. Bottom and top of boxes in (a) and (d) represent the first quartile (Q₁) and third quartile (Q₃) with indicated median (bar inside box). Lower and upper whiskers represent minimum and maximum values within 1.5 x the interquartile range (IQR) of Q₁ or Q₃. Closed (black) circles represent statistical outlier.

4.6 *In vitro* analysis of the UPR

The development of NAFLD in *Creld2*^{-/-} mice may be the consequence of diverse factors, for example, obesity or genetic disorders. *Creld2* is known to be induced by ER stress due to an ERSE consensus sequence in its promoter [10]. Moreover, abnormal UPR regulation is repeatedly associated with liver steatosis [75,76]. Thus, the development of liver steatosis in *Creld2*^{-/-} mutants suggests that *Creld2* is involved in the regulation of the UPR. However, UPR analyses in livers of 1-year-old mice did not show any significant dysregulations in *Creld2*^{-/-} mice. A possible reason for this may be that the liver steatotic phenotype is not 100 % penetrant, which might conceal occurring UPR dysregulations, since analyses of livers were performed on mice cohorts without a prior histological assessment of steatosis. To delineate the functional and regulatory role

of *Creld2* in the UPR, an *in vitro* system was utilised analysing wild-type and *Creld2*^{-/-} cells under ER stress. The three UPR pathways are orchestrated in a sophisticated manner to resolve ER stress [15] and reveal distinct responses to different ER stress conditions [77]. To encompass the intricate facets of UPR regulation, several ER stress models and different ER stressors were employed to investigate UPR pathways for aberrant regulation in *Creld2*^{-/-} cells. MEFs were used due to their heterogeneous nature and primary cell line characteristics enabling the in-depth study of complex pathways in genetically modified cells while conserving physiological properties, which mimic the complex interaction of various cell types present in an organ [78].

4.6.1 Chronic ER stress

Naturally, cells in an organism constantly encounter ER stress due to the permanent need for protein synthesis in response to metabolic demands. Therefore, cells need to adapt to ER stress and to relieve the stress for the establishment of normal cell function by activating the UPR [30]. In disease conditions, as in diabetes or NAFLD, it is frequently implicated that cells are unable to abolish the experienced ER stress, which eventually leads to disease progression over time [13]. To study the involvement of *Creld2* in UPR regulation, wild-type and *Creld2*^{-/-} MEFs were challenged with low doses of either thapsigargin (Tg) (2.5–10 nM) or Tm (25–100 ng/ml) to induce chronic ER stress over 1–3 days. Challenged cells were analysed for their viability and the regulation of UPR pathways on transcriptional as well as translational level.

4.6.1.1 Cell viability during chronic ER stress

To assess the ability of *Creld2*^{-/-} MEFs to sustain and to adapt to chronic ER stress, relative cell numbers as an indicator for cell proliferation were determined via crystal violet staining after treatment with different concentrations of Tg or Tm for up to 3 days (Figure 4.11). Wild-type MEFs show proliferation after treatment with up to 10 nM Tg (Figure 4.11a) and only start stagnating in growth when challenged with 50–100 ng/ml Tm (Figure 4.11b). In contrast, the chronic stress results in significantly reduced cell numbers in *Creld2*^{-/-} MEFs after two days of treatment with any dose of Tg (Figure 4.11a) or Tm (Figure 4.11b), indicating not only growth stagnation but also apoptosis.

Due to the ability of wild-type MEFs to tolerate and adapt to even the highest concentrations of Tg (10 nM) or Tm (100 ng/ml) tested, while *Creld2*^{-/-} cells are unable

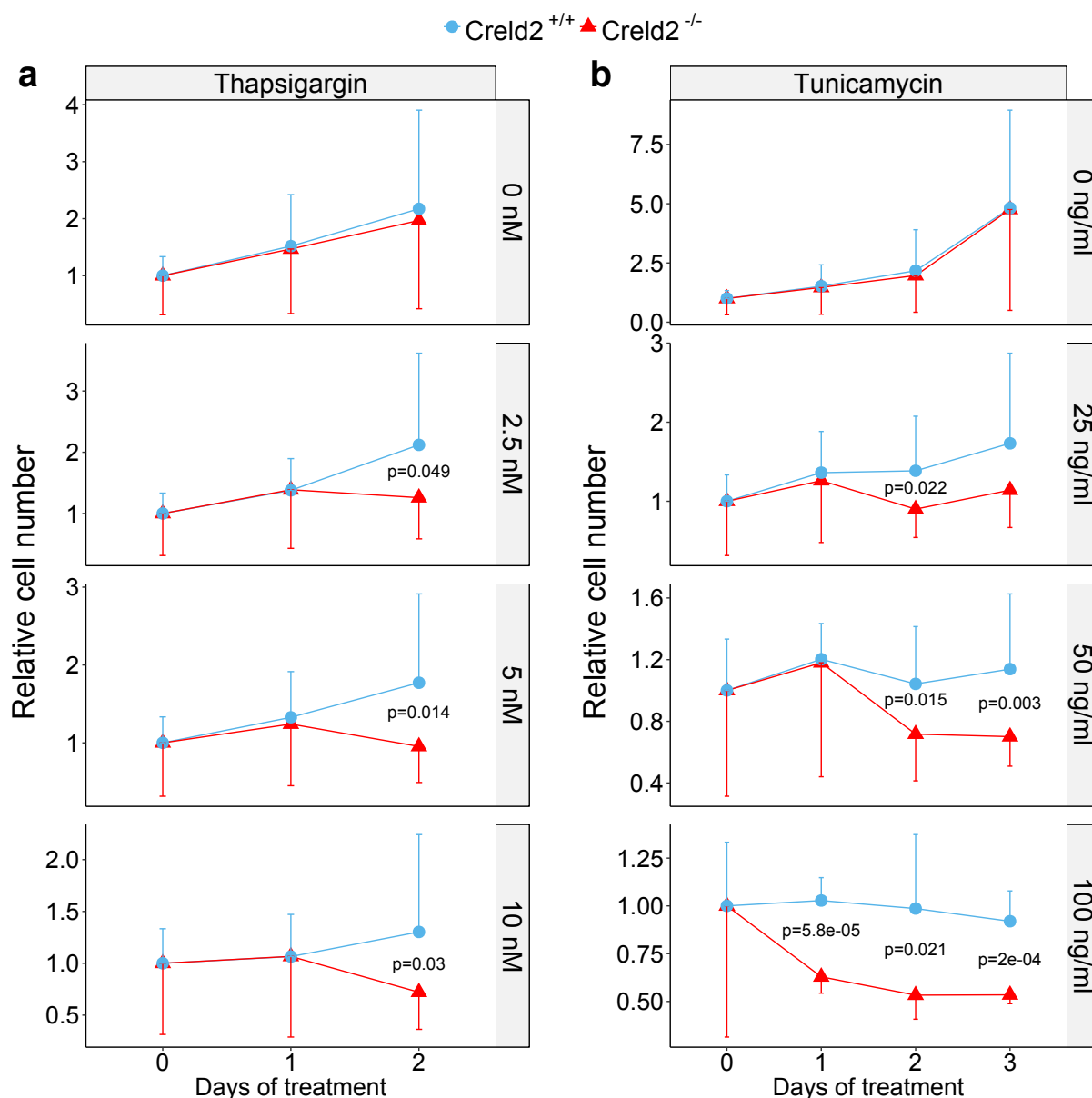


Figure 4.11: Analysis of cell viability during chronic ER stress. (a) Treatment of *Creld2*^{-/-} and *Creld2*^{+/+} MEFs with various Tg concentrations (top to bottom: 0 nM, 2.5 nM, 5 nM, 10 nM) for up to 2 days. *Creld2*^{-/-} MEFs show significant reduction in cell numbers compared to wild-type control after 2 days of treatment with any Tg concentration. **(b)** Same as in (a) but treatment of MEFs with Tunicamycin (top to bottom: 0 ng/ml, 25 ng/ml, 50 ng/ml, 100 ng/ml) for up to 3 days. *Creld2*^{-/-} MEFs show significant reduction in cell numbers compared to wild-type control after 2 days of treatment with 25–50 ng/ml Tunicamycin and already after day 1 with 100 ng/ml. Data are represented as mean ± SD. P-values were calculated using unpaired, two-tailed Student's t-test. n=12–16, except for 100 ng/ml Tunicamycin (n=6) per genotype.

to maintain their viability under these conditions, further chronic ER stress studies were performed using the highest Tg and Tm concentrations.

4.6.1.2 Regulation of ER stress markers during chronic ER stress

All of the three UPR pathways induce different gene expression programs to resolve ER stress. However, there are downstream targets, which are induced by a combination of two or more UPR branches [16]. Here, such targets are categorised as general ER stress marker. Analysis of these markers gives an insight into the efficiency of the UPR. Gene expression analyses of *Grp78*, *Grp94* and *Chop* show an initial upregulation and subsequent reduction of those genes in Tg and Tm treated cells, whereas *Dr5* remains unaltered in both genotypes (Figure 4.12a). However, ER stress induction with Tm elicits a stronger upregulation of *Grp78*, *Grp94* and *Chop* than treatment with Tg. Contrary to the dynamically regulated transcript, Grp78 protein levels increase slightly after Tg or Tm challenge and remain on the same level (Figure 4.12b,c). Chop protein expression is upregulated by Tm treatment resembling the gene expression behaviour. Interestingly, *Creld2*^{-/-} cells display slightly decreased Chop protein levels during steady state when compared to wild-type controls. Nevertheless, *Creld2*^{-/-} MEFs upregulate Chop after ER stress induction similar to *Creld2*^{+/+} cells (Figure 4.12c).

4.6.1.3 Perk pathway regulation during chronic ER stress

For the analysis of the Perk pathway, gene expression of *Perk* and *Gadd34* was assessed. *Gadd34* is induced by Chop but belongs to the Perk pathway because it dephosphorylates eIF2 α , which is a direct target of Perk [20]. Both treatments induce *Perk* expression in wild-type cells to the same extent, whereas *Perk* is not upregulated in *Creld2*^{-/-} MEFs, albeit not significant due to high variability in fibroblast clones. *Gadd34* shows equal induction in both genotypes (Figure 4.13a) and reflects the gene expression pattern of Chop (Figure 4.12a). However, on protein level *Gadd34* remains unaltered throughout the experiment (Figure 4.13c). Furthermore, Perk pathway activation was analysed by determination of the phosphorylation state of eIF2 α (Figure 4.13c), which remains unaltered in both genotypes.

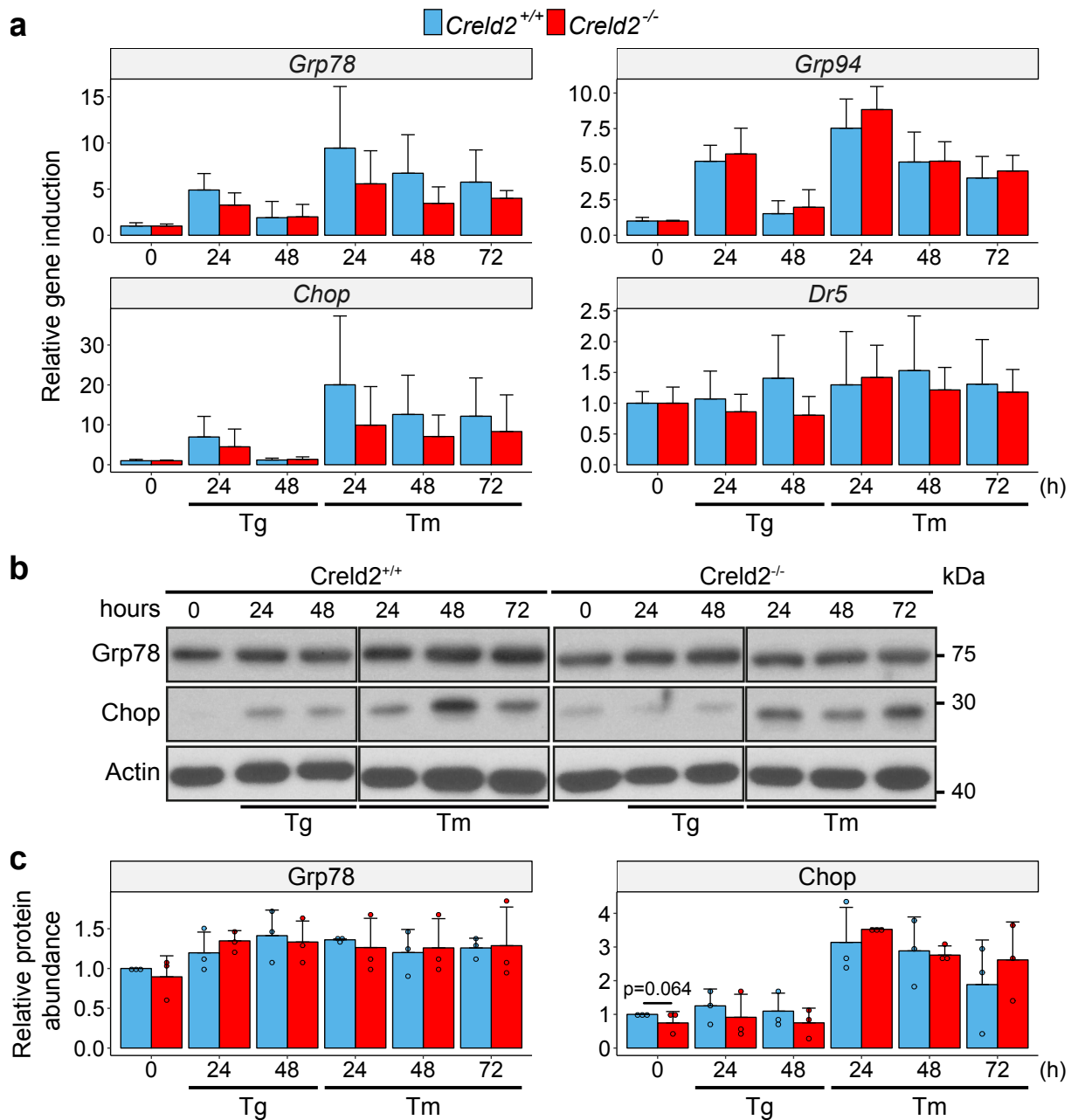


Figure 4.12: Regulation of general ER stress maker during chronic ER stress. (a) Gene expression analysis of *Grp78*, *Grp94*, *Chop* and *Dr5* in *Creld2*^{+/+} (n=5) and *Creld2*^{-/-} (n=8) MEFs. Transcriptional induction of *Grp78* is reduced at 24 h of Tg and 48 h of Tm treatment in *Creld2*^{-/-} fibroblasts compared to the wild-type controls. Gene expression is presented relative to the 0 h controls, which were set to 1. **(b-c)** Immunoblot analysis and quantification of Grp78 and Chop protein levels. Coloured circles represent individual MEF clones (*Creld2*^{+/+} and *Creld2*^{-/-}, n=3). Protein levels were normalized to β -Actin and presented relative to the 0 h wild-type controls, which were set to 1. P-values below p=0.1 are indicated. Gene and protein expression is presented as mean \pm SD. P-values were calculated using unpaired, two-tailed Student's t-test.

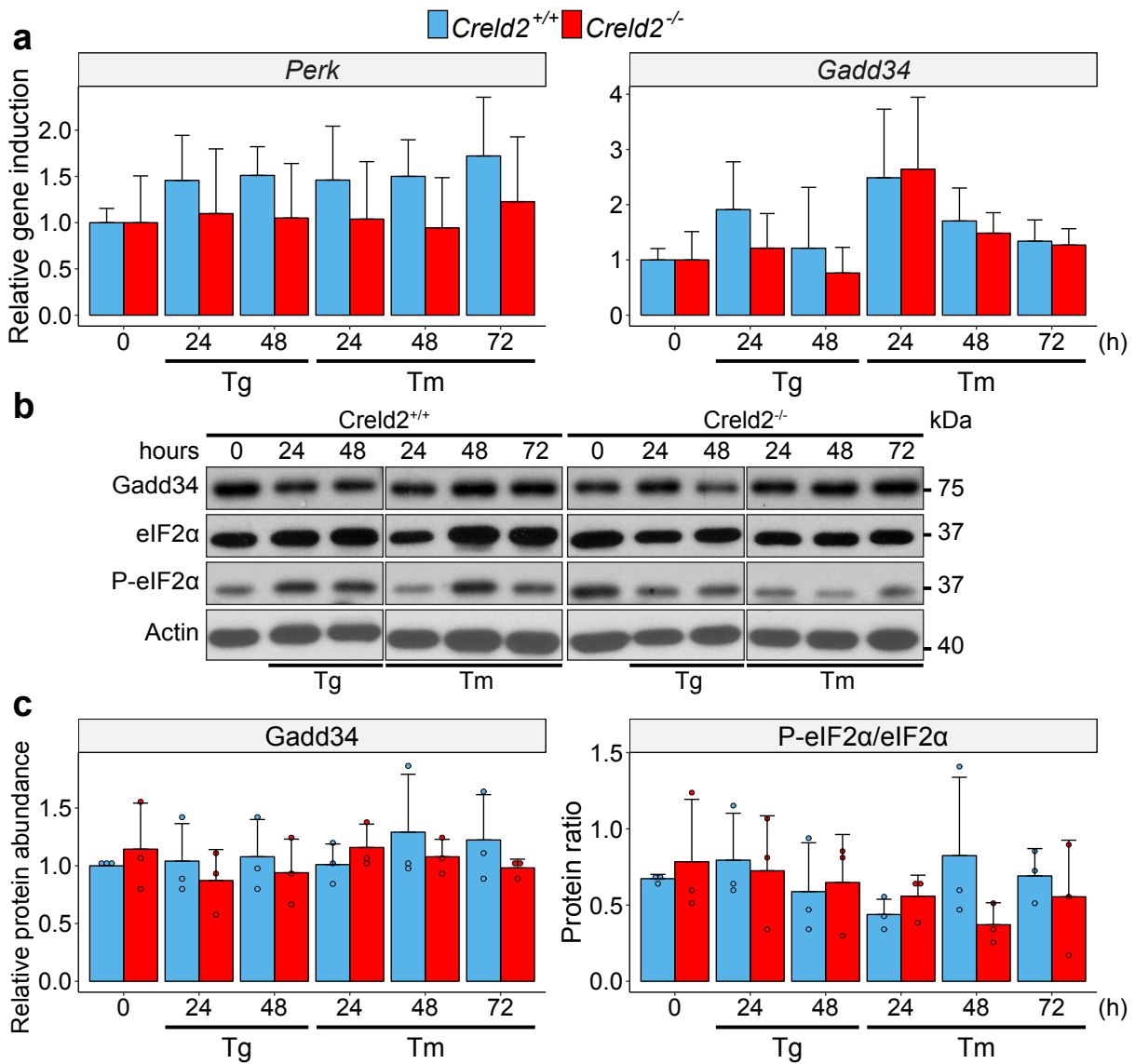


Figure 4.13: Perk pathway regulation during chronic ER stress. (a) Gene expression analysis of *Perk* and *Gadd34* in *Creld2*^{+/+} (n=5) and *Creld2*^{-/-} (n=8) MEFs. Transcriptional induction of these genes is not altered in *Creld2*^{-/-} fibroblasts compared to the wild-type controls. Gene expression is presented relative to the 0 h controls, which were set to 1. (b) Immunoblot analysis of Perk pathway activation by assessment of *Gadd34* and phosphorylated eIF2 α protein levels. (c) Quantification of immunoblots in (b). Coloured circles represent individual MEF clones (*Creld2*^{+/+} and *Creld2*^{-/-}, n=3). Protein levels were normalized to β -Actin, ratios of phosphorylated to unphosphorylated proteins were determined and presented relative to the 0 h wild-type controls, which were set to 1. P-values below p=0.1 are indicated. Gene and protein expression is presented as mean \pm SD. P-values were calculated using unpaired, two-tailed Student's t-test.

4.6.1.4 Atf6 α pathway regulation during chronic ER stress

In the assessment of Atf6 α pathway activation, gene expression of *Atf6 α* , *Edem1* and *Derl3* was measured (Figure 4.14a). Furthermore, *Creld2* expression in *Creld2*^{+/+} cells and *GFP* expression in *Creld2*^{-/-} cells was assessed since the *GFP* reporter gene replaces the endogenous *Creld2* locus in *Creld2*^{-/-} mice. *Atf6 α* shows a minor increase of gene expression after 24 h of Tg or Tm treatment, followed by a decrease of expression. To measure Atf6 α transcriptional activity, *Creld2* and *GFP* gene expression was measured. *Creld2* displays strong upregulation after challenge with either ER stressor, followed by a decline close to baseline levels after 48 h of Tg treatment and a slower decrease in cells stressed with Tm for 48 h and 72 h. However, gene expression of the reporter *GFP* shows only a minor induction when compared to *Creld2* transcripts. Moreover, *Creld2*^{-/-} MEFs reveal significantly reduced induction of *Edem1* and *Derl3* after 24 h Tg and 48 h Tm treatment in comparison to wild-type cells. The gene expression induction of *Creld2* and the insignificant induction of *GFP* can be confirmed by immunoblot probing against *Creld2* and *GFP* (Figure 4.14b,c). While *Creld2*^{-/-} cells do not show an elevation of *GFP*, *Creld2* protein expression level is increased 24 h after the beginning of treatment and is maintained until the end of observations. Furthermore, treatment with Tm, an inhibitor of N-glycosylation, results in a double band when immunoblotting against *Creld2*. The lower protein band, likely being the unglycosylated form of *Creld2*, confirms previous findings suggesting that *Creld2* is a glycoprotein [10].

4.6.1.5 Ire1 α pathway regulation during chronic ER stress

To analyse Ire1 α pathway induction, *Ire1 α* gene expression was determined and shows slight upregulation in cells challenged with Tm for 24 h and 48 h (Figure 4.15). Additionally, the mRNA level of *sXbp1* was assessed to measure Ire1 α activation. *sXbp1* abundance is elevated at 24 h in both treatments and declines afterwards. However, *sXbp1* mRNA is not falling to the baseline level but plateaus at approximately the 15-fold of the initial value in the wild-type MEFs and circa 10-fold in *Creld2*^{-/-} cells.

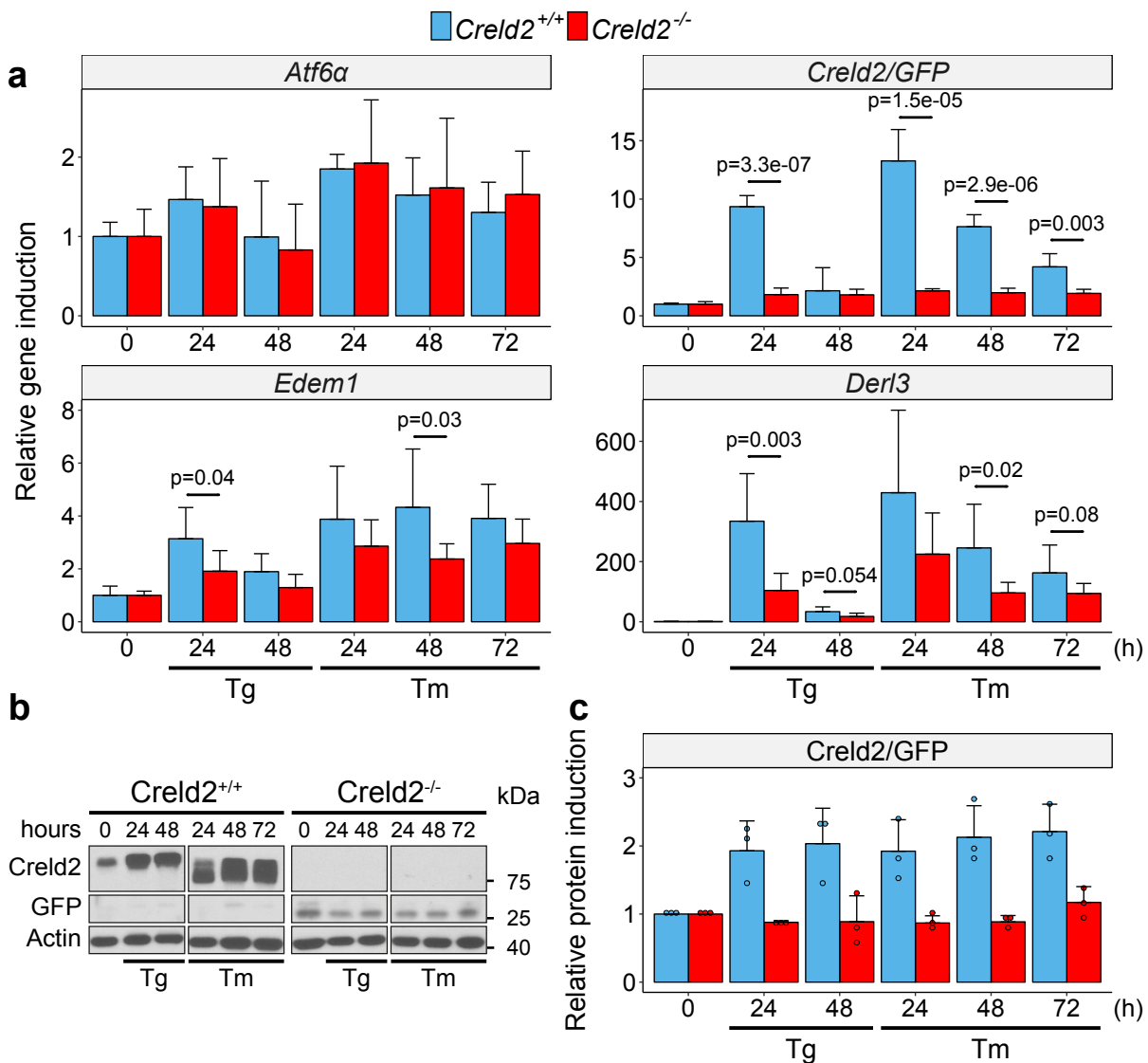


Figure 4.14: Atf6 α pathway during chronic ER stress. (a) Gene expression analysis of *Atf6 α* , *Creld2* in *Creld2*^{+/+} and *GFP* in *Creld2*^{-/-}, *Edem1* and *Derl3* in MEFs. *GFP* induction is significantly reduced in *Creld2*^{-/-} MEFs compared to *Creld2* in *Creld2*^{+/+} fibroblasts. Transcriptional induction of *Edem1* is significantly lower in *Creld2*^{-/-} fibroblasts at 24 h of Tg and 48 h of Tm treatment compared to the wild-type controls. *Derl3* shows diminished expression in *Creld2*^{-/-} MEFs. Gene expression is presented relative to the 0 h controls, which were set to 1. n=5 for wild-type and n=8 for *Creld2*^{-/-} MEFs. (b-c) Immunoblot analysis (b) and quantification of immunoblots (c) of *Creld2* and *GFP* protein levels. *GFP* expression in *Creld2*^{-/-} cells is not induced during Tg or Tm challenge. Coloured circles represent individual MEF clones (*Creld2*^{+/+} and *Creld2*^{-/-}, n=3). Protein levels were normalized to β -Actin and presented relative to the 0 h controls, which were set to 1. P-values below p=0.1 are indicated. Gene and protein expression is presented as mean \pm SD. P-values were calculated using unpaired, two-tailed Student's t-test.

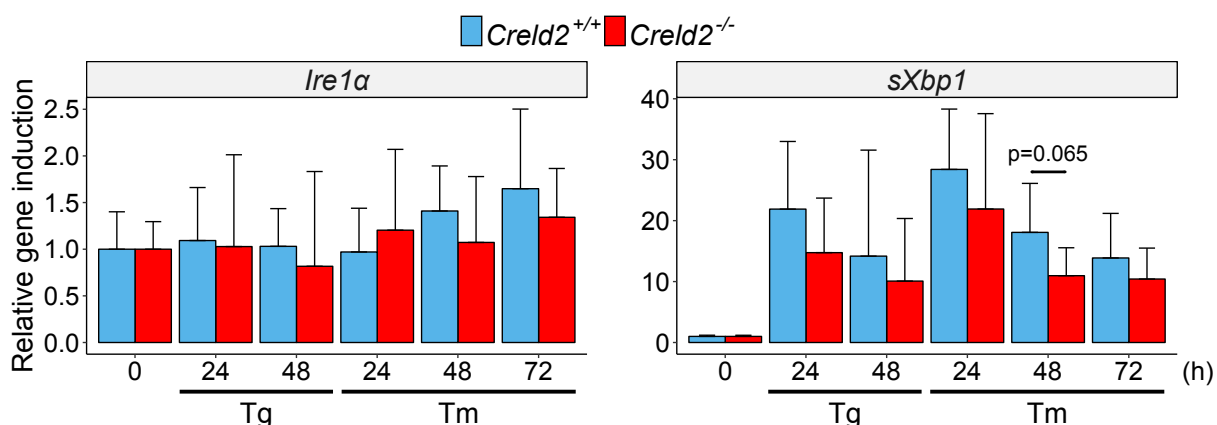


Figure 4.15: Regulation of the *Ire1α* pathway during chronic ER stress. Gene expression analysis of *Ire1α* and *sXbp1* in *Creld2*^{+/+} (n=5) and *Creld2*^{-/-} (n=8) MEFs. Gene expression is presented relative to the 0 h controls, which were set to 1. P-values below p=0.1 are indicated. Gene expression is presented as mean±SD. P-values were calculated using unpaired, two-tailed Student's t-test.

4.6.2 ER stress recovery

Ongoing research of UPR pathways reveals increasing importance of the UPR for the maintenance of healthy organ function. One approach to investigate the UPR is the analysis of knockout mice deficient in the main sensors *Atf6α* [25], *Perk* [79] or *Ire1α* [36]. Another method implies the use of cultured cells in which the UPR is induced by challenging cells with different ER stressors. However, *in vitro* studies usually focus on analysing the UPR under conditions of steady acute [30] or chronic ER stress [80]. Only little research was carried out regarding the investigation of ER stress recovery in mammalian cells [25] or plants [81], making a transfer of results and experimental set up more challenging. Therefore, experimental conditions had to be established to study the ability of wild-type and *Creld2*^{-/-} cells to recover after a short pulse of stress, which would rather recapitulate physiological conditions.

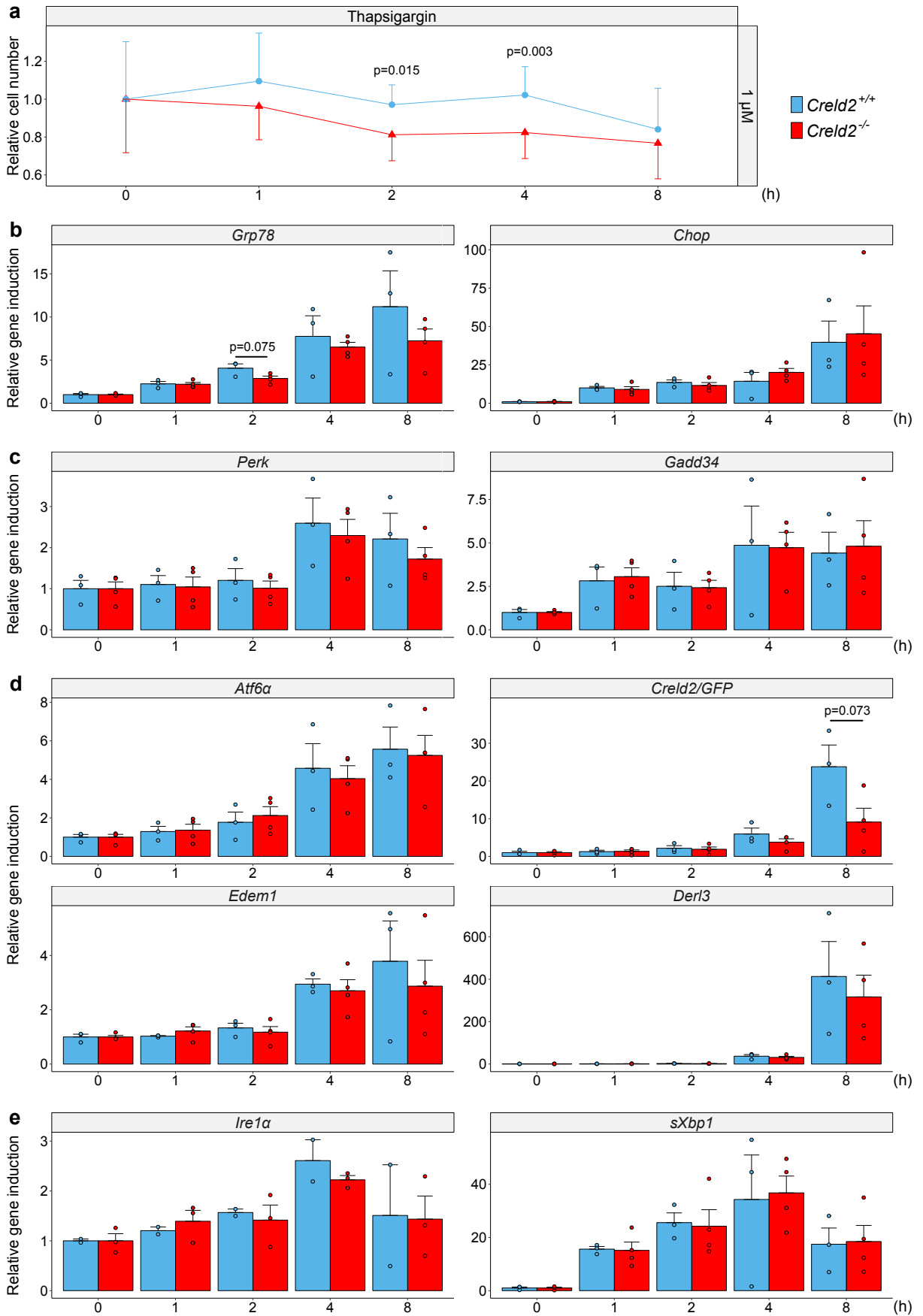
4.6.2.1 Establishment of the ER stress recovery model

A critical aspect in studying ER stress recovery is the duration of ER stress induction, which on the one hand should be sufficient to trigger a decent UPR activation, but on the other hand enable cells to overcome this burden, since it is known that prolonged, strong ER stress irreversibly leads to apoptosis [82, 83].

For this purpose *Creld2*^{+/+} and *Creld2*^{-/-} MEFs were challenged with 1 μM Tg for up to

8 h. Transcriptional activation of UPR components was assessed during the treatment and cell viability was determined 5 days after treatment (Figure 4.16). Here, cell viability served as an indicator of the capability of cells to cope with and diminish the induced ER stress and thus cells displaying similar cell numbers as the untreated controls five days after treatment would be considered to be recovered. Cells that show a reduction in relative cell numbers after the recovery phase, would still be burdened with ER stress and therefore either be unable to reach the same proliferation rate or even become apoptotic. In these assays *Creld2*^{+/+} cells show no differences in cell numbers after Tg challenge ranging from 1–4 h compared to the wild-type untreated controls. However, *Creld2*^{-/-} MEFs display significantly reduced relative cell numbers when treated for 2 h and 4 h with Tg compared to wild-type cells. After 8 h treatment, both genotypes show decreased cell numbers, indicating that cells experienced excessive ER stress (Figure 4.16a). For the assessment of the Tg challenge duration, which is sufficient for the activation of all three UPR pathways, gene expression of selected pathway components was determined during the treatment time. ER stress marker *Grp78* and *Chop* show an upregulation already after 1 h of Tg treatment (Figure 4.16b). This is also observed for *Gadd34* in the Perk pathway, whereas *Perk* expression itself is increasing at 4 h (Figure 4.16c). *Atf6α* pathway components *Edem1*, *Derl3* and *Creld2* start to be upregulated notably after 4 h Tg, while *Atf6α* shows first upregulation after 2 h of treatment (Figure 4.16d). An explanation for the delayed induction of *Edem1*, *Derl3* and *Creld2* might be the initial processing of *Atf6α* in the Golgi, which is needed to release the transcriptionally active form of *Atf6α*. Furthermore, as observed in the chronic ER stress model (Figure 4.14a-c), the expression of *GFP* is not induced in the same amplitude as *Creld2*. Similar to ER stress marker genes and *Gadd34*, 1 h Tg treatment leads to the activation of the *Ire1α* pathway, indicated by increasing *sXbp1* levels. Notably, *sXbp1* levels peak at 4 h, but are reduced thereafter to levels observed after 1 h Tg treatment. *Ire1α* displays upregulation after 4 h followed by a decrease in gene expression at 8 h of treatment (Figure 4.16e).

In considerations of choosing the appropriate ER stress pulse duration, the cell viability analyses narrow down the time span to 2–4 h, since *Creld2*^{+/+} cells show equal proliferation rates as the untreated controls, while *Creld2*^{-/-} MEFs fail to do so. For



a full UPR activation the induction of ER stress marker genes, as well as most UPR pathways, 1 h is sufficient. Although *Atf6 α* pathway induction is initiated after 2 h, a complete response is seen only after 4–8 h. Taking the observed differences in cell viability and the time-frame of UPR initiation into account, a 2 h pulse of Tg was used in subsequent experiments to analyse ER stress recovery.

To determine how wild-type and *Creld2*^{-/-} MEFs cope with a short but strong ER stress stimulus provoked by Tg and how the UPR machinery is orchestrated to enable recovery of cells, the ER stress markers and components of all three UPR pathways were analysed on transcriptional and translational level over a period of up to 46 h post 2 h ER stress challenge with 1 μ M Tg.

4.6.2.2 Marker regulation during ER stress recovery

During ER stress recovery (Figure 4.17a) *Grp94* and *Chop* gene expression is upregulated after the Tg pulse and slowly decreases over time. This behaviour of gene expression is observed in both genotypes. However, *Creld2*^{-/-} cells show reduced *Grp78* and *Grp94* gene expression levels the later recovery phase compared to *Creld2*^{+/+} MEFs. Furthermore, *Creld2*^{-/-} cells display increased *Dr5* expression at the beginning and the end of the recovery phase. Additionally, protein expression of Grp78 and Chop was assessed (Figure 4.17b,c). Notably, initial Grp78 levels show a 2-fold increase in *Creld2*^{-/-} cells in comparison to the wild-type and also Chop expression starts to increase in *Creld2*^{-/-} MEFs after 10 h, while *Creld2*^{+/+} cells reveal steady Chop levels until 30 h with reduction of Chop at 48 h.

Figure 4.16 (preceding page): Establishment of the ER stress recovery model in MEFs. (a) Analysis of cell viability after acute ER stress. *Creld2*^{-/-} (n=8) and *Creld2*^{+/+} (n=5) MEFs were treated with 1 μ M Tg for 0–8 h with subsequent incubation without Tg for 5 days following assessment of viability. *Creld2*^{-/-} cells show significant reduction in cell numbers compared to the wild-type control after 2 h and 4 h of Tg challenge. (b) Gene expression of *Grp78* and *Chop* is induced in MEFs after 1 h of Tg incubation. (c) Perk pathway activation. *Gadd34* is induced after 1 h Tg treatment. (d) Transcriptional upregulation of *Atf6 α* pathway components is begins after 4 h Tg treatment. (e) *Ire1 α* pathway activation. *sXbp1* expression is induced after 1 h Tg challenge and increases until 4 h followed by a reduction at time point 8 h. Gene expression is presented as mean \pm SD relative to the 0 h controls, which were set to 1. Coloured circles represent individual MEF clones (n=3 for wild-type and n=4 for *Creld2*^{-/-} MEFs, except for *Ire1 α* , where n=2 for *Creld2*^{+/+} and n=3 for *Creld2*^{-/-}. P-values below p=0.1 are indicated. P-values were calculated using unpaired, two-tailed Student's t-test.

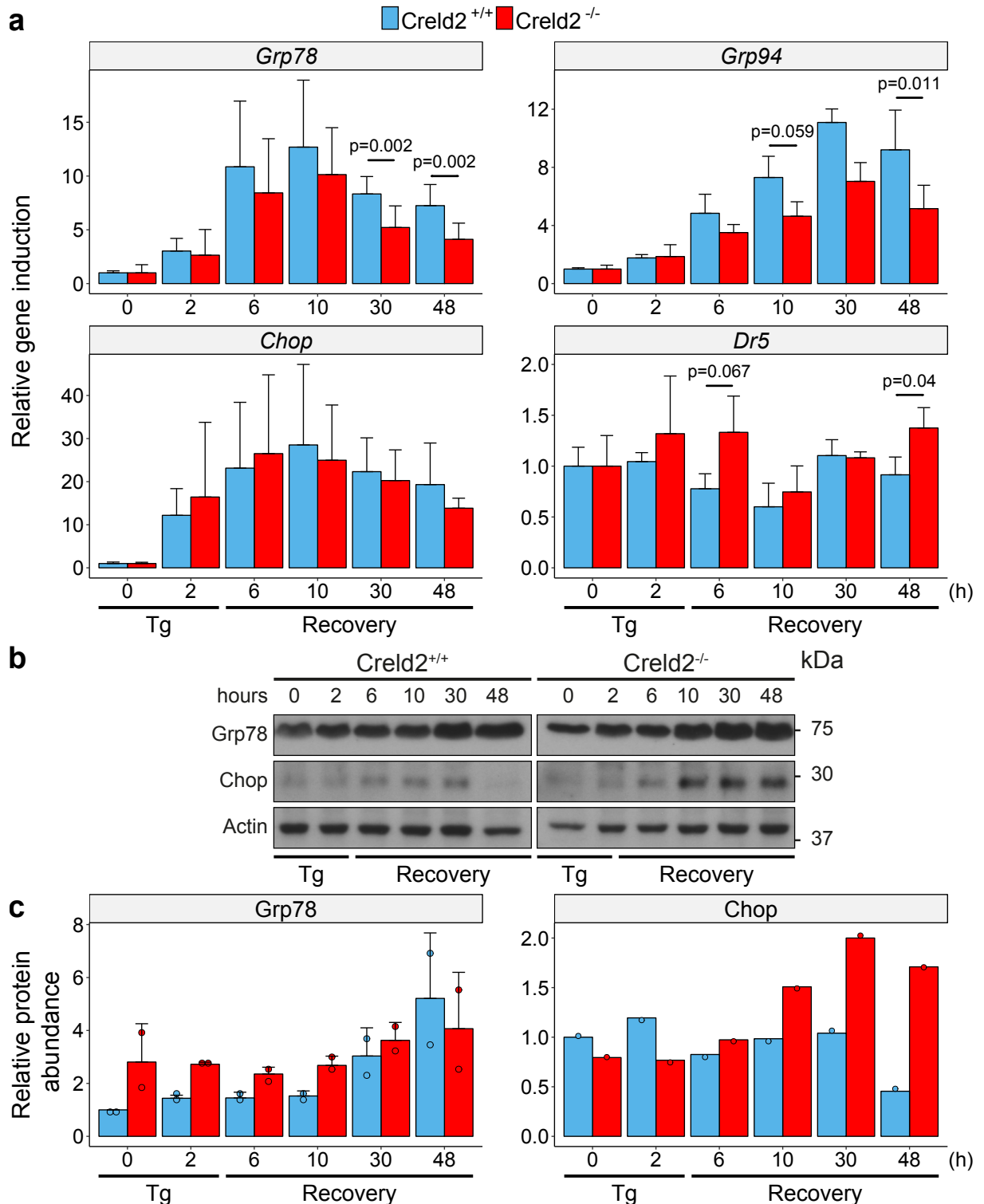


Figure 4.17: Regulation of ER stress markers during ER stress recovery. (a) Gene expression analysis of *Grp78*, *Grp94*, *Chop* and *Dr5* in *Creld2*^{+/+} (n=10, except for *Dr5* where n=3) and *Creld2*^{-/-} (n=8, except of *Dr5* where n=3) MEFs. *Grp78* and *Grp94* show significantly reduced induction after 10–48 h in *Creld2*^{-/-} fibroblasts compared to the wild-type controls. *Dr5* expression is elevated in *Creld2*^{-/-} MEFs at 6 h and 48 h. (b) Immunoblot analysis and (c) quantification of *Grp78* and *Chop*. *Creld2*^{-/-} cells show upregulated *Grp78* from 0–10 h and elevated *Chop* levels after 10–48 h. Protein levels were normalized to β -Actin. Coloured circles represent measured MEF clones (for *Grp78* n=2 and for *Chop* n=1 for both genotypes). Gene expression and protein quantification data are presented as mean \pm SD. P-values were calculated using unpaired, two-tailed Student's t-test.

4.6.2.3 Perk pathway regulation during ER stress recovery

Further differences in the UPR are noticeable in the Perk pathway (Figure 4.18). While gene expression of *Perk* and *Gadd34* in *Creld2*^{-/-} cells are similar to wild-type cells (Figure 4.18a), activation of Perk and eIF2 α on protein level differ between the two groups (Figure 4.18c). Under steady state, *Creld2*^{-/-} MEFs show reduced P-Perk/Perk and P-eIF2 α /eIF2 α ratios. After ER stress induction, wild-type cells display an increase of the P-Perk/Perk ratio at 48 h, whereas *Creld2*^{-/-} cells show no increase in Perk phosphorylation ratio from 6–48 h. In addition, wild-type MEFs exhibit increasing P-eIF2 α /eIF2 α ratios until 10 h of the experiment, which is followed by a decrease to baseline values after 30 h. In contrast, *Creld2*^{-/-} cells show a delayed phosphorylation of eIF2 α with a peak after 30 h without reaching baseline levels even after 46 h (Figure 4.18b,c).

4.6.2.4 Atf6 α pathway regulation during ER stress recovery

In the Atf6 α pathway *Creld2* expression peaks at 30 h of experiment with extents of 15-fold, whereas *GFP* gene expression in *Creld2*^{-/-} cells is marginal during recovery (Figure 4.19a). Reduced induction of GFP in *Creld2*^{-/-} cells recovery is similar to what has been observed in the chronic ER stress model (Figure 4.14a) and in the establishment of the ER recovery model (Figure 4.16d). The same is true on protein level, where GFP induction is not detectable (Figure 4.19b), while *Creld2* protein levels are elevated after 30 h and 48 h. Further, *Derl3* gene expression is significantly reduced in the *Creld2*^{-/-} MEFs after 30–48 h in comparison to *Creld2*^{+/+} cells (Figure 4.19b,c).

4.6.2.5 Ire1 α pathway regulation during ER stress recovery

In the Ire1 α branch, *Creld2*^{-/-} and wild-type MEFs show similar behaviour after the ER stress challenge (Figure 4.20). Both, *Ire1 α* gene expression and splicing of *Xbp1* (s*Xbp1*) during the recovery phase is increased, and remains at high levels even after 48 h.

Taken together, the results from *in vitro* ER stress studies reveal reduced cell viability in *Creld2*^{-/-} MEFs, which is consistent in both ER stress models. Additionally, *Creld2*^{-/-}

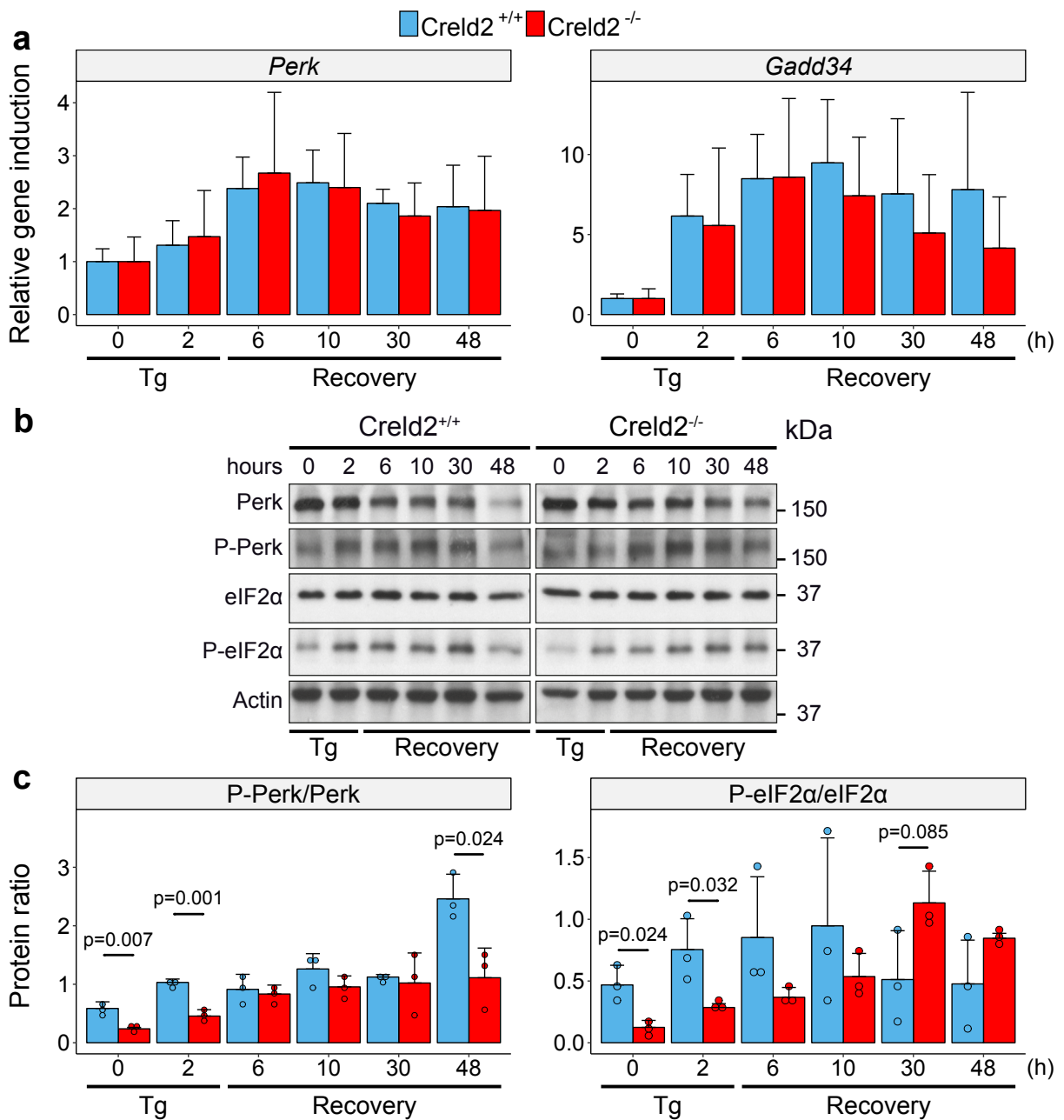


Figure 4.18: Regulation of Perk pathway induced components during ER stress recovery. (a) Gene expression analysis of *Perk* and *Gadd34* in *Creld2*^{+/+} (n=10) and *Creld2*^{-/-} (n=8) MEFs. Transcriptional induction of these genes is not altered in *Creld2*^{-/-} fibroblasts compared to the wild-type controls. (b) Immunoblot analysis and (c) quantification and assessment of Perk and eIF2α activation by determination of their phosphorylation levels. Protein levels were normalised to β-Actin and ratios of phosphorylated to unphosphorylated proteins were determined. *Creld2*^{-/-} cells show reduced levels of P-Perk and P-eIF2α from the start of the experiment. Phosphorylation of Perk in *Creld2*^{+/+} MEFs peaks at 48 h while it stagnates in *Creld2*^{-/-} cells after 6 h. Phosphorylation of eIF2α increases until 10 h and drops to control levels afterwards in wild-type MEFs, whereas P-eIF2α levels in *Creld2*^{-/-} increase slower and reach the peak at 30 h of the experiment. Coloured circles represent measured MEF clones (*Creld2*^{+/+} and *Creld2*^{-/-}, n=3). Gene expression and protein phosphorylation ratio data are presented as mean ± SD. P-values were calculated using unpaired, two-tailed Student's t-test.

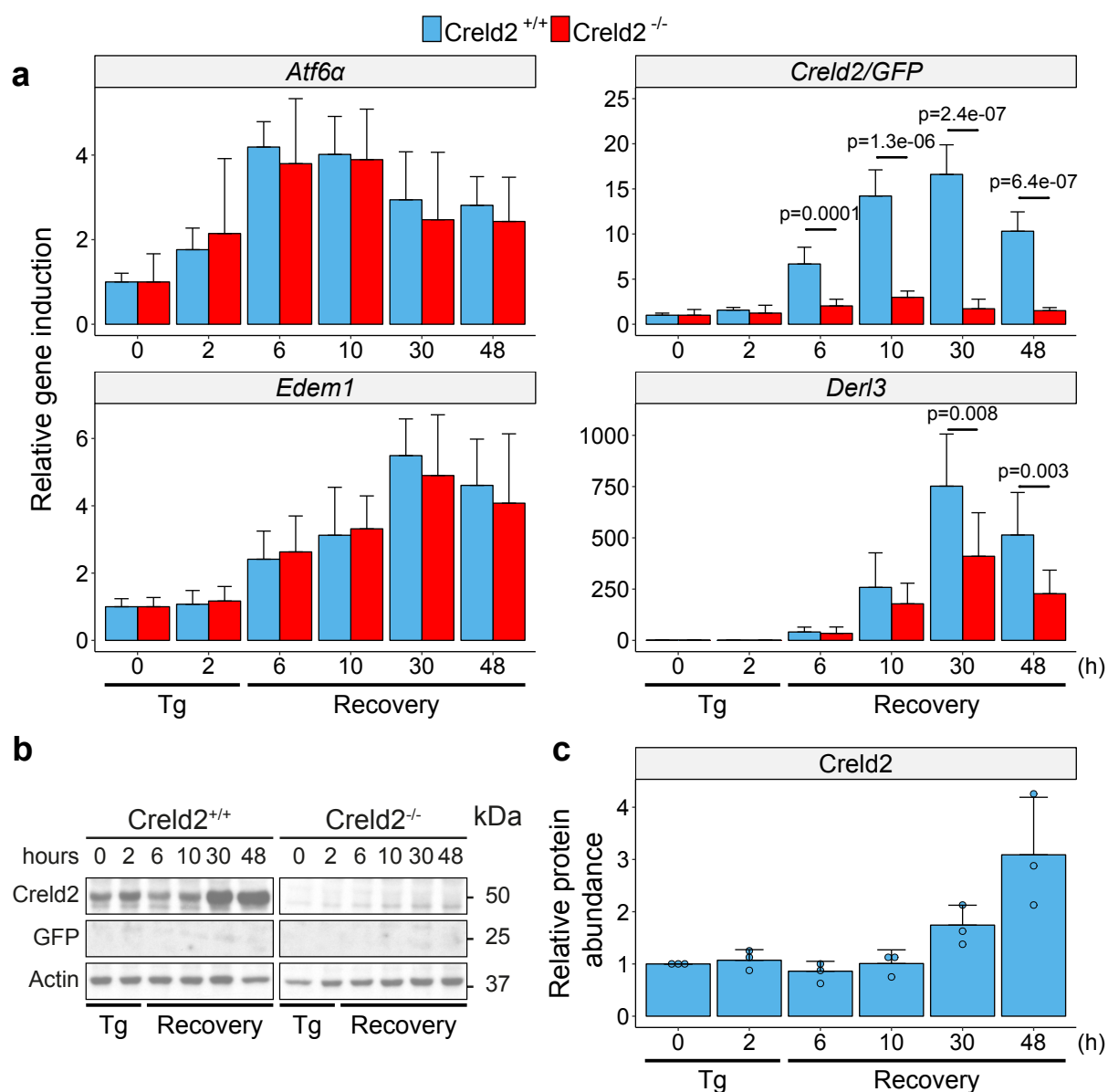


Figure 4.19: Regulation of *Atf6α* pathway induced components. (a) Gene expression analysis of *Atf6α*, *Creld2* in *Creld2*^{+/+} and *GFP* in *Creld2*^{-/-}, *Edem1* and *Derl3* in MEFs (n=10 for *Creld2*^{+/+} and n=5–8 for *Creld2*^{-/-}). Transcriptional induction of *Atf6α* and *Edem1* is not altered in *Creld2*^{-/-} fibroblasts compared to the wild-type controls. Gene expression of *Creld2* is induced after 6 h of experiment, while expression of *GFP* remains approximately at the baseline level over the whole time course. *Derl3* is significantly reduced in *Creld2*^{-/-} cells after 30–48 h of experiment. (b-c) Immunoblot analysis (b) and quantification of immunoblots (c) of *Creld2* and *GFP* protein levels. Determination of *GFP* protein levels was unattainable in *Creld2*^{-/-} cells and was omitted in the evaluation. *Creld2* protein abundance increases after 30 h and is rising until the end of the monitoring time. Coloured circles represent individual MEF clones (n=3). Protein levels were normalized to β -Actin and presented relative to the 0 h controls. Gene expression and immunoblot analyses are presented as mean \pm SD. P-values are indicated and were calculated using unpaired, two-tailed Student's t-test.

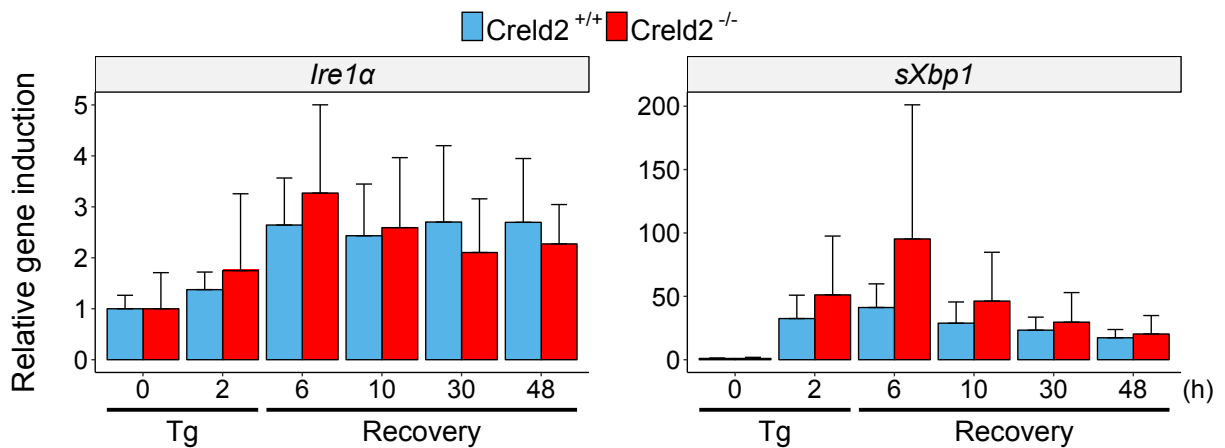


Figure 4.20: Regulation of the *Ire1α* pathway during ER stress recovery. Gene expression analysis of *Ire1α* and *sXbp1* in *Creld2*^{+/+} (n=10) and *Creld2*^{-/-} (n=8) MEFs. Gene expression is presented relative to the 0 h controls, which were set to 1. Gene expression is presented as mean ± SD.

cells display a late and insufficient response to ER stress during ER stress recovery as evidenced by UPR dysregulations in the Perk and Atf6 α branches. These results suggest that *Creld2* is involved in the regulation at least two UPR branches during ER stress.

4.7 Identification of *Creld2* interaction partners

The general *in vivo* and *in vitro* analyses of animals and cells deficient for *Creld2* provides a basic insight into emerging abnormalities due to *Creld2* absence. The observed phenotypes resulting from *Creld2* deficiency would suggest *Creld2* involvement in profoundly complex processes, for instance, in the metabolism of carbohydrates and fatty acids and the UPR. To narrow down the potential molecular function of *Creld2*, its protein interaction partners were analysed by affinity purification with subsequent mass spectrometrical identification and quantification of co-purified proteins. For this purpose, tagged *Creld2* constructs were used to co-purify protein interaction partners. To exclude inhibition of protein binding due to the fused tag, *Creld2* was tagged N- and C-terminally. Furthermore, *Creld2* was purified from either transiently or stably expressing HEK cells to enable distinction between specifically and unspecifically bound chaperones, since it is known that a strong transient overexpression increases the co-purification of heat shock proteins (HSPs) [84]. To reduce unspecific binding and for purification of proteins under native conditions, *Creld2*

was fused to the tandem affinity tag comprised of two StrepII and one Flag-tag (SF-tag) and purified by tandem affinity purification (TAP) according to Gloeckner et al. [54]. The SF-tag was fused to the N- or C-term of Creld2 with the Flag-moiety facing the N- or C-term, respectively. Purified samples from transiently or stably expressing cells transfected with a mock vector only containing the SF-tag were included in the analysis to exclude unspecific binding of proteins to the SF-tag.

Proteins identified by mass spectrometry were analysed by hierarchical clustering of mean protein intensities co-purified with each condition to visualise general differences and similarities between all five conditions (Figure 4.21a). Here, it is noticeable that samples from transiently expressing cells show a different protein profile than those from stably expressing cells. Furthermore, general differences between Creld2-containing TAP samples and their respective mock controls can be detected. To evaluate the three Creld2-containing TAP samples for common co-sedimented proteins, enriched proteins in Creld2 pull-down samples were compared and visualised in a Venn diagram (Figure 4.21b) (for a detailed protein list, which are enriched in each Creld2-containing TAP sample see Appendix A1). Comparing enriched proteins in the Creld2-containing TAP sets displays an overlap of all three sets for Creld2 and Enolase 1 (ENO1). For a better understanding of how the co-purified proteins might be biologically associated to each other, enriched proteins (Appendix A1) were analysed for functional interactions to one another using the Reactome pathway database, which contains manually curated and peer-reviewed protein interaction and pathway analysis data. Subsequently, proteins were manually separated according to their main subcellular localisation (Figure 4.21c). Co-purified proteins from virtually every cell compartment are found enriched in Creld2 TAP samples. Moreover, two-thirds of these proteins display interconnectivity, leaving one-third of the identified proteins without mapped interactions due to lacking information on protein interactions in the Reactome pathway database. In addition, pathway enrichment analysis was performed to investigate the biological processes of the enriched co-purified proteins (Table 4.1). Among the top 20 enriched pathways with an $FDR \leq 0.05$, pathways involved in glucose metabolism and the activation of the UPR are present. The potential involvement of Creld2 in the regulation of these pathways is in line with the observed glucose

metabolism (Figure 4.5) and UPR pathway regulation (Section 4.6) phenotypes in *Cred2*^{-/-} mice and cells, respectively.

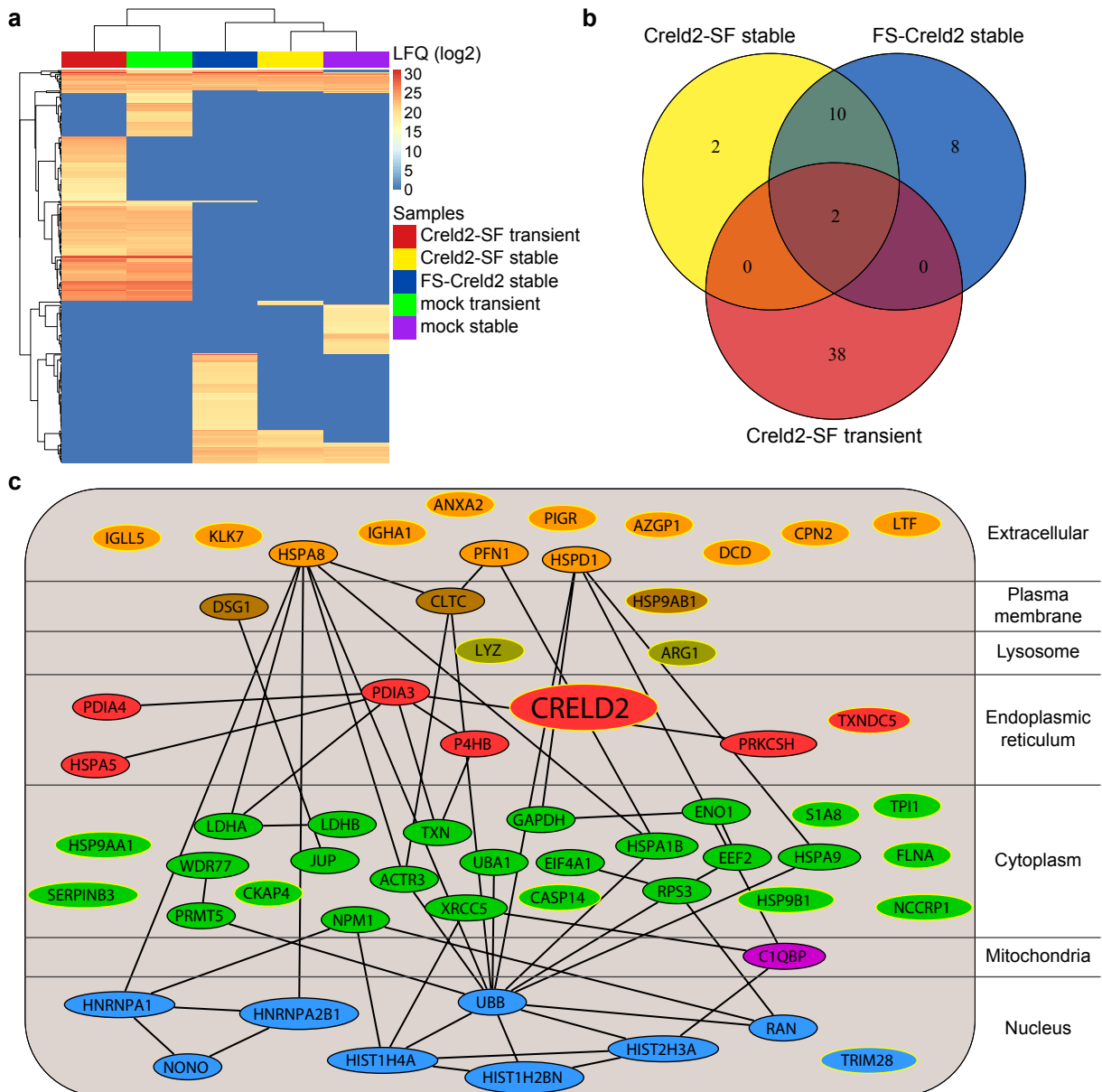


Figure 4.21: Analysis of *Cred2* interaction partners. (a) Hierarchical clustering of co-purified proteins from indicated samples. Clustering was performed on mean protein LFQ intensities (log₂-transformed) from n=3 for each sample condition. (b) Venn diagram of co-purified proteins enriched in pull downs with tagged *Cred2* vs. mock constructs. (c) Reactome analysis and spatial separation of proteins in (b). Protein nodes with yellow border indicate proteins without interaction annotation. **LFQ**: Label-free quantification **SF**: StrepII-Flag tag; **FS**: Flag-StrepII tag; **Cred2-SF**: C-terminally tagged *Cred2*; **FS-Cred2**: N-terminally tagged *Cred2*; **mock**: SF tag control; **transient**: Purification 72 h post-transfection; **stable**: Purification from stably expressing cells.

Table 4.1: Proteins affiliated to enriched pathways

Reactome Pathway	FDR	Hit proteins
RMTs methylate histone arginines	0.0115	PRMT5, WDR77, HIST1H4A
HSF1-dependent transactivation	0.0115	HSP90AB1, HSP90AA1, HSPA8
TFAP2A acts as a transcriptional repressor during retinoic acid induced cell differentiation	0,0119	HSPD1, NPM1
Metal sequestration by antimicrobial proteins	0.0119	S100A8, LTF
Glycolysis	0.0144	ENO1, TPI1, GAPDH
Gluconeogenesis	0.0147	ENO1, TPI1, GAPDH
Golgi Associated Vesicle Biogenesis	0.0149	CLTC, TXNDC5, HSPA8
RNA Polymerase I Promoter Opening	0.0157	HIST2H3A, HIST1H4A
Gene Silencing by RNA	0.0217	HSP90AA1, HIST2H3A, HIST1H4A, RAN
DNA methylation	0.0217	HIST2H3A, HIST1H4A
ATF6 (ATF6-alpha) activates chaperone genes	0.0250	HSP90B1, HSPA5
Activated PKN1 stimulates transcription of AR (androgen receptor) regulated genes KLK2 and KLK3	0.0273	HIST2H3A, HIST1H4A
SIRT1 negatively regulates rRNA Expression	0.0273	HIST2H3A, HIST1H4A
HSF1 activation	0.0273	HSP90AB1, HSP90AA1
ATF6 (ATF6-alpha) activates chaperones	0.0273	HSP90B1, HSPA5
The NLRP3 inflammasome	0.0273	HSP90AB1, TXN
trans-Golgi Network Vesicle Budding	0.0273	CLTC, TXNDC5, HSPA8
Clathrin derived vesicle budding	0.0273	CLTC, TXNDC5, HSPA8
Transcriptional regulation by small RNAs	0.0333	HIST2H3A, HIST1H4A, RAN
Formation of the cornified envelope	0.0375	CASP14, DSG1, JUP

5 Discussion

5.1 General phenotype of the *Creld2*-knockout-mouse

Consistent with other studies of the *Atf6 α* pathway, which show that most of *Atf6 α* downstream targets are dispensable during fetal and postpartal development [85–87], *Creld2* function also does not seem to be relevant for embryonic development, as evidenced by similar Mendelian distributions of *Creld2*^{+/+} and *Creld2*^{-/-} mice (Figure 4.1a). Additionally, *Creld2*^{-/-} mice show normal body weight gain during ageing (Figure 4.1b) when compared to wild-type mice and exhibit equal live expectancies as *Creld2*^{+/+} littermates. Nevertheless, the liver, which experiences constant ER stress, seems to require *Creld2* function. Despite showing no major differences in body weights, liver weights of aged, 12-months-old, *Creld2*^{-/-} mice are significantly reduced (Figure 4.1c) and *Creld2*^{-/-} mice also show reduced liver to body weight ratios (Figure 4.1d), although not significant, which might be accountable to the high variability of measured individual mice. Histological examination of *Creld2*^{-/-} mice livers shows that young (1-month-old) *Creld2*^{+/+} and *Creld2*^{-/-} mice display a healthy liver structure (Figure 4.2a), while circa 75% of aged *Creld2*^{-/-} mice show accumulation of neutral lipids in hepatocytes with abnormal GS expression (Figure 4.2b). These results indicate that *Creld2* is involved in metabolic homeostasis of the liver during ageing.

5.2 Metabolic aberrations in the *Creld2*-knockout-mouse

5.2.1 Gender-specific differences

To assess whether *Creld2* deficiency leads to gender-specific phenotypes, metabolic phenotypes of male and female mice were analysed separately. Even though young *Creld2*^{-/-} males do not show any histological signs of steatosis (Figure 4.2a), elevated levels of FFAs, DAGs, TAGs, cholesterol and cholesteryl esters can already be observed when compared to age-matched wild-type controls (Figure 4.3a) indicating that male *Creld2*^{-/-} mice are prone to steatosis development. Both, histological and quantitative analysis of livers in 1-year-old *Creld2*^{-/-} mice show a clear accumulation of

lipids (Figure 4.2b), which is not observed in littermate controls. The hepatosteatosis in aged *Creld2*^{-/-} males is accompanied by dysregulated gene expression of the master regulator of mitochondrial biogenesis *Pgc1α* (Figure 4.4a), and *Apoc2* and *Dgat2*, which are involved in TAG metabolism (Figure 4.4b). Further, *Creld2*^{-/-} males exhibit insulin resistance and reduced gene expression of glucose transporters *Glut2* and *Glut4* (Figure 4.5b,e). Interestingly, 1-year-old female *Creld2*^{-/-} mice seem to be protected from liver steatosis, since they neither show any differences in hepatic lipid levels compared to age-matched wild-type controls (Figure 4.3b), nor do they exhibit drastic differences in gene expression of metabolic markers (Figure 4.4a-d) or in glucose metabolism (Figure 4.5e,f).

Gender-specific hormonal regulation differences might explain the lack of liver steatosis in female mice. It is well known that women entering the menopause or those with genetic defects in oestrogen production exhibit increased risks of developing liver steatosis [88, 89], which is also true for mice [90], and that supplementation with oestrogen protects against metabolic syndrome [91] and improves liver functionality [92].

Therefore, *Creld2*^{-/-} female mice are most likely protected against hepatosteatosis due to the increased production of estrogen. The susceptibility for metabolic imbalances and the development of liver steatosis in female *Creld2*^{-/-} mice would potentially increase on entering the menopause.

The following discussion will focus upon the phenotype of male *Creld2*^{-/-} mice if not otherwise mentioned.

5.2.2 NAFLD in *Creld2*^{-/-} mice

NAFLD and insulin resistance are known to be closely correlated with one another, but until now it is still uncertain which condition is the cause and which the consequence. Presumably, both metabolic aberration states can trigger the other one, which is due to impairment of either the lipid or glucose metabolism evoking insulin resistance or hepatosteatosis, respectively [93, 94]. This, in turn, creates a vicious cycle leading to aggravating conditions. To unveil the metabolic dysregulations, which might lead to insulin resistance and hepatosteatosis in 1-year-old *Creld2*^{-/-} males, mice were

analysed for their glucose and lipid metabolism states.

To analyse the systemic glucose metabolism in 1-year-old males, glucose tolerance tests (GTTs) and insulin tolerance tests (ITTs) were performed, which are suited to show the metabolic situation of the major glucose up-taking organs, namely skeletal muscle, liver and adipose tissue. GTTs show a slower glucose clearance from the blood (Figure 4.5b) and ITTs reveal insulin resistance (Figure 4.5b) in *CreId2*^{-/-} males. Since it is known that skeletal muscle is the main site of insulin-stimulated glucose uptake, followed by adipose tissue [95], these results suggest that *CreId2*^{-/-} mice show insulin resistance likely due to impaired glucose uptake in extrahepatic organs, such as muscle and adipose tissue.

Further evidence, which would support this assumption, is the reduction of *Glut2* and *Glut4* gene expression (Figure 4.5e), which indicate a decreased ability of the cell to take up glucose. Especially the reduction of *Glut4* implicates that the muscle or adipose tissue is the primary cause of insulin resistance. This is because *Glut4* is the main insulin-driven glucose transporter in myocytes and adipocytes [69].

In addition, the elevated P-Akt/Akt ratio in *CreId2*^{-/-} livers (Figure 4.5c,d) might be a compensatory mechanism to increase glucose uptake because activated Akt induces Glut4 translocation to the plasma membrane [66]. Analysis of skeletal muscle or adipose tissue insulin resistance combined with gene and protein expression assessment in these tissues could verify this assumption.

Notably, the impaired glucose influx into adipose tissue leads to an elevated release of FFAs by adipocytes into the bloodstream. These FFAs are taken up by the liver and skeletal muscle for, e.g. ATP synthesis via β -oxidation. When the abundance of FFAs exceeds a certain level, the β -oxidation rate diminishes due to mitochondrial overload, triggering mitochondrial dysfunction and the accumulation of lipids in these organs, which eventually results in steatosis and increased insulin resistance [96]. Such an increased FFA release from adipose tissue under this condition might explain the elevated FFA levels (Figure 4.3a) and the reduced ATP levels (Figure 4.5f) in livers of 1-year-old *CreId2*^{-/-} mice.

Unlike adipose tissue, the liver cannot store excess amounts of lipids without impairment of metabolic processes. Therefore, hepatocytes convert these FFAs to

TAGs for secretion into the bloodstream in very low density lipoproteins (VLDLs). In conditions of FFA overload, the liver fails to meet the demand of FFA conversion to TAGs, which results in increased levels of DAGs causing metabolic dysregulations [97]. This suggests that DAGs in *Creld2*^{-/-} livers (Figure 4.3a) indeed accumulate as a result of increased FFA influx. Additionally, as mentioned in Section 5.2.1, gene expression of *Apoc2* and *Dgat2* (Figure 4.4b) is decreased in *Creld2*^{-/-} mice, which would affirm the inability of the liver to process the FFA overflow.

The liver is also the site of cholesterol synthesis with acetyl-CoA as the fundamental building block. Since the liver is oxidising excess FFAs and each cycle of FFA β -oxidation produces one acetyl-CoA molecule, this might cause increased cholesterol synthesis and accumulation as is observed in livers of aged *Creld2*^{-/-} mice (Figure 4.3a). Taken together, assessment of the metabolic *Creld2*^{-/-} phenotype suggests that *Creld2* is a potential genetic risk factor in the development of NAFLD and metabolic syndrome. The results imply that *Creld2*^{-/-} mice suffer from skeletal muscle and adipose tissue insulin resistance, which consequently leads to lipid accumulation and dysregulated metabolic processes in the liver. Instead of letting the mice age to accumulate more and more lipids over a long time, one could challenge mice with a high-fat diet. This could reveal an essential function of *Creld2* to ameliorate liver stress caused by excess lipid influx, especially with regards to a western diet, since obesity and overnutrition are the leading cause of NAFLD, nowadays.

5.3 Liver injury and inflammation

The accumulation of lipids in hepatocytes for extended periods leads to lipotoxicity, disturbed signalling pathways and lipid-induced apoptosis [98]. Exacerbation of NAFLD to further stages accompanied by increased apoptosis of hepatocytes results in inflammatory responses [99, 100]. Since the severity of liver steatosis in *Creld2*^{-/-} males cannot be determined by simply assessing liver lipids and glucose metabolism, the steatosis progression grade was determined by analysing gene expression of markers mirroring liver health state (Figure 4.6).

To determine imbalances in proliferation and apoptosis the genes *Erk1/2* and *Dr5* were assessed. *Erk1/2* are kinases belonging to the mitogen-activated protein kinase family

and, among other functions, play important roles in cell proliferation [71]. Increased *Dr5* gene expression is observed during ER stress-induced apoptosis [22] and is also correlated to lipotoxicity in liver steatosis [101]. Thus, dysregulated *Erk1/2* or *Dr5* gene expression in *Creld2^{-/-}* mice would indicate pathologic cell fates. Yet, *Creld2^{-/-}* mice do not show differences in cell proliferation or apoptosis compared to *Creld2^{+/+}* mice as evidenced by similar gene expression of *Erk1/2* and *Dr5*. Further, gene expression of the acute phase response markers *Apcs* and *Saa3* remain unchanged (Figure 4.6b) and expression levels of pro-inflammatory cytokines *Tnf α* and *Il6* are slightly decreased in *Creld2^{-/-}* males when compared to littermate controls (Figure 4.6c). This indicates that *Creld2^{-/-}* mice rather experience a benign liver steatosis since aggravation of hepatosteatosis is correlated with increased acute phase response genes as well as inflammatory cytokines.

The absence of inflammation could be the result of either reduced recruitment of leukocytes from the bone-marrow to injured liver tissue sites or a deficiency in the response by Kupffer cells, which are major producers of pro-inflammatory cytokines. Both processes are essential for the replenishment of tissue-resident macrophages, which in turn maintain and repair tissue by eliciting pro-inflammatory responses [102, 103]. However, Kupffer cell numbers are unchanged in *Creld2^{-/-}* males compared to *Creld2^{+/+}* males (Figure 4.7a). Further, BMDMs that would give rise to pro-inflammatory immune cells in the liver during steatosis [104, 105] were tested for their inflammatory response to stimulation. LPS stimulation of BMDMs and assessing the gene expression of pro-inflammatory cytokines *Tnf α* , *Il1 β* and *Il6* reveals proper immune responses in *Creld2^{-/-}* BMDMs.

Hence, analyses of liver injury and inflammation states imply that *Creld2^{-/-}* males still exhibit a benign form of steatosis.

5.4 Impaired UPR as the trigger of hepatosteatosis

The UPR is a crucial machinery for the maintenance and re-establishment of cellular homeostasis and activity. Unresolved ER stress leads to attenuation of cellular processes, directing the cell into apoptosis and consequently impedes organ function. Besides the three major tasks of halting global protein synthesis, increasing folding

capacity and enhancing unfolded protein degradation, the UPR reveals more and more crucial metabolic functions reaching beyond the sole elimination of ER stress. The UPR receives increasing importance in the regulation of genes involved in lipid metabolism and is frequently linked to the development of fatty liver during conditions of disturbed activity in any of the three UPR pathways [15, 36, 34, 16, 32].

Creld2 is induced by the Atf6 α pathway during ER stress and lack of Creld2 increases susceptibility for fatty liver development and thus might constitute a connecting element between UPR regulation and metabolism homeostasis.

However, the mode of function of Creld2 and which pathways are downstream of Creld2 remain enigmatic. Hence, the aim was to unravel whether Creld2 is at the intersection of metabolism and UPR by contributing to proper regulation of the UPR.

For this purpose, UPR pathways in livers of 1-year-old mice were investigated to test whether UPR downstream signalling cascades are impaired in *Creld2*^{-/-} mice (Figure 4.8). The results display similar steady state levels of assessed UPR components, except for increased gene expression of *Grp94* (Figure 4.8a) and slightly reduced P-eIF2 α /eIF2 α ratios (Figure 4.8e,f) in *Creld2*^{-/-} males. This would imply that ablation of Creld2 does not affect UPR regulation and that increased *Grp94* expression might be a compensatory mechanism to ameliorate the metabolic phenotype, due to Grp94 involvement in various processes, such as in pancreatic β -cell functionality [106] and maintenance of liver parenchymal health state [107]. However, some experimental issues could have masked the results. First, the steatotic phenotype in aged *Creld2*^{-/-} males is not 100% penetrant and only observed in circa 75%. This phenotypic heterogeneity might conceal effects in UPR regulation since analyses of livers were performed on mice cohorts without a prior histological assessment of steatosis. Second, UPR analyses in unchallenged livers with only mild steatosis (as discussed in section 5.3) might not be a proper assessment of UPR regulation, since changes in the UPR at steady state may be minor or too transient to be revealed.

Therefore, an isolated *in vitro* system approach was chosen for in-depth analysis of UPR regulation under various ER stress challenge conditions enabling constant measurements of cellular and molecular changes. Two conditions, termed chronic ER stress and ER stress recovery, were applied as an approach to challenge cells while

mimicking potential stress situations in the liver.

These experimental setups revealed that *Creld2*^{-/-} MEFs are unable to resolve chronic stress conditions (Figure 4.11). Also in the recovery model, where a short pulse of a moderately strong ER stress was evoked with subsequent recovery for five days, *Creld2*^{-/-} cells were unable to overcome the challenge and display reduced cell numbers compared to *Creld2*^{+/+} MEFs (Figure 4.16a).

Thus, in contrast to analyses of biologically heterogenous livers, the results from *in vitro* experiments strongly indicate a need for Creld2 when cells experience emerging ER stress.

5.4.1 Chronic ER stress

Analysis of UPR pathways including general ER stress marker during chronic ER stress, reveals dysregulation of Atf6 α downstream target genes *Edem1* and *Derl3* in *Creld2*^{-/-} cells (Figure 4.14a). Both *Edem1* and *Derl3* are important components of the ERAD machinery, implying that *Creld2*^{-/-} cells are unable to properly resolve ER stress due to deficiencies in degradation of unfolded proteins. However, components of the Perk and Ire1 α pathways and also ER stress markers do not show remarkable dysregulation of UPR components, which would indicate that Creld2 largely influences Atf6 α downstream targets.

5.4.2 ER stress recovery

In contrast to the chronic ER stress model, *Creld2*^{-/-} cells analysed during ER stress recovery exhibit extensive regulatory aberrations in various UPR pathways. Monitoring of general ER stress marker reveals reduced induction of chaperones *Grp78* and *Grp94* (Figure 4.17a), which is indicative for impaired activation of at least one UPR pathway since these markers are regulated by a combination of two or more UPR branches. However, Grp78 protein levels, which are elevated already in control (0 h) *Creld2*^{-/-} cells until 10 h of the experiment when compared to *Creld2*^{+/+} cells (Figure 4.17b,c), indicate that a homogenous cell population deficient for Creld2 undergoes UPR activation already during steady state conditions. In addition, gene expression of *Dr5* is elevated in *Creld2*^{-/-} MEFs after 48 h (Figure 4.17a) suggesting that *Creld2*^{-/-} cells are more susceptible for ER stress-induced apoptosis, which reflects the observed

reduction of cell number in *Creld2*^{-/-} cells left for recovery after 2 h and 4 h of Tg challenge (Figure 4.16a).

In this recovery model, lack of *Creld2* further impacts the Perk pathway (Figure 4.18) as *Creld2*^{-/-} cells display a reduced and delayed phosphorylation of Perk and eIF2 α , which is indicative for an inefficient and late activation of Perk and subsequent inhibition of eIF2 α (Figure 4.18b,c). Thus, during ER stress, global protein synthesis is not attenuated immediately in *Creld2*^{-/-} cells leading to exacerbation of ER stress through continuous influx of proteins into the ER, thereby burdening the ER with an abundance of non-native proteins for processing. Consequently, cells experience ER stress for a prolonged period, because the ER is overloaded and requires more time to fold and process the abundant proteins eventually leading to apoptosis.

Furthermore, dysregulated Perk pathway activation likely implicates altered Atf4 protein expression. Atf4 was reported to induce expression of pivotal genes for cholesterol metabolism, while Atf4 deletion results in accumulation of free cholesterol in livers of knockout mice [34]. Since it is crucial for the cell to esterify free cholesterol for storage, cholesteryl esters in *Creld2*^{-/-} male livers (Figure 4.3a) might be increased as a consequence of esterifying the excess free cholesterol.

These findings indicate that aberrant Atf4 regulation likely causes the increased cholesterol levels in *Creld2*^{-/-} males (Figure 4.3a) during ER stress.

Further deficiencies of UPR activation were observed in components regulated by the Atf6 α pathway. Consistent with results obtained in the chronic ER stress model (Figure 4.14a), induction of *Der13* gene expression during ER stress recovery is insufficient in *Creld2*^{-/-} MEFs (Figure 4.19a). The coherence of reduced *Der13* induction in both models suggests that *Creld2* is upstream of *Der13* gene expression and possibly also plays a role in regulating other components of the ERAD machinery.

Der13 accelerates clearance of the ER from unfolded proteins by re-translocating non-native glycoproteins from the ER to the cytosol for degradation. Hence, the insufficient induction of *Der13* would lead to sustained ER stress due to a slower removal of non-native proteins from the ER.

Combining the reduced *Der13* induction with the simultaneous delay in Perk pathway activation, thereby causing additional ER overload with non-native protein, would mean

an even stronger accumulation of ER stress.

To verify increased total protein accumulation in the ER of challenged *Creld2*^{-/-} cells, the ER distension could be assessed by electron microscopy [108]. Alternatively, the total amount of glycoproteins in different cellular fractions could be determined, as this would give insights on translocation efficiency of non-native glycoproteins since Der13 is reported to aid in the re-translocation of glycoproteins [109].

Of note, both chronic and recovery models display reduced or almost absent expression of the *GFP* reporter (Figure 4.14a,b and Figure 4.19a,b), indicating either loss of intron-mediated enhancer sequences due to the replacement of the complete *Creld2* gene locus with the *GFP* reporter, or a potential positive feedback loop of *Creld2* leading to its own induction. A possible mechanism for this feedback loop might be enhanced *Atf6* α shuttling to the Golgi and possibly also its proteolytic cleavage leading to increased *Atf6* α transcriptional activity, which could be tested in an *in vitro* overexpression model.

In the *Ire1* α pathway, *Creld2*^{-/-} cells show similar induction of *Ire1* α gene expression and splicing of *Xbp1* when compared to wild-type cells (Figure 4.20a), which would indicate that this pathway is not impaired in its function. However, sXbp1 was found to dimerise with the active transcription factor *Atf6* α to induce gene expression of ERAD components [25]. Further evidence provided by RNA-seq studies show that these two pathways function synergistically [16] so that the possibility of aberrant *Ire1* α pathway function cannot be excluded. Analysing *Atf6* α nuclear translocalisation together with RNA-sequencing in challenged *Creld2*^{+/+} and *Creld2*^{-/-} cells could clarify potentially dysregulated sXbp1 transcriptional activity.

5.4.3 Chronic ER stress versus ER stress recovery

Comparing the two *in vitro* ER stress models reveals consistent impairments in the regulation of *Atf6* α pathway components, suggesting a feed-forward loop influence of *Creld2* on its gene expression and the expression of *Der13*. Additional dysregulations in the Perk branch in the recovery model strongly suggest that *Creld2* is involved the regulation of several UPR branches. Since it is known that the three UPR branches regulate metabolic processes, these UPR signalling impairments caused by *Creld2*

absence might be the trigger of NAFLD in 1-year-old *Creld2*^{-/-} male mice.

Interestingly, the ER stress recovery model unveils considerably more defects in UPR activation than the chronic ER stress model. One possible reason might be a masking effect in the chronic model due to the challenge of cells with too high doses of ER stressors. Another explanation could be that the duration of ER stress over 48 h-72 h is inappropriate and fails to mimic physiological states, especially when cells are challenged by pharmacological ER stressors [110].

Naturally, most organs experience a temporary stimulus of ER stress, e.g. after taking in a meal or just after awakening, as this results in a rapid increase of metabolic demands, such as the instant production of large insulin amounts or processing of nutrients by the liver. Hence, the condition of persistent activation of the UPR might be too artificial and mostly unphysiological.

What remains uncertain in this study is to which extent *Creld2*^{-/-} cells are able to adapt to short but recurring ER stress, since in the recovery model cells were burdened only with a single transient pulse of ER stress. It would be interesting to investigate UPR activation and regulation in *Creld2*^{-/-} cells that have been challenged several times - in a recurring manner, as one would expect to happen under physiological conditions. This could give insights and possibly further clarify the development of liver steatosis in *Creld2*^{-/-} males. However, evidence from the recovery model point towards a delayed and insufficient UPR activation, which eventually would lead to accumulation of ER stress and thereby result in impaired organ function. Thus, the phenotype of *Creld2*^{-/-} livers may originate from incomplete resolution of ER stress, which is accumulating with time, thereby disabling the cells to respond to upcoming ER stress stimuli properly.

5.5 *Creld2* in bone development and maintenance

Several studies investigated *Creld2* involvement in bone development and growth. First, *Creld2* was found to be upregulated in growth plates of bones suffering from MCDS [41], a pathophysiological condition caused by collagen X mutation. Other studies indicate that *Creld2* plays a role in proper epiphyseal growth plate development, whereby *Creld2* is suggested to possess PDI activity and to be a component of the ECM [50, 73].

However, the previous studies did not have the advantage of possessing a knockout model to study bone formation. Therefore, the epiphyseal growth plate of 1-month-old *Creld2*^{-/-} mice was analysed. Indeed, derangements of chondrocytes in the proliferating zone and increased hypertrophic zone width in *Creld2*^{-/-} mice compared to *Creld2*^{+/+} controls (Figure 4.9a) suggest an important role of *Creld2* in chondrocyte differentiation. However, main characteristics of MCDS are defects in bone growth resulting in mild dwarfism with short limbs and unbalanced gait [111], which could not be observed in full *Creld2*-knockout mice, albeit mice with cartilage-specific deficiency of *Creld2*^{-/-} allegedly show retarded growth [73]. The reason for this controversy in observations remains unclear. However, due to the complexity of a whole organism with a myriad of metabolic process interactions and cross-talk between diverse organs, the possibility of a different phenotype in conditional knockout mice compared to a full knockout quite persists.

Zhang et al. reported that *Creld2* augments BMP9-induced osteogenic differentiation of MSCs leading to enhanced bone formation, while knockdown of *Creld2* shows reduced osteogenic differentiation [51]. Additionally, osteogenic differentiation itself demands the production of high protein amounts, which automatically leads to ER stress. Confirming evidence from analyses of *Atf6α* functionality in MCDS mice shows an *Atf6α*-dependent amelioration of disease severity [112], which supports the findings that *Creld2* is upregulated and found in chondrocytes of growth plates during ER stress conditions.

However, the observations by Zhang and colleagues are contradictory to the findings in 1-year-old *Creld2*^{-/-} mice. Here, the bone mineral density is increased in femurs of aged *Creld2*^{-/-} males and females when compared to age-matched wild-type controls (Figure 4.9b,c) indicating the onset of osteopetrosis.

To analyse the severity of increased bone density, the cellularity and abundance of stem cells were tested, since drastic changes in bone mass may have an impact on the bone-marrow niche. *Creld2*^{-/-} mice do not show any deviation in total cell numbers (Figure 4.10a) nor differences in HSC sub-populations in comparison to *Creld2*^{+/+} and *Creld2*^{+/-} mice (Figure 4.10d) although *Creld2* expression in LSK progenitor cells is present (Figure 4.10c). This indicates that the osteopetrosis in *Creld2*^{-/-} femurs is still

mild since differences in total cell numbers or LSK and HSC populations would be altered due to a displacement of bone-marrow by over-growing bone in the case of severe osteopetrosis.

A reason for this discrepancy could be that Zhang et al. do not use genetic models, but implanted MSCs transfected with murine Creld2 or with Creld2 siRNA so that it is not clear which effects might be provoked by the absence of Creld2 after extended periods of time on bone structure.

In summary, all of the reported studies of chondrodysplasia mice models showed Creld2 upregulation because the disease is mainly induced through unfolded proteins, which induce ER stress. Despite the discrepancies with previous studies, the results from *Creld2*^{-/-} mice suggest that Creld2 plays a role in bone formation, growth and maintenance by regulating proper UPR pathway activation (as discussed in Section 5.4).

5.6 Creld2 interaction partners

The abnormalities mentioned above in *Creld2*^{-/-} mice and MEFs suggest that Creld2 is involved in the regulation of metabolic processes and the activation of the UPR. However, these biological processes are extremely complex, and each is comprised of numerous pathways involving thousands of proteins cooperating in a myriad of reactions [113]. Thus, to identify the up- or downstream signalling pathways of Creld2, its molecular interaction partners were determined.

Creld2 interactome pathway enrichment analysis shows that protein interaction partners are involved in glucose metabolism and UPR regulation via the Atf6 α branch (Table 4.1). The regulation of these pathways by Creld2, which is consistent with the metabolic phenotype of *Creld2*^{-/-} mice (Figures 4.2, 4.3 and 4.5) and the observed dysregulations in UPR activation (Figures 4.14, 4.17, 4.18 and 4.19).

Evaluation of enriched proteins from Creld2 pull-downs versus their respective mock controls (Figure 4.21b) shows that the purification from transiently expressing cells co-precipitates many HSPs and PDIs (Table A1), albeit mean Creld2 abundance in all Creld2 precipitation conditions is similar. This implies that Creld2 requires extensive folding aid, thereby drawing chaperones, such as Grp78 (HSPA5), to oneself.

Conclusively, the attraction of numerous chaperones might result in the activation of UPR branches, since these chaperones need to dissociate from the ER stress sensors to assist in the folding of Creld2. In this case, Creld2 would function as a kind of decoy molecule, which indirectly triggers enhanced UPR activation. This assumption would be backed up by evidence from previous analyses, which show that a mere Creld2 overexpression induces gene expression of UPR downstream targets *Chop* and *sXbp1* after 48 h, although Creld2 protein levels are already increased 24 h post transfection [2].

Additionally, the idea of Creld2 being a decoy protein would be supported by the obtained results from ER stress recovery experiments, which show delayed phosphorylation of Perk and eIF2 α , and hence a late activation of the Perk downstream signalling cascade (Figure 4.18c) as well as insufficient induction of *Der13* gene expression (Figure 4.19a). The native Creld2 proteins residing in the ER might unfold during emerging ER stress resulting in chaperone attraction. The reason of Creld2 unfolding may be due to the shift from an oxidising to a reducing ER milieu [114] as a consequence of ROS production [115], which would lead to the reduction of disulfide bonds in the EGF-like domains of Creld2 (see structure in Figure 1.1).

Another mode of function of Creld2 to augment UPR activation might be to enhance the secretion of chaperones, such as Grp78 or HSPs in general. Creld2 is a glycoprotein [10, 2] and can be secreted [8, 50]. Likewise, Grp78 was found to be translocated to the plasma membrane [116], especially during ER stress [117], where it regulates and favours proliferation and cell survival [118, 119]. This would suggest that Creld2 might also serve as a protein shuttling guide for numerous chaperones and ECM proteins since several HSPs and ECM proteins were identified as Creld2 co-precipitates (Figure 4.21c). Increased Grp78 shuttling to the plasma membrane would consequently reduce Grp78 abundance in the ER, leading to less Grp78 for inactivation of the three ER stress sensors.

Taken together, these results suggest that Creld2 might function as a decoy molecule, sequestering HSPs, such as Grp78 (HSPA5), from the ER stress sensors due to its folding needs and thereby leads to enhanced activation of the UPR.

Further analysis of proteins enriched in Creld2 pull-downs (Figure 4.21b) revealed

the presence of ENO1 in all three Creld2 pull-down conditions (Table A1). ENO1 is a glycolytic enzyme involved in the break down of glucose to pyruvate [120] and is reported to take part in numerous other cellular processes, such as immune responses and development [121]. In addition, pull-down from stably expressing cells show common enrichment of two further proteins involved in glucose metabolism, namely lactate dehydrogenase (LDH) A and LDHB. LDHA converts pyruvate to lactate and is not affected by substrate or product inhibition, while LDHB reverses this reaction and is inhibited by high pyruvate concentrations [122].

Taking into account that *Creld2*^{-/-} males exhibit liver steatosis (Figure 4.2b, Figure 4.3), insulin resistance (Figure 4.5b) and decreased ATP levels (Figure 4.5f), the interaction of Creld2 with enzymes involved in glucose metabolism strongly suggests that Creld2 additionally plays a role in regulation of glucose processing.

To clarify whether Creld2 influences carbohydrate metabolism via regulating of ENO1 and LDHA/LDHB activity, biochemical assays for the determination of glycolysis and pyruvate conversion rates in *Creld2*^{+/+} and *Creld2*^{-/-} liver lysates could be performed.

In summary, Creld2 co-purification results further affirm that Creld2 most probably is involved in the regulation of metabolic processes and enhancement of UPR activation and thereby helps in maintaining metabolic homeostasis in an organism.

5.7 Conclusion

The present study reveals new insights into the function of Creld2 in an organism and its role in the orchestration of the UPR. *Creld2*^{-/-} mice reveal susceptibility to the development of a benign liver steatosis accompanied by insulin resistance and dysregulation of genes involved in glucose and lipid metabolism. These findings render Creld2 as a novel genetic risk factor for the development of NAFLD and metabolic syndrome. The general phenotypic observations probably are the consequence of the incapability of cells to cope with ER stress. This is evidenced by *in vitro* analyses of UPR regulation, which imply that Creld2 is involved in the orchestration of a prompt and robust response to ER stress. Here, the loss of Creld2 results in a delayed attenuation of global protein synthesis and an insufficient induction of important components for protein degradation. Cues obtained by protein interaction studies suggest that under ER stress conditions, Creld2 is bound by chaperones, which triggers activation of the UPR. On top of that, Creld2 co-precipitated proteins, such as ENO1 and LDHA/LDHB, suggest that Creld2 additionally is involved in carbohydrate metabolism.

6 Summary

The aim of this thesis was to investigate the role of Creld2 in the maintenance of metabolic homeostasis under steady state conditions and in the regulation of the UPR under ER stress conditions. Metabolic analyses of *Creld2*^{-/-} mice revealed a susceptibility of 1-year-old males for the development of hepatosteatosis and insulin resistance, accompanied with dysregulated gene expression of *Pgc1α*, and a reduced gene expression of the glucose transporters *Glut2* and *Glut4*. Female *Creld2*^{-/-} mice were protected from liver steatosis probably due to gender-specific hormonal regulation differences. *In vitro* ER stress analyses of wild-type and *Creld2*-deficient MEFs showed that *Creld2*^{-/-} cells cannot tolerate the emerging stress as well as *Creld2*^{+/+} cells and consequently become apoptotic when challenged with ER stress. In-depth analyses of the three UPR branches displayed a delayed and deficient response to ER stress, which leads to incomplete ER stress relief and to ER-stress accumulation rendering the cells dysfunctional. These *in vitro* results support the hypothesis that lack of Creld2 results in unresolved ER stress and the subsequent development of liver steatosis. In addition, Creld2 co-precipitation studies reveal an enrichment of numerous chaperones and proteins involved in carbohydrate metabolism, which indicates that Creld2 may bind to and effect the function of these proteins. Concluding, the results of this thesis suggest that Creld2 is involved in the regulation of metabolic processes by enhancing and orchestrating the UPR to enable proper ER stress resolution.

Acknowledgements

Firstly, I would like to express my gratitude to my doctoral adviser Prof. Dr. Dr. Michael Hoch for allowing me to do my PhD studies in his laboratory and for his constant support despite his extremely time-consuming duty as the rector of the University of Bonn.

Likewise, I would like to thank PD Dr. Reinhard Bauer, who was continuously addressable to discuss my ongoing project and to give valuable advice.

My sincere gratitude goes to Dr. Elvira Mass, who took the matter of supervision in her hands in times when I was locked in a stalemate, and not only guided me in the way out of the impasse but also motivated, encouraged and helped me with seemingly endless efforts in finishing my studies.

I thank Lorenzo Bonaguro for the countless constructive and critical discussions, and Melanie Thielisch for the infinite aid in histology, and I want to express my sincere gratitude to both for the great assistance in my experiments and for making the laboratory ambience bearable when despair was about to take over.

Last but not least, I want to thank my friends and family who always cheered me up, especially my parents who, in the first place, made all that possible and never ceased to believe in me.

References

- [1] P. A. Rupp, G. T. Fouad, C. A. Egelston, C. A. Reifsteck, S. B. Olson, W. M. Knosp, R. W. Glanville, K. L. Thornburg, S. W. Robinson, and C. L. Maslen, "Identification, genomic organization and mRNA expression of CRELD1, the founding member of a unique family of matricellular proteins," *Gene*, vol. 293, pp. 47–57, jun 2002.
- [2] E. Mass, "Functional analyses of the conserved Cysteine-rich with EGF-like domains (Creld) protein family in *Mus musculus*," 2013.
- [3] S. W. Robinson, C. D. Morris, E. Goldmuntz, M. D. Reller, M. A. Jones, R. D. Steiner, and C. L. Maslen, "Missense mutations in CRELD1 are associated with cardiac atrioventricular septal defects.," *American journal of human genetics*, vol. 72, pp. 1047–52, apr 2003.
- [4] M. Zatyka, M. Priestley, E. J. Ladusans, A. E. Fryer, J. Mason, F. Latif, and E. R. Maher, "Analysis of CRELD1 as a candidate 3p25 atrioventricular septal defect locus (AVSD2) [1]," mar 2005.
- [5] C. L. Maslen, D. Babcock, S. W. Robinson, L. J. Bean, K. J. Dooley, V. L. Willour, and S. L. Sherman, "CRELD1 mutations contribute to the occurrence of cardiac atrioventricular septal defects in Down syndrome," nov 2006.
- [6] J. K. Redig, G. T. Fouad, D. Babcock, B. Reshey, E. Feingold, R. H. Reeves, and C. L. Maslen, "Allelic Interaction between CRELD1 and VEGFA in the Pathogenesis of Cardiac Atrioventricular Septal Defects," *AIMS Genet*, vol. 1, no. 1, pp. 1–19, 2014.
- [7] E. Mass, D. Wachten, A. C. Aschenbrenner, A. Voelzmann, and M. Hoch, "Murine Creld1 controls cardiac development through activation of calcineurin/NFATc1 signaling.," *Developmental cell*, vol. 28, pp. 711–26, mar 2014.
- [8] K. Oh-hashii, R. Kunieda, Y. Hirata, and K. Kiuchi, "Biosynthesis and secretion

- of mouse cysteine-rich with EGF-like domains 2.," *FEBS letters*, vol. 585, pp. 2481–7, aug 2011.
- [9] C. L. Maslen, D. Babcock, J. K. Redig, K. Kapeli, Y. M. Akkari, and S. B. Olson, "CRELD2: gene mapping, alternate splicing, and comparative genomic identification of the promoter region.," *Gene*, vol. 382, pp. 111–20, nov 2006.
- [10] K. Oh-hashii, H. Koga, S. Ikeda, K. Shimada, Y. Hirata, and K. Kiuchi, "CRELD2 is a novel endoplasmic reticulum stress-inducible gene.," *Biochemical and biophysical research communications*, vol. 387, pp. 504–10, sep 2009.
- [11] Y. Kim, S.-J. Park, S. R. Manson, C. A. Molina, K. Kidd, H. Thiessen-Philbrook, R. J. Perry, H. Liapis, S. Kmoch, C. R. Parikh, A. J. Bleyer, and Y. M. Chen, "Elevated urinary CRELD2 is associated with endoplasmic reticulum stress-mediated kidney disease," *JCI Insight*, vol. 2, dec 2017.
- [12] J. a. Ortiz, M. Castillo, E. D. del Toro, J. Mulet, S. Gerber, L. M. Valor, S. Sala, F. Sala, L. M. Gutiérrez, and M. Criado, "The cysteine-rich with EGF-like domains 2 (CRELD2) protein interacts with the large cytoplasmic domain of human neuronal nicotinic acetylcholine receptor alpha4 and beta2 subunits.," *Journal of neurochemistry*, vol. 95, pp. 1585–96, dec 2005.
- [13] H. Malhi and R. J. Kaufman, "Endoplasmic reticulum stress in liver disease.," *Journal of hepatology*, vol. 54, pp. 795–809, apr 2011.
- [14] K. Mori, "Tripartite Management of Unfolded Proteins in the Endoplasmic Reticulum," *Cell*, vol. 101, pp. 451–454, may 2000.
- [15] D. T. Rutkowski, J. Wu, S.-H. Back, M. U. Callaghan, S. P. Ferris, J. Iqbal, R. Clark, H. Miao, J. R. Hassler, J. Fornek, M. G. Katze, M. M. Hussain, B. Song, J. Swathirajan, J. Wang, G. D.-Y. Yau, and R. J. Kaufman, "UPR pathways combine to prevent hepatic steatosis caused by ER stress-mediated suppression of transcriptional master regulators.," *Developmental cell*, vol. 15, pp. 829–40, dec 2008.

- [16] B. Adamson, T. M. Norman, M. Jost, M. Y. Cho, J. K. Nuñez, Y. Chen, J. E. Villalta, L. A. Gilbert, M. A. Horlbeck, M. Y. Hein, R. A. Pak, A. N. Gray, C. A. Gross, A. Dixit, O. Parnas, A. Regev, and J. S. Weissman, “A Multiplexed Single-Cell CRISPR Screening Platform Enables Systematic Dissection of the Unfolded Protein Response,” *Cell*, vol. 167, no. 7, pp. 1867–1882.e21, 2016.
- [17] S. J. Marciniak and D. Ron, “Endoplasmic reticulum stress signaling in disease.,” *Physiological reviews*, vol. 86, pp. 1133–49, oct 2006.
- [18] D. G. Breckenridge, M. Germain, J. P. Mathai, M. Nguyen, and G. C. Shore, “Regulation of apoptosis by endoplasmic reticulum pathways.,” *Oncogene*, vol. 22, pp. 8608–18, nov 2003.
- [19] E. Kojima, A. Takeuchi, M. Haneda, A. Yagi, T. Hasegawa, K.-i. Yamaki, K. Takeda, S. Akira, K. Shimokata, and K.-i. Isobe, “The function of GADD34 is a recovery from a shutoff of protein synthesis induced by ER stress: elucidation by GADD34-deficient mice.,” *FASEB journal : official publication of the Federation of American Societies for Experimental Biology*, vol. 17, pp. 1573–5, aug 2003.
- [20] M. H. Brush, D. C. Weiser, and S. Shenolikar, “Growth arrest and DNA damage-inducible protein GADD34 targets protein phosphatase 1 alpha to the endoplasmic reticulum and promotes dephosphorylation of the alpha subunit of eukaryotic translation initiation factor 2.,” *Molecular and cellular biology*, vol. 23, no. 4, pp. 1292–303, 2003.
- [21] S. J. Marciniak, C. Y. Yun, S. Oyadomari, I. Novoa, Y. Zhang, R. Jungreis, K. Nagata, H. P. Harding, and D. Ron, “CHOP induces death by promoting protein synthesis and oxidation in the stressed endoplasmic reticulum.,” *Genes & development*, vol. 18, pp. 3066–77, dec 2004.
- [22] H. Yamaguchi and H. G. Wang, “CHOP is involved in endoplasmic reticulum stress-induced apoptosis by enhancing DR5 expression in human carcinoma cells,” *Journal of Biological Chemistry*, vol. 279, pp. 45495–45502, oct 2004.
- [23] Y. Wang, J. Shen, N. Arenzana, W. Tirasophon, R. J. Kaufman, and R. Prywes,

- “Activation of ATF6 and an ATF6 DNA Binding Site by the Endoplasmic Reticulum Stress Response,” *J. Biol. Chem.*, vol. 275, pp. 27013–27020, sep 2000.
- [24] Y. Adachi, K. Yamamoto, T. Okada, H. Yoshida, A. Harada, and K. Mori, “ATF6 Is a Transcription Factor Specializing in the Regulation of Quality Control Proteins in the Endoplasmic Reticulum,” *Cell Structure and Function*, vol. 33, no. 1, pp. 75–89, 2008.
- [25] K. Yamamoto, T. Sato, T. Matsui, M. Sato, T. Okada, H. Yoshida, A. Harada, and K. Mori, “Transcriptional induction of mammalian ER quality control proteins is mediated by single or combined action of ATF6alpha and XBP1.,” *Developmental cell*, vol. 13, pp. 365–76, sep 2007.
- [26] W. Tirasophon, A. A. Welihinda, and R. J. Kaufman, “A stress response pathway from the endoplasmic reticulum to the nucleus requires a novel bifunctional protein kinase/endoribonuclease (Ire1p) in mammalian cells,” *Genes and Development*, vol. 12, no. 12, pp. 1812–1824, 1998.
- [27] X. Shen, R. E. Ellis, K. Lee, C.-y. Y. Liu, K. Yang, A. Solomon, H. Yoshida, R. Morimoto, D. M. Kurnit, K. Mori, R. J. Kaufman, and A. Arbor, “Complementary Signaling Pathways Regulate the Unfolded Protein Response and Are Required for *C. elegans* Development,” *Cell*, vol. 107, pp. 893–903, 2001.
- [28] A.-H. Lee, N. N. Iwakoshi, and L. H. Glimcher, “XBP-1 regulates a subset of endoplasmic reticulum resident chaperone genes in the unfolded protein response.,” *Molecular and cellular biology*, vol. 23, pp. 7448–59, nov 2003.
- [29] K. Yamamoto, H. Yoshida, K. Kokame, R. J. Kaufman, and K. Mori, “Differential contributions of ATF6 and XBP1 to the activation of endoplasmic reticulum stress-responsive cis-acting elements ERSE, UPRE and ERSE-II,” *Journal of Biochemistry*, vol. 136, no. 3, pp. 343–350, 2004.
- [30] J. Wu and R. J. Kaufman, “From acute ER stress to physiological roles of the Unfolded Protein Response.,” *Cell death and differentiation*, vol. 13, pp. 374–84, mar 2006.

- [31] H. Jo, S. S. Choe, K. C. Shin, H. Jang, J. H. Lee, J. K. Seong, S. H. Back, and J. B. Kim, "Endoplasmic reticulum stress induces hepatic steatosis via increased expression of the hepatic very low-density lipoprotein receptor," *Hepatology*, vol. 57, no. 4, pp. 1366–1377, 2013.
- [32] J. Han and R. J. Kaufman, "The role of ER stress in lipid metabolism and lipotoxicity," *Journal of Lipid Research*, vol. 57, no. 8, pp. 1329–1338, 2016.
- [33] A. Lee, E. Scapa, D. Cohen, and L. Glimcher, "Regulation of hepatic lipogenesis by the transcription factor XBP1," *Science*, vol. 320, no. 5882, pp. 1492–1496, 2008.
- [34] M. E. Fusakio, J. A. Willy, Y. Wang, E. T. Mirek, R. J. T. Al Baghdadi, C. M. Adams, T. G. Anthony, and R. C. Wek, "Transcription factor ATF4 directs basal and stress-induced gene expression in the unfolded protein response and cholesterol metabolism in the liver," *Molecular Biology of the Cell*, vol. 27, no. 9, pp. 1536–1551, 2016.
- [35] T. Iwawaki, R. Akai, S. Yamanaka, and K. Kohno, "Function of IRE1 alpha in the placenta is essential for placental development and embryonic viability," *Proceedings of the National Academy of Sciences*, vol. 106, no. 39, pp. 16657–16662, 2009.
- [36] K. Zhang, S. Wang, J. Malhotra, J. R. Hassler, S. H. Back, G. Wang, L. Chang, W. Xu, H. Miao, R. Leonardi, Y. E. Chen, S. Jackowski, and R. J. Kaufman, "The unfolded protein response transducer IRE1 α prevents ER stress-induced hepatic steatosis.," *The EMBO journal*, vol. 30, pp. 1357–75, apr 2011.
- [37] M. Usui, S. Yamaguchi, Y. Tanji, R. Tominaga, Y. Ishigaki, M. Fukumoto, H. Katagiri, K. Mori, Y. Oka, and H. Ishihara, "Atf6 α -null mice are glucose intolerant due to pancreatic β -cell failure on a high-fat diet but partially resistant to diet-induced insulin resistance.," *Metabolism: clinical and experimental*, vol. 61, pp. 1118–28, aug 2012.
- [38] X. Chen, F. Zhang, Q. Gong, A. Cui, S. Zhuo, Z. Hu, Y. Han, J. Gao, Y. Sun, Z. Liu,

- Z. Yang, Y. Le, X. Gao, L. Q. Dong, X. Gao, and Y. Li, "Hepatic ATF6 increases fatty acid oxidation to attenuate hepatic steatosis in mice through peroxisome proliferator-activated receptor α ," *Diabetes*, vol. 65, no. 7, pp. 1904–1915, 2016.
- [39] A. M. Reimold, N. N. Iwakoshi, J. Manis, P. Vallabhajosyula, E. Szomolanyi-Tsuda, E. M. Gravellese, D. Friend, M. J. Grusby, F. Alt, and L. H. Glimcher, "Plasma cell differentiation requires the transcription factor XBP-1," *Nature*, vol. 412, no. July, pp. 300–307, 2001.
- [40] N. N. Iwakoshi, M. Pypaert, and L. H. Glimcher, "The transcription factor XBP-1 is essential for the development and survival of dendritic cells," *The Journal of Experimental Medicine*, vol. 204, no. 10, pp. 2267–2275, 2007.
- [41] T. L. Cameron, K. M. Bell, L. Tatarczuch, E. J. Mackie, M. H. Rajpar, B. T. McDermott, R. P. Boot-Handford, and J. F. Bateman, "Transcriptional profiling of chondrodysplasia growth plate cartilage reveals adaptive ER-stress networks that allow survival but disrupt hypertrophy," *PLoS ONE*, vol. 6, p. e24600, sep 2011.
- [42] T. L. Cameron, K. M. Bell, I. L. Gresshoff, L. Sampurno, L. Mullan, J. Ermann, L. H. Glimcher, R. P. Boot-Handford, and J. F. Bateman, "XBP1-Independent UPR Pathways Suppress C/EBP- β Mediated Chondrocyte Differentiation in ER-Stress Related Skeletal Disease," *PLoS Genetics*, vol. 11, p. e1005505, sep 2015.
- [43] J. M. Berg, J. L. Tymoczko, G. J. Gatto Jr., and L. Stryer, *No Title*. W.H. Freeman and Company, 8 ed., 2015.
- [44] N. Stefan, K. Kantartzis, and H. U. Häring, "Causes and metabolic consequences of fatty liver," *Endocrine Reviews*, vol. 29, no. 7, pp. 939–960, 2008.
- [45] L. C. Bertot and L. A. Adams, "The natural course of non-alcoholic fatty liver disease," *International Journal of Molecular Sciences*, vol. 17, no. 5, 2016.
- [46] C. Wang, Q. Tao, X. Wang, X. Wang, and X. Zhang, "Impact of high-fat diet on liver genes expression profiles in mice model of nonalcoholic fatty liver disease," *Environmental Toxicology and Pharmacology*, vol. 45, pp. 52–62, 2016.

- [47] C. G. Bell, "The Epigenomic Analysis of Human Obesity," *Obesity*, vol. 25, no. 9, pp. 1471–1481, 2017.
- [48] S. Wahl, A. Drong, B. Lehne, M. Loh, W. R. Scott, S. Kunze, P. C. Tsai, J. S. Ried, W. Zhang, Y. Yang, S. Tan, G. Fiorito, L. Franke, S. Guarrera, S. Kasela, J. Kriebel, R. C. Richmond, M. Adamo, U. Afzal, M. Ala-Korpela, B. Albetti, O. Ammerpohl, J. F. Apperley, M. Beekman, P. A. Bertazzi, S. L. Black, C. Blancher, M. J. Bonder, M. Brosch, M. Carstensen-Kirberg, A. J. De Craen, S. De Lusignan, A. Dehghan, M. Elkalaawy, K. Fischer, O. H. Franco, T. R. Gaunt, J. Hampe, M. Hashemi, A. Isaacs, A. Jenkinson, S. Jha, N. Kato, V. Krogh, M. Laffan, C. Meisinger, T. Meitinger, Z. Y. Mok, V. Motta, H. K. Ng, Z. Nikolakopoulou, G. Nteliopoulos, S. Panico, N. Pervjakova, H. Prokisch, W. Rathmann, M. Roden, F. Rota, M. A. Rozario, J. K. Sandling, C. Schafmayer, K. Schramm, R. Siebert, P. E. Slagboom, P. Soininen, L. Stolk, K. Strauch, E. S. Tai, L. Tarantini, B. Thorand, E. F. Tigchelaar, R. Tumino, A. G. Uitterlinden, C. Van Duijn, J. B. Van Meurs, P. Vineis, A. R. Wickremasinghe, C. Wijmenga, T. P. Yang, W. Yuan, A. Zhernakova, R. L. Batterham, G. D. Smith, P. Deloukas, B. T. Heijmans, C. Herder, A. Hofman, C. M. Lindgren, L. Milani, P. Van Der Harst, A. Peters, T. Illig, C. L. Relton, M. Waldenberger, M. R. Jarvelin, V. Bollati, R. Soong, T. D. Spector, J. Scott, M. I. McCarthy, P. Elliott, J. T. Bell, G. Matullo, C. Gieger, J. S. Kooner, H. Grallert, and J. C. Chambers, "Epigenome-wide association study of body mass index, and the adverse outcomes of adiposity," *Nature*, vol. 541, pp. 81–86, jan 2017.
- [49] F. Lazner, M. Gowen, D. Pavasovic, and I. Kola, "Osteopetrosis and osteoporosis: Two sides of the same coin," sep 1999.
- [50] C. L. Hartley, S. Edwards, L. Mullan, P. a. Bell, M. Fresquet, R. P. Boot-Handford, and M. D. Briggs, "Armet/Manf and Creld2 are components of a specialized ER stress response provoked by inappropriate formation of disulphide bonds: implications for genetic skeletal diseases.," *Human molecular genetics*, vol. 22, pp. 5262–75, dec 2013.
- [51] J. Zhang, Y. Weng, X. Liu, J. Wang, W. Zhang, S. H. Kim, H. Zhang, R. Li,

- Y. Kong, X. Chen, W. Shui, N. Wang, C. Zhao, N. Wu, Y. He, G. Nan, X. Chen, S. Wen, H. Zhang, F. Deng, L. Wan, H. H. Luu, R. C. Haydon, L. L. Shi, T.-C. He, and Q. Shi, "Endoplasmic reticulum (ER) stress inducible factor cysteine-rich with EGF-like domains 2 (Creld2) is an important mediator of BMP9-regulated osteogenic differentiation of mesenchymal stem cells.," *PloS one*, vol. 8, p. e73086, jan 2013.
- [52] Servier, "Smart Servier Medical Art."
- [53] P. Schatz, "Bone Formation and Development, Anatomy and Physiology," 2016.
- [54] C. J. Gloeckner, K. Boldt, A. Schumacher, R. Roepman, and M. Ueffing, "A novel tandem affinity purification strategy for the efficient isolation and characterisation of native protein complexes," *PROTEOMICS*, vol. 7, pp. 4228–4234, dec 2007.
- [55] P. Shannon, A. Markiel, . Owen Ozier, N. S. Baliga, J. T. Wang, D. Ramage, N. Amin, B. Schwikowski, and T. Ideker, "Cytoscape: a software environment for integrated models of biomolecular interaction networks," *Genome Research*, no. 13, pp. 2498–2504, 2003.
- [56] M. Serrano, A. Ormazábal, M. A. Vilaseca, N. Lambruschini, R. Garcia-Romero, S. Meavilla, B. Perez-Dueñas, M. Pineda, A. Garcia-Cazorla, J. Campistol, and R. Artuch, "Assessment of plasma ammonia and glutamine concentrations in urea cycle disorders," *Clinical Biochemistry*, vol. 44, pp. 742–744, jun 2011.
- [57] J. Long, H. Wang, Z. Lang, T. Wang, M. Long, and B. Wang, "Expression level of glutamine synthetase is increased in hepatocellular carcinoma and liver tissue with cirrhosis and chronic hepatitis B," *Hepatology International*, vol. 5, no. 2, pp. 698–706, 2011.
- [58] V. Soontornniyomkij, J. P. Kesby, B. Soontornniyomkij, J. J. Kim, C. L. Achim, S. Semenova, and D. V. Jeste, "Age and High-Fat Diet Effects on Glutamine Synthetase Immunoreactivity in Liver and Hippocampus and Recognition Memory in Mice," *Curr Aging Sci*, vol. 9, no. 4, pp. 301–309, 2016.

- [59] R. Gebhardt and D. Mecke, "Heterogeneous distribution of glutamine synthetase among rat liver parenchymal cells in situ and in primary culture.," *The EMBO journal*, vol. 2, no. 4, pp. 567–70, 1983.
- [60] Z. Wu, P. Puigserver, U. Andersson, C. Zhang, G. Adelmant, V. Mootha, A. Troy, S. Cinti, B. Lowell, R. C. Scarpulla, and B. M. Spiegelman, "Mechanisms controlling mitochondrial biogenesis and respiration through the thermogenic coactivator PGC-1," *Cell*, vol. 98, pp. 115–124, jul 1999.
- [61] R. B. Vega, J. M. Huss, and D. P. Kelly, "The Coactivator PGC-1 Cooperates with Peroxisome Proliferator-Activated Receptor alpha in Transcriptional Control of Nuclear Genes Encoding Mitochondrial Fatty Acid Oxidation Enzymes," *Molecular and Cellular Biology*, vol. 20, pp. 1868–1876, mar 2000.
- [62] R. J. Havel, V. G. Shore, B. Shore, and D. M. Bier, "Role of specific glycopeptides of human serum lipoproteins in the activation of lipoprotein lipase.," *Circulation research*, vol. 27, no. 4, pp. 595–600, 1970.
- [63] J. C. LaRosa, R. I. Levy, P. Herbert, S. E. Lux, and D. S. Fredrickson, "A specific apoprotein activator for lipoprotein lipase," *Biochemical and Biophysical Research Communications*, vol. 41, pp. 57–62, oct 1970.
- [64] S. Cases, S. J. Stone, P. Zhou, E. Yen, B. Tow, K. D. Lardizabal, T. Voelker, and R. V. Farese, "Cloning of DGAT2, a Second Mammalian Diacylglycerol Acyltransferase, and Related Family Members," *Journal of Biological Chemistry*, vol. 276, pp. 38870–38876, oct 2001.
- [65] J. Shao, H. Yamashita, L. Qiao, and J. E. Friedman, "Decreased Akt kinase activity and insulin resistance C57BL/KsJ-Lepr(db/db) mice," *Journal of Endocrinology*, vol. 167, pp. 107–115, oct 2000.
- [66] E. Hajduch, G. J. Litherland, and H. S. Hundal, "Protein kinase B (PKB/Akt) - a key regulator of glucose transport?," *FEBS Lett.*, vol. 492, pp. 199–203, mar 2001.

- [67] H. Fukumoto, S. Seino, H. Imura, Y. Seino, R. L. Eddy, Y. Fukushima, M. G. Byers, T. B. Shows, and G. I. Bell, "Sequence, tissue distribution, and chromosomal localization of mRNA encoding a human glucose transporter-like protein.," *Proceedings of the National Academy of Sciences*, vol. 85, no. 15, pp. 5434–5438, 1988.
- [68] B. Thorens, H. K. Sarkar, H. R. Kaback, and H. F. Lodish, "Cloning and functional expression in bacteria of a novel glucose transporter present in liver, intestine, kidney, and β -pancreatic islet cells," *Cell*, vol. 55, pp. 281–290, oct 1988.
- [69] M. MUECKLER, "Facilitative glucose transporters," *European Journal of Biochemistry*, vol. 219, no. 3, pp. 713–725, 1994.
- [70] K. Kotani, O. D. Peroni, Y. Minokoshi, O. Boss, and B. B. Kahn, "GLUT4 glucose transporter deficiency increases hepatic lipid production and peripheral lipid utilization," *Journal of Clinical Investigation*, vol. 114, pp. 1666–1675, dec 2004.
- [71] Y. Mebratu and Y. Tesfaigzi, "How ERK1/2 Activation Controls Cell Proliferation and Cell Death Is Subcellular Localization the Answer?," *Cell cycle (Georgetown, Tex.)*, vol. 8, pp. 1168–1175, apr 2009.
- [72] E. Gruys, M. J. M. Toussaint, T. A. Niewold, and S. J. Koopmans, "Acute phase reaction and acute phase proteins.," *Journal of Zhejiang University. Science. B*, vol. 6, pp. 1045–56, nov 2005.
- [73] M. D. Briggs, P. A. Bell, M. J. Wright, and K. A. Pirog, "New therapeutic targets in rare genetic skeletal diseases," *Expert Opinion on Orphan Drugs*, vol. 3, no. 10, pp. 1137–1154, 2015.
- [74] M. J. Kiel, Ö. H. Yilmaz, T. Iwashita, O. H. Yilmaz, C. Terhorst, and S. J. Morrison, "SLAM family receptors distinguish hematopoietic stem and progenitor cells and reveal endothelial niches for stem cells," *Cell*, vol. 121, no. 7, pp. 1109–1121, 2005.
- [75] S. Basseri and R. C. Austin, "ER Stress and Lipogenesis: A Slippery Slope toward Hepatic Steatosis," dec 2008.

- [76] X.-Q. Zhang, C.-F. Xu, C.-H. Yu, W.-X. Chen, and Y.-M. Li, "Role of endoplasmic reticulum stress in the pathogenesis of nonalcoholic fatty liver disease.," *World journal of gastroenterology : WJG*, vol. 20, pp. 1768–76, feb 2014.
- [77] J. Wu, J. L. Ruas, J. L. Estall, K. A. Rasbach, J. H. Choi, L. Ye, P. Boström, H. M. Tyra, R. W. Crawford, K. P. Campbell, D. T. Rutkowski, R. J. Kaufman, and B. M. Spiegelman, "The unfolded protein response mediates adaptation to exercise in skeletal muscle through a PGC-1 α /ATF6 α complex," *Cell Metabolism*, vol. 13, no. 2, pp. 160–169, 2011.
- [78] P. K. Singhal, S. Sassi, L. Lan, P. Au, S. C. Halvorsen, D. Fukumura, R. K. Jain, and B. Seed, "Mouse embryonic fibroblasts exhibit extensive developmental and phenotypic diversity," *Proceedings of the National Academy of Sciences*, vol. 113, no. 1, pp. 122–127, 2016.
- [79] P. Zhang, B. McGrath, S. Li, A. Frank, F. Zambito, J. Reinert, M. Gannon, K. Ma, K. McNaughton, and D. R. Cavener, "The PERK eukaryotic initiation factor 2 alpha kinase is required for the development of the skeletal system, postnatal growth, and the function and viability of the pancreas.," *Molecular and cellular biology*, vol. 22, pp. 3864–3874, jun 2002.
- [80] H. Urra, E. Dufey, F. Lisbona, D. Rojas-Rivera, and C. Hetz, "When ER stress reaches a dead end," *Biochimica et Biophysica Acta - Molecular Cell Research*, vol. 1833, no. 12, pp. 3507–3517, 2013.
- [81] C. Ruberti, Y. S. Lai, and F. Brandizzi, "Recovery from temporary endoplasmic reticulum stress in plants relies on the tissue-specific and largely independent roles of bZIP28 and bZIP60, as well as an antagonizing function of BAX-Inhibitor 1 upon the pro-adaptive signaling mediated by bZIP28," *Plant Journal*, vol. 93, no. 1, pp. 155–165, 2018.
- [82] I. Tabas and D. Ron, "Integrating the mechanisms of apoptosis induced by endoplasmic reticulum stress," mar 2011.

- [83] R. Iurlaro and C. Muñoz-Pinedo, "Cell death induced by endoplasmic reticulum stress," *FEBS Journal*, vol. 283, pp. 2640–2652, 2016.
- [84] S. Flag, C. J. Gloeckner, C. J. Gloeckner, K. Boldt, A. Schumacher, and M. Ueffing, "Proteomics," *Methods in molecular biology (Clifton, N.J.)*, vol. 564, no. February, 2009.
- [85] J. Wu, D. T. Rutkowski, M. Dubois, J. Swathirajan, T. Saunders, J. Wang, B. Song, G. D.-Y. Yau, and R. J. Kaufman, "ATF6alpha optimizes long-term endoplasmic reticulum function to protect cells from chronic stress.," *Developmental cell*, vol. 13, pp. 351–64, sep 2007.
- [86] Y. Ariyama, H. Shimizu, T. Satoh, T. Tsuchiya, S. Okada, S. Oyadomari, M. Mori, and M. Mori, "Chop-deficient mice showed increased adiposity but no glucose intolerance," *Obesity*, vol. 15, pp. 1647–1656, jul 2007.
- [87] Y. Eura, H. Yanamoto, Y. Arai, T. Okuda, T. Miyata, and K. Kokame, "Derlin-1 deficiency is embryonic lethal, derlin-3 deficiency appears normal, and herp deficiency is intolerant to glucose load and ischemia in mice," *PLoS ONE*, vol. 7, no. 3, p. e34298, 2012.
- [88] J. Munoz, A. Derstine, and B. A. Gower, "Fat distribution and insulin sensitivity in postmenopausal women: Influence of hormone replacement," *Obesity Research*, vol. 10, pp. 424–431, jun 2002.
- [89] D. Roulot, "Liver involvement in Turner syndrome," jan 2013.
- [90] S. Hart-Unger, Y. Arao, K. J. Hamilton, S. L. Lierz, D. E. Malarkey, S. C. Hewitt, M. Freemark, and K. S. Korach, "Hormone signaling and fatty liver in females: Analysis of estrogen receptor α mutant mice," *International Journal of Obesity*, vol. 41, pp. 945–954, jun 2017.
- [91] T. M. D'Eon, S. C. Souza, M. Aronovitz, M. S. Obin, S. K. Fried, and A. S. Greenberg, "Estrogen regulation of adiposity and fuel partitioning: Evidence of genomic and non-genomic regulation of lipogenic and oxidative pathways," *Journal of Biological Chemistry*, vol. 280, pp. 35983–35991, oct 2005.

- [92] O. Koulouri, J. Ostberg, and G. S. Conway, "Liver dysfunction in Turner's syndrome: Prevalence, natural history and effect of exogenous oestrogen," *Clinical Endocrinology*, vol. 69, pp. 306–310, aug 2008.
- [93] T. Matsuzaka and H. Shimano, "Molecular mechanisms involved in hepatic steatosis and insulin resistance," *Journal of Diabetes Investigation*, vol. 2, no. 3, pp. 170–175, 2011.
- [94] E. Fabbrini, S. Sullivan, and S. Klein, "Obesity and Nonalcoholic Fatty Liver Disease: Biochemical, Metabolic and Clinical Implications NIH Public Access," *Hepatology*, vol. 51, no. 2, pp. 679–689, 2010.
- [95] R. A. DeFronzo and D. Tripathy, "Skeletal muscle insulin resistance is the primary defect in type 2 diabetes.," *Diabetes care*, vol. 32 Suppl 2, 2009.
- [96] J. Delarue and C. Magnan, "Free fatty acids and insulin resistance," mar 2007.
- [97] V. T. Samuel and S. G. I, "Integratin Mechanisms for Insulin Resistance: Common Threads and Missing Links," *Cell*, vol. 148, no. 5, pp. 852–871, 2012.
- [98] H. Malhi and G. J. Gores, "Molecular mechanisms of lipotoxicity in nonalcoholic fatty liver disease," nov 2008.
- [99] J. K. Reddy and M. S. Rao, "Lipid metabolism and liver inflammation. II. Fatty liver disease and fatty acid oxidation.," *American Journal Of Physiology Gastrointestinal Liver Physiology*, pp. G852–G858, 2006.
- [100] E. Hijona, L. Hijona, J. I. Arenas, and L. Bujanda, "Inflammatory Mediators of Hepatic Steatosis," *Mediators of Inflammation*, vol. 2010, pp. 1–7, mar 2010.
- [101] H. Malhi, F. J. Barreyro, H. Isomoto, S. F. Bronk, and G. J. Gores, "Free fatty acids sensitise hepatocytes to TRAIL mediated cytotoxicity," *Gut*, vol. 56, pp. 1124–1131, aug 2007.
- [102] F. Geissmann, M. G. Manz, S. Jung, M. H. Sieweke, M. Merad, and K. Ley, "Development of monocytes, macrophages, and dendritic cells.," *Science (New York, N.Y.)*, vol. 327, pp. 656–61, feb 2010.

- [103] F. Ginhoux and M. Guilliams, "Tissue-Resident Macrophage Ontogeny and Homeostasis," mar 2016.
- [104] C. L. Scott, F. Zheng, P. De Baetselier, L. Martens, Y. Saeys, S. De Prijck, S. Lippens, C. Abels, S. Schoonooghe, G. Raes, N. Devoogdt, B. N. Lambrecht, A. Beschin, and M. Guilliams, "Bone marrow-derived monocytes give rise to self-renewing and fully differentiated Kupffer cells," *Nature Communications*, vol. 7, p. 10321, jan 2016.
- [105] L. Beattie, A. Sawtell, J. Mann, T. C. Frame, B. Teal, F. de Labastida Rivera, N. Brown, K. Walwyn-Brown, J. W. Moore, S. MacDonald, E. K. Lim, J. E. Dalton, C. R. Engwerda, K. P. MacDonald, and P. M. Kaye, "Bone marrow-derived and resident liver macrophages display unique transcriptomic signatures but similar biological functions," *Journal of Hepatology*, vol. 65, pp. 758–768, oct 2016.
- [106] D.-s. Kim, L. Song, J. Wang, H. Wu, G. Gu, Y. Sugi, Z. Li, and H. Wang, "GRP94 Is an Essential Regulator of Pancreatic β -Cell Development, Mass, and Function in Male Mice," *Endocrinology*, vol. 159, pp. 1062–1073, feb 2018.
- [107] W. T. Chen, D. Ha, G. Kanel, and A. S. Lee, "Targeted Deletion of ER Chaperone GRP94 in the Liver Results in Injury, Repopulation of GRP94-Positive Hepatocytes, and Spontaneous Hepatocellular Carcinoma Development in Aged Mice," *Neoplasia*, vol. 16, pp. 617–626, aug 2014.
- [108] C. M. Osowski and F. Urano, "Measuring ER stress and the unfolded protein response using mammalian tissue culture system," *Methods in Enzymology*, vol. 490, no. 508, pp. 71–92, 2013.
- [109] Y. Oda, T. Okada, H. Yoshida, R. J. Kaufman, K. Nagata, and K. Mori, "Derlin-2 and Derlin-3 are regulated by the mammalian unfolded protein response and are required for ER-associated degradation," *Journal of Cell Biology*, vol. 172, pp. 383–393, jan 2006.
- [110] T. J. Bergmann, I. Fregno, F. Fumagalli, A. Rinaldi, F. Bertoni, P. J. Boersema, P. Picotti, and M. Molinari, "Chemical stresses fail to mimic the unfolded protein

- response resulting from luminal load with unfolded polypeptides,” *Journal of Biological Chemistry*, no. 9, p. jbc.RA117.001484, 2018.
- [111] R. S. Lachman, D. L. Rimoïn, and J. Spranger, “Metaphyseal chondrodysplasia, Schmid type Clinical and radiographic deliniation with a review of the literature,” 1988.
- [112] M. Forouhan, K. Mori, and R. P. Boot-Handford, “Paradoxical roles of ATF6 α and ATF6 β in modulating disease severity caused by mutations in collagen X,” mar 2018.
- [113] “KEGG PATHWAY: Metabolic pathways - Reference pathway,” 2018.
- [114] M. Csala, G. Bánhegyi, and A. Benedetti, “Endoplasmic reticulum: A metabolic compartment,” *FEBS Letters*, vol. 580, no. 9, pp. 2160–2165, 2006.
- [115] H. Zeeshan, G. Lee, H.-R. Kim, and H.-J. Chae, “Endoplasmic Reticulum Stress and Associated ROS,” *International Journal of Molecular Sciences*, vol. 17, no. 3, p. 327, 2016.
- [116] C. Liu, G. Bhattacharjee, W. Boisvert, R. Dilley, and T. Edgington, “In Vivo Interrogation of the Molecular Display of Atherosclerotic Lesion Surfaces,” *American Journal of Pathology*, vol. 163, pp. 1859–1871, nov 2003.
- [117] Y. Zhang, R. Liu, M. Ni, P. Gill, and A. S. Lee, “Cell surface relocalization of the endoplasmic reticulum chaperone and unfolded protein response regulator GRP78/BiP,” *Journal of Biological Chemistry*, vol. 285, pp. 15065–15075, may 2010.
- [118] Y. Liu, S. C. Steiniger, Y. S. Kim, G. F. Kaufmann, B. Felding-Habermann, and K. D. Janda, “Mechanistic studies of a peptidic GRP78 ligand for cancer cell-specific drug delivery,” *Molecular Pharmaceutics*, vol. 4, pp. 435–447, jun 2007.
- [119] A. A. Birukova, P. A. Singleton, G. Gawlak, X. Tian, T. Mirzapoiazova, B. Mambetsariev, O. Dubrovskiy, O. V. Oskolkova, V. N. Bochkov, and K. G.

- Birukov, "GRP78 is a novel receptor initiating a vascular barrier protective response to oxidized phospholipids.," *Molecular biology of the cell*, vol. 25, pp. 2006–16, jul 2014.
- [120] B. Y. H. Stern and A. E. Mirsky, "THE ISOLATION OF WHEAT GERM NUCLEI AND SOME ASPECTS OF THEIR GLYCOLYTIC METABOLISM," *The Journal of General Physiology*, no. 1, pp. 181–200, 1952.
- [121] H. Ji, J. Wang, J. Guo, Y. Li, S. Lian, W. Guo, H. Yang, F. Kong, L. Zhen, L. Guo, and Y. Liu, "Progress in the biological function of alpha-enolase," *Animal Nutrition*, vol. 2, no. 1, pp. 12–17, 2016.
- [122] R. Stambaugh and D. Post, "Substrate and Product Inhibition of Rabbit Substrate and Product Inhibition of Rabbit Muscle Lactic Dehydrogenase Heart (HJ and Muscle (MJ Isozymes *," *The Journal of Biological Chemistry*, vol. 241, no. 7, pp. 4–10, 1966.

List of Figures

1.1	Predicted Creld2 protein structure is conserved between different species.	2
1.2	Overview of the unfolded protein response.	6
1.3	Overview of fatty acid metabolism.	9
1.4	Histological analysis of <i>Creld2</i> KO liver sections.	11
1.5	Long bone growth and structure.	13
4.1	Genotype distribution and comparison of mouse weights.	39
4.2	Histological analysis of livers.	40
4.3	Thin layer chromatography of total lipid extracts from young and old <i>Creld2</i> ^{-/-} and litter mate control mice livers.	42
4.4	Gene expression analysis of lipid metabolism components.	44
4.5	Analysis of glucose metabolism and energy state in 1-year-old mice.	46
4.6	Determination of liver health state in aged mice.	48
4.7	Analysis of Kupffer cells and macrophage activation.	49
4.8	Analysis of UPR pathways in livers of 1-year-old mice.	52
4.9	Analysis of bones in 1-month and 1-year-old mice.	54
4.10	Bone-marrow analysis in 1-year-old male mice.	55
4.11	Analysis of cell viability during chronic ER stress.	57
4.12	Regulation of general ER stress marker during chronic ER stress.	59
4.13	Perk pathway regulation during chronic ER stress.	60
4.14	Atf6 α pathway during chronic ER stress.	62
4.15	Regulation of the Ire1 α pathway during chronic ER stress.	63
4.16	Establishment of the ER stress recovery model in MEFs.	66
4.17	Regulation of ER stress markers during ER stress recovery.	67
4.18	Regulation of Perk pathway induced components during ER stress recovery.	69
4.19	Regulation of Atf6 α pathway induced components.	70
4.20	Regulation of the Ire1 α pathway during ER stress recovery.	71
4.21	Analysis of Creld2 interaction partners.	73

List of Tables

2.1	Equipment	15
2.2	Consumables	16
2.3	Chemicals	17
2.4	Standards and Kits	17
2.5	Bacterial strains	18
2.6	Buffers	18
2.7	Media for bacterial culture	20
2.8	Media for cell culture	21
2.9	Antibodies	21
2.10	Plasmids used	23
2.11	Primer for genotyping	24
2.12	Primer for cloning	24
2.13	Primer for quantitative real time PCR	24
2.14	Gene blocks used for cloning	26
3.1	Genotyping PCR Protocol	30
3.2	Genotyping PCR program	30
3.3	PCR Protocol <i>Creld2</i> cDNA amplification	31
3.4	<i>Creld2</i> cDNA amplification PCR program	31
3.5	PCR Protocol SF-mock tag amplification	32
3.6	SF-mock tag amplification PCR program	32
3.7	qRT-PCR Protocol	32
4.1	Proteins affiliated to enriched pathways	74
A1	Enriched proteins in <i>Creld2</i> affinity precipitations	114

List of abbreviations

Akt	Protein kinase B
Apcs	Serum amyloid P-component
Apoc2	Apolipoprotein C-II
APR	Acute phase response
Atf4	Activating transcription factor 4
Atf6 α	Activating transcription factor 6 alpha
ATP	Adenosine triphosphate
AVSD	Atrioventricular septal defect
BMD	Bone mineral density
BMDM	Bone-marrow derived macrophages
BMP9	Bone morphogenic protein 9
CAC	Citric acid cycle
Chop	CCAAT-enhancer-binding protein homologous protein
CoA	Coenzyme A
Creld2	Cysteine-rich with EGF-like domains 2
DAG	Diacylglycerol
Derl3	Derlin 3
Dgat1/2	Diacylglycerol O-acyltransferase
Dr5	Death receptor 5
ECM	Extracellular matrix
Edem1	ER degradation enhancing alpha-mannosidase like protein 1
EGF-like	Epidermal growth factor- like
ENO1	Enolase 1
ER	Endoplasmic reticulum
ERAD	ER-associated protein degradation
Erk1/2	Extracellular signal-regulated kinase 1/2
ERSE	ER stress response element
eIF2 α	Eukaryotic initiation factor 2 alpha

EWAS	Epigenome-wide association studies
FFA	Free fatty acid
Fit2	Fat storage-inducing transmembrane protein 2
Fsp27	Fat specific protein 27
Gadd34	Growth arrest and DNA damage-inducible protein
GFP	Green fluorescent protein
Glut2/4	Glucose transporter 2/4
Grp78/Grp94	78/94 kDa glucose-regulated protein
GS	Glutamine synthetase
GTT	Glucose tolerance test
HE staining	Hematoxylin/Eosin staining
HFD	High-fat diet
HSC	Hematopoietic stem cells
HSP	Heat shock protein
<i>Il1β</i>	Interleukin 1 β
Il6	Interleukin 6
Ire1 α	Inositol-requiring protein 1 alpha
ITT	Insulin tolerance test
LDHA/B	Lactate dehydrogenase A/B
LPS	Lipopolysaccharide
LSK cells	Lin ⁻ Sca1 ⁺ cKit ⁺ cells
MCDS	Schmid metaphyseal chondrodysplasia
MED	Multiple epiphyseal dysplasia
MEFs	Mouse embryonic fibroblasts
MSC	Mesenchymal stem cell
nAtf6 α	nuclear Atf6 α
NAFLD	Non-alcoholic induced fatty liver disease
NFATc1	Nuclear factor of activated T cells 1
PDI	Protein disulfide isomerase
Perk	PRKR-like endoplasmic reticulum kinase

List of abbreviations

Pgc1 α	Peroxisome proliferative activated receptor, gamma, coactivator 1 alpha
ROS	Reactive oxygen species
S1P/S2P	Site-1/2 protease
Saa3	Serm amyloid A-3 protein
SF-tag	StreptII-StreptII-Flag tag
sXbp1	Spliced X-box binding protein 1
TAG	Triacylglycerol
TAP	Tandem affinity purification
Tg	Thapsigargin
Tm	Tunicamycin
Tnf α	Tumor necrosis factor α
UPR	Unfolded protein response
VLDL	Very low density lipoprotein
WE domain	Tryptophane and glutamic acid-rich domain

Appendix

Table A1: Enriched proteins in Creld2 affinity precipitations

Creld2-SF transient	Creld2-SF stable	FS-Creld2 stable
ANXA2	ACTR3	ACTR3
AZGP1	CRELD2	ARG1
CKAP4	DSG1	C1QBP
CPN2	EEF2	CASP14
CRELD2	EIF4A1	CLTC
DCD	ENO1	CRELD2
ENO1	HIST1H2BN	EEF2
FLNA	HIST1H4A	EIF4A1
GAPDH	HIST2H3A	ENO1
HSP90AA1	LDHA	HIST1H2BN
HSP90AB1	LDHB	HIST1H4A
HSP90B1	PFN1	HIST2H3A
HSPA1B	UBA1	HNRNPA1
HSPA5	XRCC5	HNRNPA2B1
HSPA8		HSPD1
HSPA9		LDHA
IGHA1		LDHB
IIGLL5		NONO
JUP		PFN1
KLK7		UBA1
LTF		
LYZ		
NCCRP1		
NPM1		
P4HB		
PDIA3		
PDIA4		
PIGR		
PRKCSH		
PRMT5		
RAN		
RPS3		
S100A8		
SERPINB3		
TPI1		
TRIM28		
TXN		
TXNDC5		
UBB		
WDR77		